Electron spin resonance studies of doped magnesium oxide

Hossain, Delawer,

ELECTRON SPIN RESONANCE STUDIES

OF DOPED MAGNESIUM OXIDE

by

MD. DELAWER HOSSAIN, M.Sc.
(Graduate Society)

A Thesis submitted to the University of Durham

in Candidature for the degree of Doctor of Philosophy.

JUNE 1980

Department of Applied Physics
and Electronics,
Science Laboratories,
DURHAM.

To the memory of my Father.

To my Mother.

ACKNOWLEDGEMENTS

Many people have helped with this thesis in one way or another, and I would like to express my very grateful appreciation to them all.

I wish to thank the University of Rajshahi, Bangladesh, for the award of a research scholarship to study for the degree of Ph.D. in the United Kingdom.

My thanks are due to Professor G G Roberts for allowing me to use the facilities of the Department of Applied Physics and Electronics and to the technical staff, led by Mr. F Spence for their assistance. In particular, I am grateful to Mr. R T Harcourt for his patient, painstaking efforts in cutting and polishing specimens ; to Mr. C Savage and Mr. W Mounsey for their continued assistance during the course of the work.

I would like to give thanks to my colleagues, Mr. A D Inglis, Mr. L J C Bluck, Mr. T G Bushell, and other members of the 'Ceramics and Resonance Group', for their many useful discussions and cooperation.

I am also indebted to Mrs. S Mellanby for her careful typing of this thesis and to Dr. K M Elahi for his assistance in drawing the diagrams.

A thesis such as this becomes part of one's life and that part of my life was made very pleasant by my good fortune in having such an excellent supervisor. I am very grateful to my supervisor, Dr. J S Thorp, for his enthusiàstic guidance, advice, encouragement, and every possible help throughout the work and the preparation of this thesis.

Finally, I must thank my wife, Fazilatun Nessa, whose patience, encouragement and support,made it possible for me to undertake this work.

ABSTRACT

Electron spin resonance linewidths of Cr^{3+}, Co^{2+}, Fe^{3+}, Ni^{2+} and Gd^{3+}, doped in single crystal MgO, were examined both experimentally at 9 GHz and theoretically for a range of concentrations (310 ppm to 15100 ppm) over the temperature range from 4.2 K to 293 K. The theoretical dipolar linewidths were 5 to 100 times larger (according to the electronic configuration of the dopant) than the experimental peak-to-peak linewidths for the $\frac{1}{2} \longleftrightarrow -\frac{1}{2}$ transition. These factors were higher for trivalent Cr^{3+}, Fe^{3+}, and Gd^{3+} than for divalent Co^{2+} and Ni^{2+}

The experimental linewidths of Cr^{3+}/MgO and Fe^{3+}/MgO were independent of concentration, which was in marked contrast to the $(\text{concentration})^{\frac{1}{2}}$ variation expected from dipolar theory. The slight increase observed in linewidth of Co^{2+}/MgO with concentration, which was not as much as the $(\text{concentration})^{\frac{1}{2}}$ behaviour, was due to cross-relaxation between Co^{2+} ions.

The linewidth was observed to be independent of polar angle for Cr^{3+}/MgO (from 15 K to 293 K) ; for Co^{2+}/MgO (from 4.2 K to 65 K) and Gd^{3+} (from 4.2 K to 293 K), which was also in contrast to the dipolar theory. Some variation of linewidth with polar angle was seen for Cr^{3+}/MgO (4.2 K to 15 K) and for Ni^{2+}/MgO (20 K to 180 K) but this was not in accordance with the dipolar theory predictions and, on the contrary, confirmed the presence of internal strain in the crystals.

The temperature dependence of linewidths in Co^{2+}/MgO and Ni^{2+}/MgO were observed and in particular the line broadening of Fe^{3+}/MgO and Cr^{3+}/MgO were also examined at liquid helium temperatures. These line broadenings were interpreted as follows : for Fe^{3+}/MgO as due to non-secular line broadening mechanisms (the '10/3' effect) originally

proposed by Anderson and Weiss ; for Cr^{3+}/MgO as arising from the combined effects of strain due to charge misfit of Cr^{3+} and the host cation, and temperature, which causes both exchange striction and departure from the cubic symmetry to a lower symmetry.

For all the dopants (Cr^{3+}, Fe^{3+}, Co^{2+}, Ni^{2+} and Gd^{3+}) in the single crystal MgO, the ratios of moments $M_4^{\frac{1}{4}}/M_2^{\frac{1}{2}}$ derived from the experimental data were greater than 1.33 and the lineshapes were markedly Lorentzian. The data suggested that all the above ions entered the lattice substitutionally, occupying magnesium sites, without disturbing the local symmetry, though the dopants differ in valency and ionic radius from the host cation Mg^{2+} and the linewidths were determined by exchange narrowing over the whole concentration range examined. The exchange energy J and Weiss constant Θ, were calculated from the experimental data and varied linearly with concentration; the exchange energies for the S-state ions were greater than F-state ions. The evaluated exchange energies and Weiss constants compared well with the literature values obtained from independent, different measurements.

Calculations of the predicted dipolar linewidths of trivalent Cr^{3+}, Fe^{3+} and Gd^{3+} in the host lattices of alkaline earth oxides (MgO, CaO and SrO) showed that the dipolar linewidth of a given ion decreases linearly with the increase of the host lattice parameter and that, in a given host lattice, the linewidths are proportional to the electron spin value of the dopant.

The dielectric properties of pure and doped (Ni^{2+} and Co^{2+}) MgO have also been measured in the temperature range 293 K to 100 K, over the frequency range 500 Hz to 30 kHz. The dielectric constant ε' of doped MgO has been found to be slightly higher than undoped MgO. Low

temperature measurements of ε' indicate that Co^{2+}/MgO has the greater temperature dependence of polarizability than pure MgO and Ni^{2+}/MgO. At room temperature, the variation of the real part of the conductivity with frequency over the measured frequency range followed $Re\sigma(\omega) \alpha \omega^{n}$, with $n = 0.86$ for Co^{2+}/MgO and $n = 0.853$ for Ni^{2+}/MgO and undoped MgO. The data fits well with the "Universal dielectric law" $\varepsilon'' \alpha \omega^{n-1}$ $(n<1)$.

CONTENTS

CHAPTER ONE

INTRODUCTION

1.1 THE AIM OF THE WORK

Magnesium oxide is widely used in industry as an insulating material which, because of its refractory nature, can be used at high temperatures ; a common example is as an insulator in heating elements. It has been found that at a rather high temperature (approximately 1100^{o}K) the insulating behaviour of MgO collapses and consequently the material conducts leading to the failure of the heating element. It has been suggested that the diffusion of impurities from the sheath of the element, whose constituents are mainly iron, with some chromium, cobalt and manganese, into the MgO lattice, could be an explanation of this phenomenon, but this argument has not yet been proved. A programme of measurements of the electrical conductivity and dielectric losses in pure and doped magnesia is being undertaken in this department. In the interpretation of these dielectric phenomena it is very helpful to have detailed structural information on the exact location and interactions of the impurity ions. This need led to the present work, which was a chracterisation, using primarily electron spin resonance techniques, of the behaviour of iron, chromium, cobalt and nickel as substitutional dopants in MgO.

Some electron spin resonance (e.s.r.) measurements on doped magnesium oxide have been reported and there are several papers, dealing with magnesium oxide doped with various ions (e.g. Fe^{3+}, Cr^{3+}, Co^{2+}, Ni^{2+} and Gd^{3+}). However, the emphasis of all these has been to determine the parameters of the spin Hamiltonians, the g-factors, zero field splittings and so on. Indeed, almost all the iron group, ions and few rare earth ions, have been studied in the MgO lattice using magnetic resonance as a

technique, but the pattern of the investigations was different from that needed here. The approach required here depended rather on the ability to determine from lineshape analysis the interactions of the individual ions and to this extent followed the earlier work on iron doped magnesia reported by Thorp et al (1.1). In this it was found that exchange effects occur between Fe^{3+} ions in MgO, even at low concentrations in the temperature range from 293K to 77K. These ideas have been extended in order to make an investigation of similar effects in MgO containing both divalent Co^{2+} or Ni^{2+} amd trivalent Fe^{3+}, Cr^{3+} or Gd^{3+} ions over the wider temperature range from 293K to 4.2K. One consequence was that it was possible to compare the exchange energy of divalent and trivalent doped ions in the same lattice (MgO).

These main steps in the present study of doped magnesium oxide are indicated in the following summary :

(i) The theoretical prediction of dipolar linewidth and comparison with experimentally observed linewidths (both as regards lineshapes and magnitude of linewidth) in the temperature range 293K to 4.2K for the various concentrations of Cr^{3+}, Co^{2+}, Fe^{3+}, Ni^{2+} and Gd^{3+} in MgO single crystal host lattices.

(ii) Evaluation of the exchange energy for the above doping ions and a comparison between divalent and trivalent ions in the MgO lattice, to examine whether the Anderson rule (1.2) $J_{trivalent} > J_{divalent}$ held.

(iii) The theoretical prediction of dipolar linewidths of trivalent ions (Fe^{3+}, Cr^{3+} or Gd^{3+}) doped in CaO and SrO single crystal host lattices and comparison with the published results.

In addition to the e.s.r. studies some measurements of dielectric constant ε' of pure MgO and doped MgO (e.g. Co^{2+} or Ni^{2+}) in the temperature range 293K to 100K were made.

1.2 THE MAGNESIUM OXIDE STRUCTURE

The magnesium oxide structure is that of the well known sodium chloride (1.3) of the type MX, where M denotes the metal ion or atom and X an electronegative element, e.g. oxygen in the oxides, or fluorine or chlorine in halides, etc. The lattice is face-centred cubic of space group O_h^5 as indicated by Cornwell (1.4) (the point group O_h and the assignment of superscript by Schonflies is rather arbitrary). Each magnesium atom has a coordination number of six, the neighbours being at the vertices of regular octahedra as shown in Figure 1.1. In this octahedral coordination the ionic radii, according to Shannon and Prewitt (1.5) for Mg^{2+} and O^{2-} are 0.72 Å and 1.40 Å respectively. Wyckoff (1.3) gave the lattice parameter (at 21°C) as a_o = 4.2112 Å. When doping single crystals of MgO with iron group-ions (at low concentrations) it is generally assumed that the dopant enters the lattice substitutionally and that the average lattice parameter (and unit cell symmetry) is not changed.

Historically, several different sets of values of ionic radii have been obtained by investigators using different methods. The most widely accepted values are those of Goldschmidt et al (1926),(1.6), Pauling (1927),(1.7) (often with some later corrections) and Ahrens (1952),(1.8). Although agreement between these three authors is generally good there are some very important discrepancies and taken as a whole the results do not fit certain statistical tests. The most recent, and probably the most accurate estimates of ionic radii, are to be found in a massive compilation of data by Shannon and Prewitt (1969), (1.5) where they took into account both the electronic spin state and the coordination of both cations and anions. Following Shannon and Prewitt, the values of "effective ionic radii" for the doping ions used in this work based on the oxygen value $r\left(\begin{smallmatrix} vl & 2- \\ & O \end{smallmatrix}\right)$ = 1.40 Å have been compiled and these are given, together with the corresponding atomic configurations in Table 1.1.

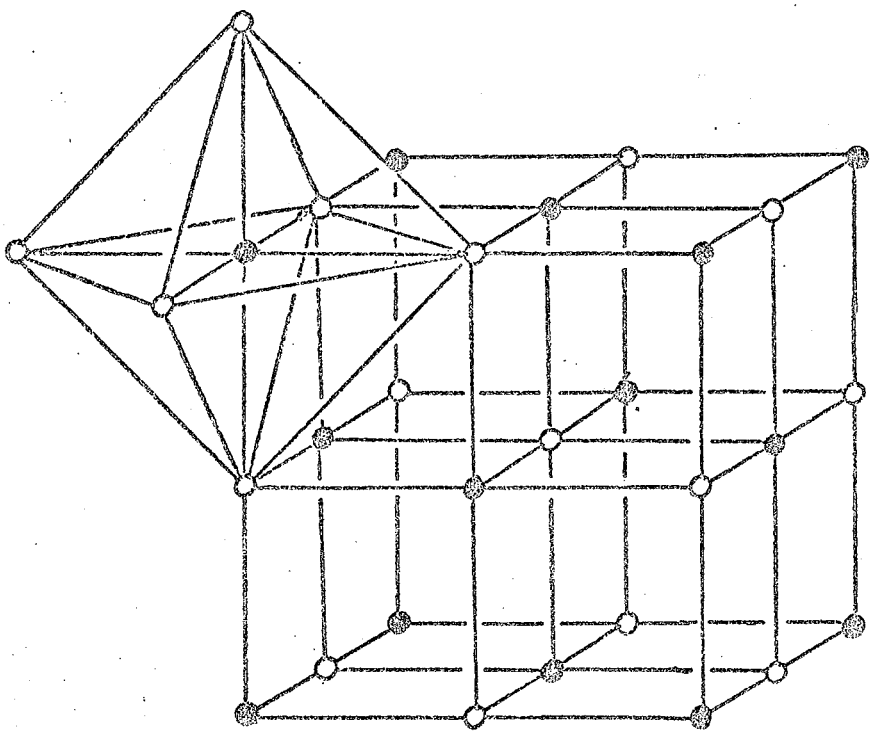

FIGURE 1.1 The structure of MgO
● = magnesium, o = oxygen,
showing octahedral coordination
of the magnesium.

Ion	Effective ionic radii Ref (1.5)	Configuration	Basic Level	Electron Spin	Natural abundance		Nuclear Spin with Reference
					Odd Isotopes	Percentage (%)	
Cr^{3+}	0.615 Å	$3d^3$	$^4F_{3/2}$	$\frac{3}{2}$	53	9.55	$\frac{3}{2}$...(1.9)
Fe^{3+}	0.645 Å	$3d^5$	$^6S_{5/2}$	$\frac{5}{2}$	57	2.25	$\frac{1}{2}$...(1.10)
Co^{2+}	0.735 Å	$3d^7$	$^4F_{9/2}$	$\frac{3}{2}$	59	100	$\frac{7}{2}$...(1.11)
Ni^{2+}	0.70 Å	$3d^8$	$^3F_4$	1	61	1.25	$\frac{3}{2}$...(1.10)
Gd^{3+}	0.938 Å	$4f^7$	$^8S_{7/2}$	$\frac{7}{2}$	155 157	14.7 15.7	$\frac{3}{2}$...(1.12)

TABLE 1.1: Ionic radii and the free ion ground state of some transition ions.

1.3 THE DOPED MAGNESIUM OXIDE CRYSTALS

A selection of single crystals of doped magnesium oxide were purchased from W & C Spicers Ltd (Cheltenham) with the following nominal concentrations in parts per million (ppm) ; all were grown by electrofusion techniques. The concentrations available were as shown below in Table 1.2.

Host	Dopant	Concentration (ppm)	Host	Dopant	Concentration (ppm)
MgO	Cr	800 A	MgO	Co	310 A
		1300 A			1250 A
		3600 X			1900 X
		4200 X			2500 A
		5000 X			3300 X
		6200 X			4800 X
		7400 X			8200 X
		9500 X			9900 X
		15100 X	MgO	Ni	130 A
MgO	Fe	2300 X			370 A
		4300 X			1400 A
MgO	Gd	310 A			

TABLE 1.2 : Composition of single crystals examined.
A = analysed by absorptionmetry.
X = analysed by X-ray methods.

The concentrations in the samples used in this work had been determined by optical spectrographic and X-ray analysis (Johnson Matthey Limited) to an accuracy of about 2%. Neither optical examination nor

X-ray back reflection photographs, used to orient the samples, revealed any evidence of macroscopic cracking, flaws, strain or mosaic formation. This led us to assume that the samples were in good single crystal form. To the eye the chromium doped crystals ranged in colour from light green to dark green, the cobalt containing crystals from clear pink to deep pink, the nickel containing crystals from clear white to pale green, the iron containing crystals were dark green and the gadolinium doped crystal was milky white. All the samples were cleaved from the (100) plane of the respective doped single crystal MgO and they were cut to suit the X-band spectrometer.

REFERENCES

CHAPTER ONE

1.1 J.S.Thorp, R.A.Vasquez, C.Adcock and W.Hutton, J.Mat.Sc. 11 (1976) 89.

1.2 P.W.Anderson, Solid State Physics, 14 (1963) 99.

1.3 R.W.G. Wyckoff, 'Crystal Structures' V-1, Interscience N.Y.(1965).

1.4 J.F.Cornwell, 'Group theory and electronic energy bands in solid ', North Holland, (1969).

1.5 R.D.Shannon and C.T.Prewitt, Acta.Cryst. B25 (1969) 925.

1.6 V.M.Goldschmidt, T.Burth, G.Lande and W.H.Zachariasen, Skr.Norske Vidensk.Akad.1.Mat.Nat. Kl No.2 (1926).

1.7 L.Pauling, J.Amer.Chem.Soc. 49 (1927) 765.

1.8 L.H.Ahrens, Geochim.Cosmochim. Acta. 2(1952) 155.

1.9 B.Bleaney and K.D.Bowers, Proc.Phys.Soc.London A64 (1951) 1135.

1.10 H.H.Woodburg and G.W.Ludwig, Phys.Rev.Letts,1 (1958) 16.

1.11 W.Low, Phys.Rev. 109 (1958) 256.

1.12 W.Low, Phys.Rev. 103 (1955) 1305.

CHAPTER TWO

GENERAL THEORY

In this chapter the basic terms and equations (which are needed to identify and analyse the e.s.r. spectra) have been introduced. These are spin Hamiltonians, different linewidth mechanisms, lineshape factors and moment ratios.

GENERAL THEORY

2.1 THE SPIN HAMILTONIAN

Paramagnetic resonance is concerned with the investigation of the lowest energy levels of paramagnetic ions. In general, a paramagnetic resonance (i.e. electron spin resonance (e.s.r.)) spectrum is rather complex, with lines due to different electronic transitions which may be further divided into subgroups of lines by interaction with a nuclear moment. Fortunately, the e.s.r. data can be described in a fairly simple way without detailed knowledge of all interactions. This is mainly because the paramagnetic entity is present in a crystalline environment and consequently the crystalline electric field is invariant under the operations of the symmetry group to which crystals belong. A Hamiltonian can be written which represents the magnetic behaviour of the ground state spin system only, since it contains polynomials in the electronic spin it is referred to as a spin Hamiltonian. According to the definition given by Low (2.1), the spin Hamiltonian is a convenient shorthand representation of the experimental results in which the measured splitting related to g-values, fine structure and hyperfine structure parameters, etc.enter as energy terms. There are numerous special forms of this spin Hamiltonian appropriate in cubic, tetragonal and lower symmetry crystals and these are fully described in several text books (e.g. Abragam and Bleaney (1970) (2.2), Wertz and Bolton (1972) (2.3)).

Here a few specific examples will be given of materials relevant to the present work. The spin Hamiltonian H_s for Cr^{3+} in the cubic lattice of single crystal MgO is given by Low in 1957 (2.4) as

$$H_s = g \beta \bar{H}.\bar{S} + A \bar{I}.\bar{S} \qquad (2.1)$$

which gives transitions at

$$h\nu = g\,\beta\,H - A\,M_I + \left(\frac{A^2}{2H}\right)\left[I(I+1) - M_I^2 + M_I(2M_s - 1)\right] \qquad (2.2)$$

where

g = Spectroscopic splitting factor

H = Applied magnetic field

β = Bohr magneton

A = Hyperfine structure constant

$\bar{I}$ = Nuclear spin

S = Electronic spin

M_I = Nuclear spin quantum number

M_s = Electronic spin quantum number

h = Planck constant

ν = Resonance frequency

Figure 2.1 shows the energy levels of the ground state in a zero magnetic field where the dotted lines indicate the energy levels of the even isotopes of chromium. Cr^{3+} has $S = \frac{3}{2}$. At high magnetic field the four energy levels diverge linearly, and the three transitions coincide at $h\nu = g\,\beta\,H$ so the theory predicts an intense singlet at $h\nu = g\,\beta\,H$ due to the even isotopes of Cr^{3+} and a less intense quartet, centred on $h\nu = g\,\beta\,H$, with separation A, due to the isotope ^{53}Cr (9.5% abundance) with $I = \frac{3}{2}$. In high magnetic fields the transitions $\Delta M_s = \pm 1$ & $\Delta M_I = 0$ are allowed and for the effective spin $S' = \frac{1}{2}$, the resonance lines can be assigned as (for H >> A as is usually the case)

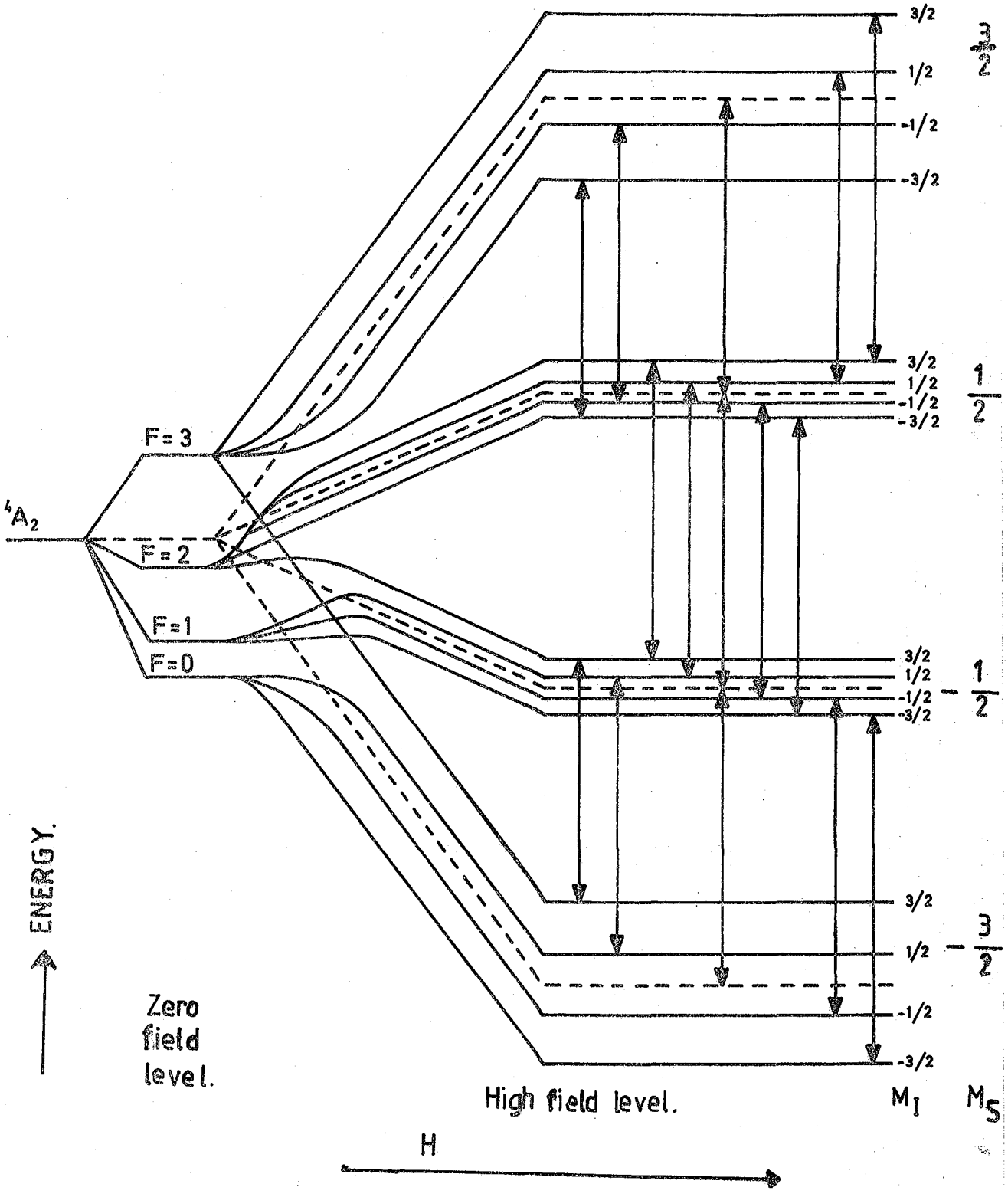

FIG.2.1 Schematic energy level diagram for MgO: Cr. Even isotopes are represented by dotted lines, ^{53}Cr with I =3/2 by solid lines. Observed transitions shown by arrows [Low. 1957(24)].

For $M_I = \frac{3}{2}$ $h\nu = g\beta H - \frac{3}{2}A$

$M_I = \frac{1}{2}$ $h\nu = g\beta H - \frac{1}{2}A$

$M_s = \pm\frac{1}{2}$ $h\nu = g\beta H$ (2.3)

$M_I = -\frac{1}{2}$ $h\nu = g\beta H + \frac{1}{2}A$

$M_I = -\frac{3}{2}$ $h\nu = g\beta H + \frac{3}{2}A$

The spin Hamiltonian for Co^{2+} in the cubic crystalline field of MgO will also contain the hyperfine term, because the only natural isotope of cobalt is ^{59}Co (100% abundance) which has a nuclear spin $I = {}^{7}/_{2}$, and the following spin Hamiltonian ($S' - \frac{1}{2}$) is appropriate

$$H_s = g\beta\ \bar{H} \cdot \bar{S} + A\,\bar{I} \cdot \bar{S} \qquad (2.4)$$

The expected spectrum of Co^{2+}/MgO as an Octet of separation A cm^{-1}, is illustrated in Figure 2.2.

Ni^{2+} has 8 d-electrons and the ground state is $^3F_4$. In an octahedral field the orbital F-state splits into two threefold levels the same as d^3 (Cr^{3+} etc) with the singlet A_2 lowest as shown in Figure 2.3. The principal difference between $3d^3$ (Cr^{3+}, $S = \frac{3}{2}$) and $3d^8$ (Ni^{2+}, $S = 1$) ions arise from spin multiplicity. Since there is no excited state close to the ground state, e.s.r. spectra of the Ni^{2+} ion can be seen at room temperature or at 77 K. The appropriate spin Hamiltonian of Ni^{2+} in the cubic crystalline field of MgO is (on neglecting the hyperfine

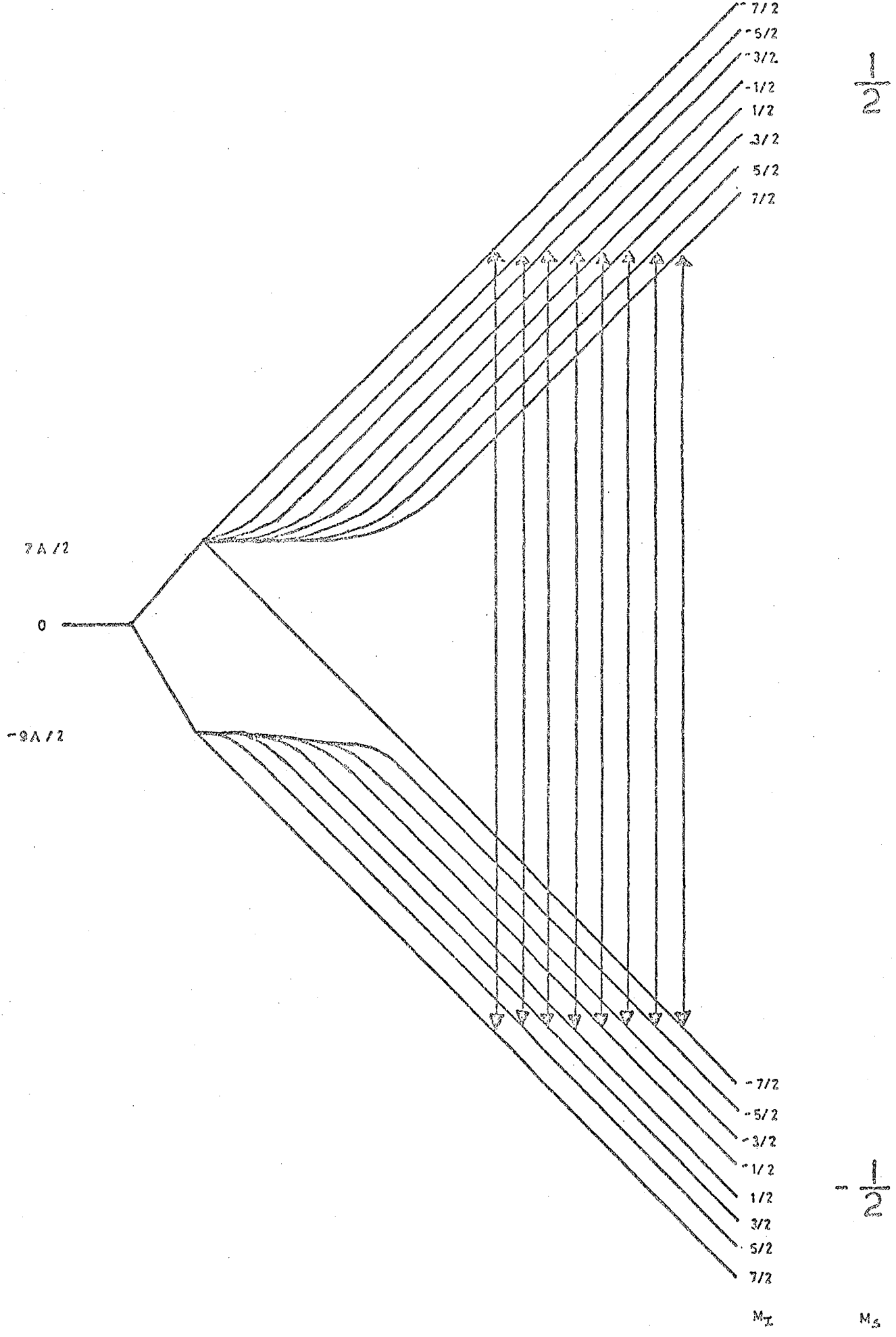

FIGURE 2.2 The electronic and nuclear Zeeman levels of Co^{2+} showing the eight transitions observed in e.s.r. [Low. 1958(2.12b)]

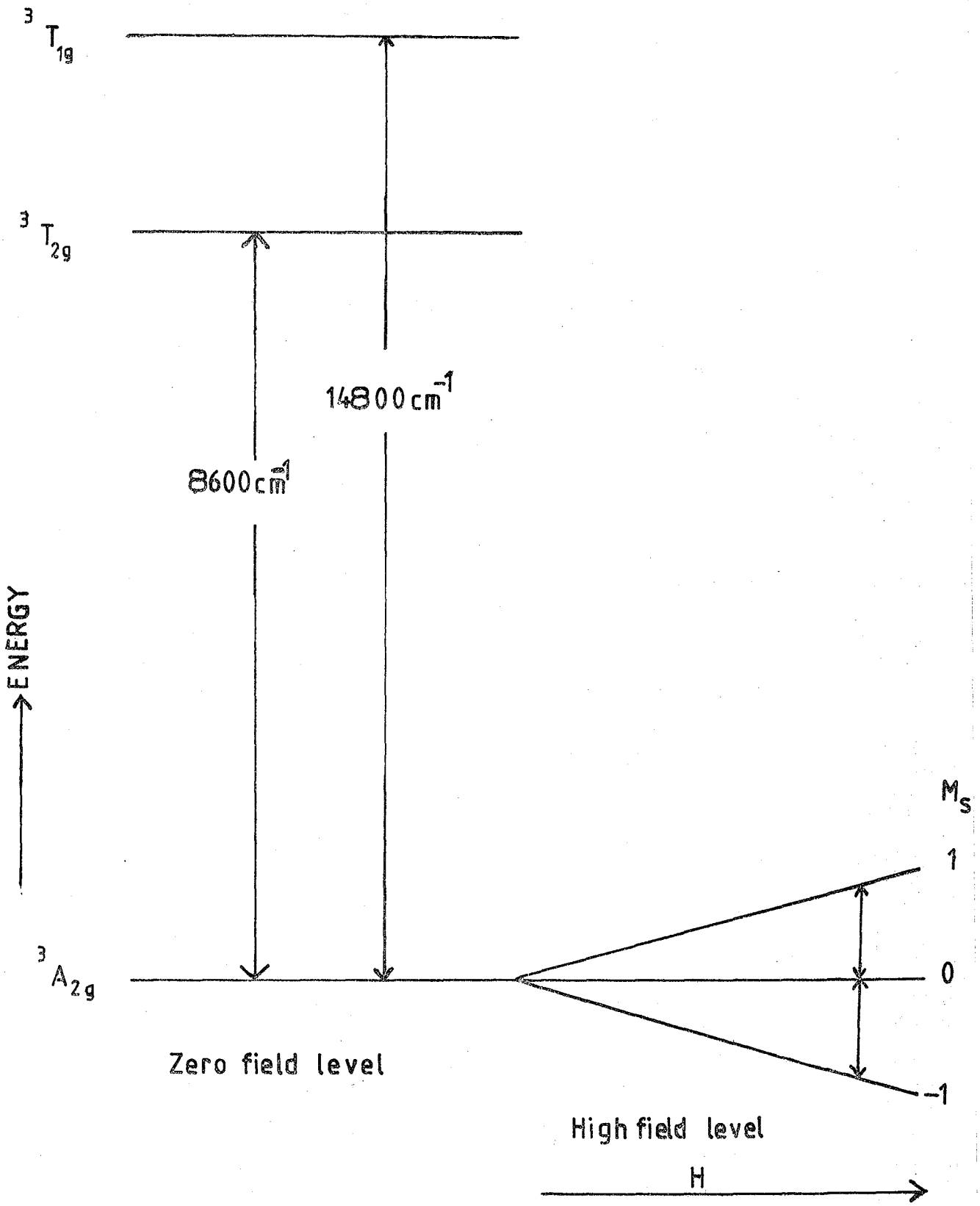

FIG, 2, 3 ENERGY LEVELS OF Ni^{2+} IN MgO [Low, 1958 (2, 12a)]

term due to the odd isotope ^{61}Ni, 1.25% abundance, $I = \frac{3}{2}$)

$$H_s = g \beta \bar{H}.\bar{S} \qquad (2.5)$$

where the transitions due to $|-1\rangle \longleftrightarrow |0\rangle$ and $|0\rangle \longleftrightarrow |+1\rangle$ are superimposed at $h\nu = g \beta H$, in the high magnetic field.

The trivalent gadolinium ion has seven unpaired electrons in the 4f unfilled shell which make it half-filled and give rise to a ground state $4f^7, {}^8S_{7/2}$. It has been reported in the reference (2.2) that for this ion the only non-zero interaction in a magnetic resonance experiment would be the Zeeman interaction

$$H_s = g \beta \bar{H}.\bar{S} \qquad (2.6)$$

2.2 LINE BROADENING MECHANISMS

There are two parameters associated with an e.s.r. line. First, the g value, which gives the actual resonance position of the line ; second, the linewidth, which gives the absorption condition of the resonance. Linewidth is determined directly by the energy spread of the levels occupied by the unpaired electrons in question. Hence a measurement of the linewidth will give information on the actual interactions which the unpaired electron is experiencing and which cause its energy to be spread out. There are two principal types of line, namely (a) homogeneously broadened lines and (b) inhomogeneously broadened lines. The distinction between these two types of broadened line in e.s.r. was first clarified by Portis (2.5). Homogeneous broadening occurs when the energy absorbed from the radiation field is distributed to all the spins, so that thermal equilibrium of the spin system is maintained throughout the paramagnetic resonance. Several sources of homogeneous broadening are :

(a) Dipolar interactions between like spins

(b) Exchange interactions

(c) Spin lattice relaxation

(d) Interaction of spins with radiation field

(e) Motion of unpaired spins in the microwave field

(f) Diffusion of excitation throughout the sample

An inhomogeneously broadened line is one which consists of a spectral distribution of individual resonance lines merged into one overall line or envelope, as shown in Figure 2.4. Sources of inhomogeneous broadening include :

(a) Unresolved fine and hyperfine structure

(b) Dipolar interaction between unlike spins, i.e. spins with different Larmor frequencies

(c) Anisotropy of the splitting energy levels

(d) Inhomogeneties in the applied d.c. magnetic field

(e) Mosaic structure (i.e. crystal lattice irregularities)

(f) Internal strain (due to point defects, charge effects and dislocations).

The inhomogeneous broadening must come from interaction outside the spin system and must be slowly varying over the time required for a spin transition. A general review of the various theories of linewidths is given by Van Vleck in 1957 (2.6).

2.2.1 Dipolar Broadening

(a) General Expressions

If two neighbouring paramagnetic centres are located at a distance r from one another, each Zeeman energy level is broadened by the value $\sim h/\beta^2 r^{-3}$ as a result of the dipole interaction. This type of broadening

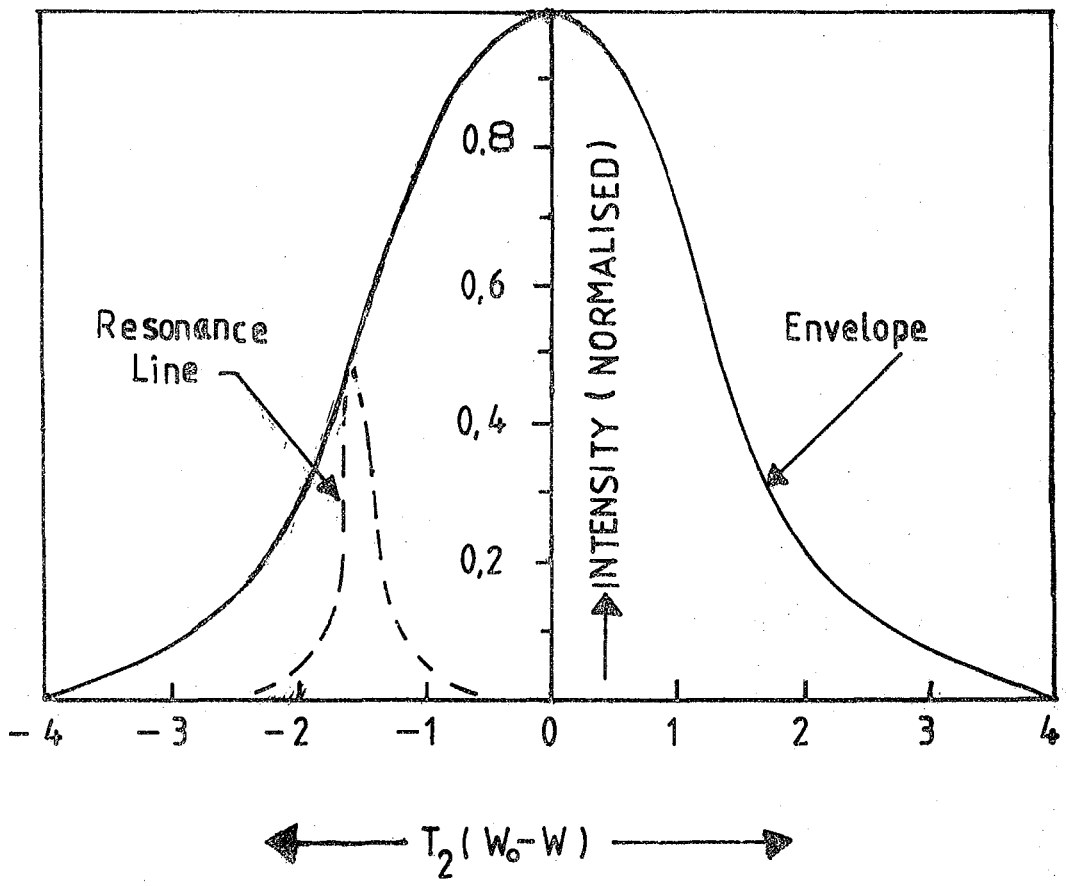

FIG, 2,4 ABSORPTION ENVELOPE AND ONE OF ITS INDIVIDUAL RESONANCE LINE. [Portis 1953,(2,5)].

is treated in detail by Van Vleck in his early paper (2.7) and in a more concise form in his review article (2.6). Considering the dynamic interaction of dipoles, he proposed the Hamiltonian for the dipolar interaction between ions as

$$H_{dip} = \sum_{k>j} g^2 \beta^2 r_{jk}^{-3} \left[\bar{S}_j . \bar{S}_k - \frac{3\left(\bar{S}_j . \bar{r}_{jk}\right)\left(\bar{S}_k . \bar{r}_{jk}\right)}{r_{jk}^2} \right] \quad (2.7)$$

where g is the Lande g factor, β is the Bohr magneton, S stands for spin and r_{jk} is the radius vector from the reference atom j to all the neighbouring atoms labelled over k. The second term of Equation 2.17 is strongly dependent om the orientation of the d.c. magnetic field relative to the crystallographic axis. The result of the simultaneous interaction of many spins, produces a Gaussian shaped resonance line and the difficulty of its analysis was overcome by Van Vleck, using the method of moments. He found that, for like atoms, the second moments $\langle \Delta\omega^2 \rangle$, can be written

$$\langle \Delta\omega^2 \rangle = \frac{3}{4} S(S+1) \left(\frac{g^2 \beta^2}{\hbar} \right)^2 .n. \sum_k \left[r_{jk}^{-6} \left(3 \cos^2 \theta_{jk} - 1 \right)^2 \right] \quad (2.8)$$

where ω is measured in radians per second, n is the concentration of interacting atoms, and θ_{jk} is the angle between the radius vector and a crystallographic reference axis.

For unlike atoms this equation becomes

$$\langle \Delta\omega^2 \rangle = \frac{1}{3} S(S+1) \left(g g' \beta^2 / \hbar \right)^2 .n. \sum_k \left[r_{jk}^{-6} \left(3 \cos^2 \theta_{jk} - 1 \right)^2 \right] \quad (2.9)$$

where g refers to the reference atom ; g' refers to the surrounding atoms. The term between brackets [ ] is a pure geometrical factor, i.e. dependent on the crystal structure, and can be evaluated using spherical harmonies, $Y_{\ell m}$, following the procedure by Brown et al (2.8).

The second moment of the linewidth caused by dipolar interaction in MgO lattice has been shown by Thorp et al (2.9) to be

(i) For like atoms,

$$\langle \Delta\omega^2 \rangle = \frac{3}{4} S (S+1) \left(\frac{g^2 \beta^2}{\hbar} \right)^2 .n. \left[\frac{4}{5} \sum_k \left(r_{jk}^{-6} \right) + \frac{32\pi}{35} Y^*_{4,0} \left(\theta_H, \phi_H \right) \sum_k r_{jk}^{-6} \; Y_{4,0} \left(\theta_k, \phi_k \right) + \frac{64\pi}{35} Y^*_{4,4} \left(\theta_H, \phi_H \right) \sum_k r_{jk}^{-6} \; Y_{4,4} \left(\theta_k, \phi_k \right) \right] \qquad (2.10)$$

and

(ii) For unlike atoms,

$$\langle \Delta\omega^2 \rangle = \frac{1}{3} S (S+1) \left(\frac{g\, g' \beta^2}{\hbar} \right)^2 .n. \left[\frac{4}{5} \sum_k \left(r_{jk}^{-6} \right) + \frac{32\pi}{35} Y^*_{4,0} \left(\theta_H, \phi_H \right) \sum_k r_{jk}^{-6} \; Y_{4,0} \left(\theta_k, \phi_k \right) + \frac{64\pi}{35} Y^*_{4,4} \left(\theta_H, \phi_H \right) \sum_k r_{jk}^{-6} \; Y_{4,4} \left(\theta_k, \phi_k \right) \right] \qquad (2.11)$$

where θ_k, ϕ_k refer the radius vector to the crystal axes while θ_H and ϕ_H

refer the radius vector to the crystal axes while Θ_H and ϕ_H refer the static magnetic field to the same axes. The standard forms of spherical harmonics are well known (2.10) and are specified completely by Θ and ϕ. The numerical factor $3/4$ in the equation for like atoms (and $\frac{1}{3}$ in the equation for unlike atoms) shows that like atoms produce a mean square broadening which is $9/4$ times greater than that produced by unlike atoms. The reason for this is that the resonances of like atoms do overlap and thus enhance the mutual coupling.

The total dipolar broadening is given by the square root of the sum of the second moments of the individual dipolar interactions. This must be converted into a peak-to-peak derivative linewidth, ΔH_{ms}, for comparison with experimental results. This is done using the equation

$$\Delta H_{ms} = \frac{\sqrt{<\Delta\omega^2>}}{\pi} \cdot \frac{\partial H}{\partial \nu} \text{ Tesla} \qquad (2.12)$$

where the parameter $\frac{\partial H}{\partial \nu}$ is obtained from the relation $\frac{\partial H}{\partial \nu} = \frac{h}{g\beta}$.

It has been shown by Vasquez (2.11) that the dipolar interaction between unlike atoms in the MgO lattice (i.e. between dopant and Mg^{2+} ; dopant and O^{2-}) gives a negligible contribution to the broadening of the lines.

(b) Particular Cases

For interactions between dopants, one needs the equation for dipolar broadening between like atoms. For Cr^{3+}, $S = \frac{3}{2}$ and the g value in the MgO lattice is 1.98 (2.4). The atomic part of the equation 2.10 can be evaluated as

$$\frac{3}{4} S(S+1) \left(\frac{g^2\beta^2}{\hbar}\right)^2 .n. = 2.8757 \times 10^{-25} .n. \left(\text{rad.sec}^{-1}\right)^2 \text{cm}^6 \qquad (2.13)$$

Using Table -11 of reference (2.9), the geometrical part of the equation can be partially evaluated leading to the final equation of second moment of like atoms for Cr^{3+}/MgO crystals as

$$\langle\Delta\omega^2\rangle_{Cr^{3+}/MgO} = 2.8757 \times 10^{20} .n.\left[15.9814-5.175\ Y^*_{4,0}(\theta_H,\phi_H) -6.218\ Y^*_{4,4}(\theta_H,\phi_H)\right] \quad (2.14)$$

For Co^{2+}, $S = \frac{3}{2}$ and g value in MgO lattice is 4.278 (2.12(b)) and the second moment of like atoms for Co^{2+}/MgO crystals is

$$\langle\Delta\omega^2\rangle_{Co^{2+}/MgO} = 6.264 \times 10^{21}.n.\left[15.9184-5.175\ Y^*_{4,0}(\theta_H,\phi_H) -6.218\ Y^*_{4,4}(\theta_H,\phi_H)\right] \quad (2.15)$$

Similarly for Ni^{2+}, S = 1 and the g value in the MgO lattice is 2.2145 (2.13) and for Gd^{3+}, S = 7/2, the g value in MgO lattice is 1.992 (2.14) ; therefore, the second moments of these ions in the MgO lattice are respectively

$$\langle\Delta\omega^2\rangle_{Ni^{2+}/MgO} = 2.3989 \times 10^{20}.n.\left[15.9184-5.175\ Y^*_{4,0}(\theta_H,\phi_H) -6.218\ Y^*_{4,4}(\theta_H,\phi_H)\right] \quad (2.16)$$

and

$$\langle\Delta\omega^2\rangle_{Gd^{3+}/MgO} = 1.2073 \times 10^{21}.n.\left[15.984-5.175\ Y^*_{4,0}(\theta_H,\phi_H) -6.218\ Y^*_{4,4}(\theta_H,\phi_H)\right] \quad (2.17)$$

For $\phi_H = 0^o$, (which corresponds to most of the experimental work) all the above equations 2.14 to 2.17 are totally real and by substituting values of n and θ_H corresponding to the experimental ones, curves of dipolar broadening as a function of polar angle, θ_H, can be drawn. Using the transformation equation 2.12, ΔH_{ms} can be calculated and compared with experimental values.

The exact shape of the dipolar broadened lines has been considered by Swarup (2.15) who concluded that in the absence of exchange effects, crystalline fields or quadrupole moments, the shape of the resonance line due to pure dipolar interaction between the spins is Gaussian. For example, it can be mentioned that Grant et al in Cr^{3+}/Al_2O_3 (2.16), Brown et al in $Nd^{3+}/CaWO_4$ (2.8), Thorp et al in $Gd^{3+}/CaWO_4$ (2.17) and in $Cr/Ti/Al_2O_3$ (2.18) all found dipolar broadening.

2.2.2 Exchange Narrowing

The phenomenon of exchange narrowing was first suggested as a possibility by Gorter and Van Vleck (2.19) and was demonstrated mathematically by Van Vleck (2.7). These authors pointed out that in most pure salts the exchange interaction cannot broaden the paramagnetic resonance line because it commutes with the components of the total magnetic moment and therefore has no direct effect on either the Zeeman energy or the radiating dipole moment. On the other hand, exchange cacause rapid motion in the spin system, which can result in averaging out the effects of the broadening interactions such as magnetic dipolar interactions, thus narrowing the line. Dirac (2.20) showed that the exchange interaction, which depends on the mutual orientation of the spins, can be described approximately by the following interaction Hamiltonian

$$H_{exch} = -2 \sum_{j>k} J_{jk} (\bar{S}_j . \bar{S}_k) \qquad (2.18)$$

where the exchange integral J decreases very rapidly with distance and is negligible in dilute crystals. In concentrated crystals, one can approximate equation 2.28 because of the strong interaction between the nearest neighbours. In this case, the interaction is the scalar product $-2J\Sigma(S_j.S_k)$ summed over the nearest neighbours only. This form of interaction is isotropic in contrast to the dipolar interaction which is a second-rank tensor. The effect of exchange interaction is electrostatic in origin and is connected with the overlap of the orbital wave functions and with the type of symmetry in the representation of the permutation group. Van Vleck's (2.7) mathematical analysis shows that for identical spins and $S' = \frac{1}{2}$, the isotropic exchange interaction contributes to the fourth moment and not to the second moment. Since the total area of the line cannot change, the effect is that the centre part of the line is narrowed, the tails broadened and the shape approximates to a Lorentzian. This peaking of the line shape (as shown in Figure 2.5) is called Exchange Narrowing.

The problem of the exact shape of an exchange narrowed line has been considered by Anderson and Weiss in 1953 (2.21), who used a mathematical model to obtain the shape factor. They predict that for an exchange narrowed line, the absorption line-half width, $\Delta\omega$, at half-height in frequency units (i.e. $\Delta\omega = \frac{2\pi g\beta}{h} \cdot \frac{1}{2} \Delta H_{\frac{1}{2}}$, where $\Delta H_{\frac{1}{2}}$ is the full-width at half intensity) can be related to the exchange energy by

$$\Delta\omega \simeq \frac{\langle \Delta\omega^2 \rangle \text{ dipolar}}{(J/\hbar)} \qquad (2.19)$$

where $\langle \Delta\omega^2 \rangle$ is the second moment of dipole-dipole interaction (which has been discussed in Section 2.2.1) and $(J/\hbar)$ is the exchange energy in frequency units. They estimated the exchange energy from the Curie-Weiss

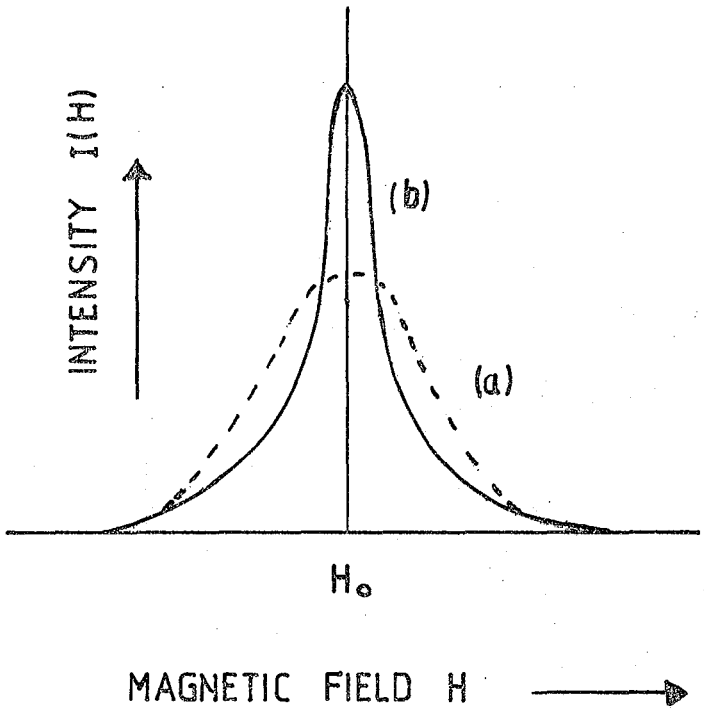

FIG, 2, 5 ABSORPTION LINESHAPES (a) WITHOUT AND (b) WITH EXCHANGE INTERACTION. [Van Vleck (2, 6)]

law $\chi = \frac{C}{T + \theta}$; here θ is obtained from the Weiss-molecular field equation

$$3K\theta = 2J\ z\ S(S + 1) \qquad (2.20)$$

in which z is the number of nearest neighbours and K is the Boltzmann constant. In the first place, Anderson and Weiss found that the value of exchange energy obtained by means of equations 2.19 and 2.20, from the experimental linewidths did not agree at all well with those obtained from the Curie temperature ; their second conclusion was that much better agreement was achieved if the '10/3' correction was introduced. This proposed '10/3' effect in exchange narrowed lines has been examined in theoretical detail by Kubo and Tomita in 1954 (2.22), who showed that the '10/3' effect will be present when the Zeeman frequency is comparable to the frequency of exchange interaction. In this region a frequency dependence of the width is generally to be expected.

2.2.3 Other Broadening Mechanisms

So far two sources of homogeneous line broadening (dipolar and exchange narrowing) have been mentioned. Other homogeneous sources of line broadening include, spin lattice relaxation and spin-diffusion. Spin lattice relaxation mechanisms produce an equilibrium population of the Zeeman states and effectively broaden the resonance line. On the other hand spin diffusion corresponds to a spatial propagation of spin magnetization through the simultaneous flipping of nearby spins and this broadens the line.

The inhomogeneity of the resonance line width may be caused by small variations in zero field splittings. Small differences in D may result from three causes (2.1) :

(a) Defects and dislocations in the neighbourhood of the magnetic ions,

(b) Thermal vibrations of the surroundings.

(c) Twinning and mosaic structure of the crystal.

Unresolved hyperfine structure and hyperfine interaction with the surrounding diamagnetic nuclei by means of covalent bonding, may also produce inhomogeneous broadening. If the inhomogeneity of the magnetic field over the sample volume exceeds the natural linewidth, then the spins in various parts of the sample will find themselves in different field strengths and the resonance will be artificially broadened in an inhomogeneous manner.

2.3 CHARACTERISTICS OF SPECTRAL LINESHAPES

2.3.1 General Equations

A great deal of information can be obtained from an analysis of the width and shape of a resonant absorption line. Two mathematical functions are commonly used to represent the shapes of spectral lines, namely the Lorentzian and the Gaussian. The analytical expression for a Lorentzian absorption lineshape as a function of the magnetic field strength is described by Poole (2.23) as

$$Y^{L}_{(H)} = \frac{y_m}{1 + \left(\frac{H - H_o}{\frac{1}{2}\Delta H_{\frac{1}{2}}} \right)^2} \tag{2.21}$$

and the corresponding expression for a Gaussian line is

$$Y^{G}_{(H)} = y_m \exp\left[- 0.693 \left(\frac{H - H_o}{\frac{1}{2}\Delta H_{\frac{1}{2}}} \right)^2 \right] \tag{2.22}$$

where y_m denotes the maximum amplitude, obtained in both cases at the

centre of the line, where $H = H_o$. The quantity $\Delta H_{\frac{1}{2}}$ is the full line-width between half-amplitude points as shown in Figure 2.6. In field modulation spectrometers (such as used in these experiments) one ordinarily detects the first derivative counterparts of equations 2.21 and 2.22. These have the forms

$$Y'^{L}_{(H)} = \frac{16\, y'_m \left(\frac{H - H_o}{\frac{1}{2}\Delta H_{ms}}\right)}{\left\{3 + \left(\frac{H - H_o}{\frac{1}{2}\Delta H_{ms}}\right)^2\right\}^2} \qquad (2.23)$$

and

$$Y'^{G}_{(H)} = 1.6487\, y'_m \left(\frac{H - H_o}{\frac{1}{2}\Delta H_{ms}}\right) \exp\left[-\frac{1}{2}\left(\frac{H - H_o}{\frac{1}{2}\Delta H_{ms}}\right)^2\right] \qquad (2.24)$$

where $1.6487 = e^{\frac{1}{2}}$, and the quantities y'_m and ΔH_{ms} are the derivative half amplitude and the peak-to-peak line width respectively, as shown in Figure 2.7.

2.3.2. Lineshape Factor

For a Gaussian line amplitude y'_m has the explicit form

$$y'^{G}_{m} = \frac{y_m}{\frac{1}{2}\Delta H_{ms}\, e^{\frac{1}{2}}} \qquad (2.25)$$

and the peak-to-peak linewidth ΔH_{ms} is related to the half-amplitude

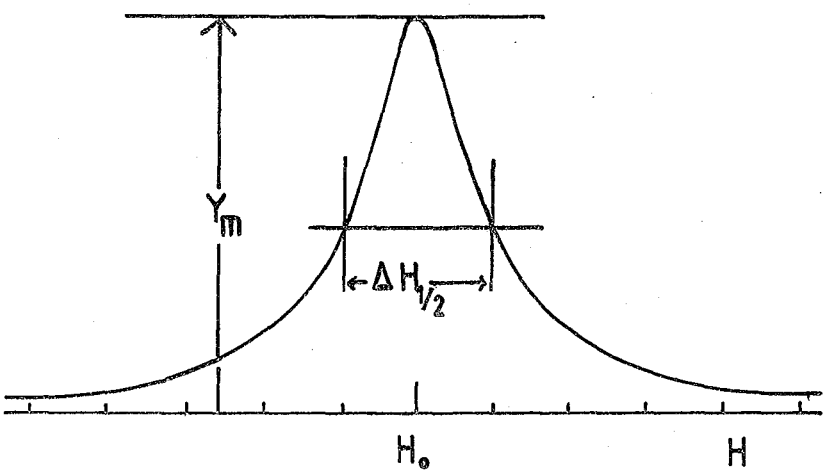

(a)

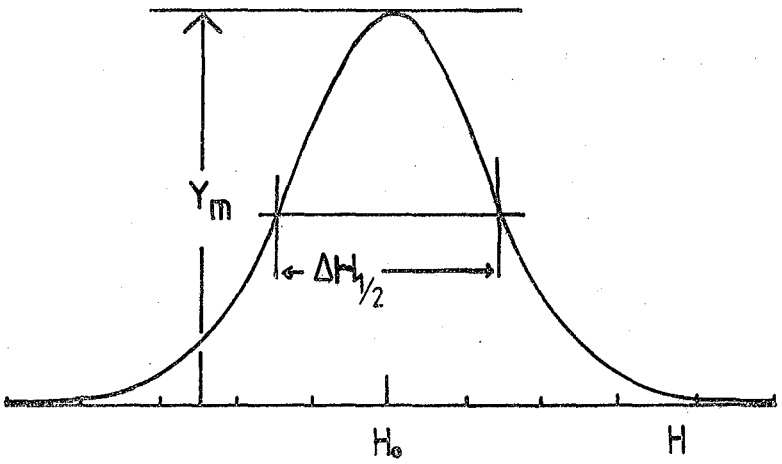

(b)

FIG, 2, 6 ABSORPTION LINESHAPES

(a) LORENTZIAN AND (b) GAUSSIAN.

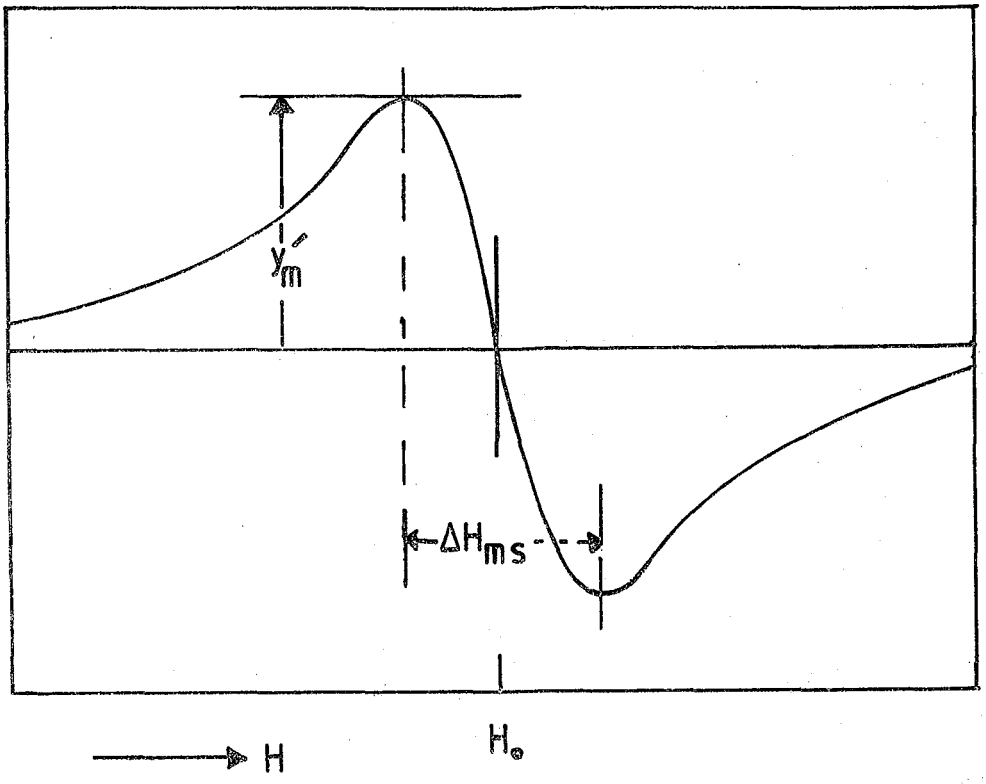

(a)

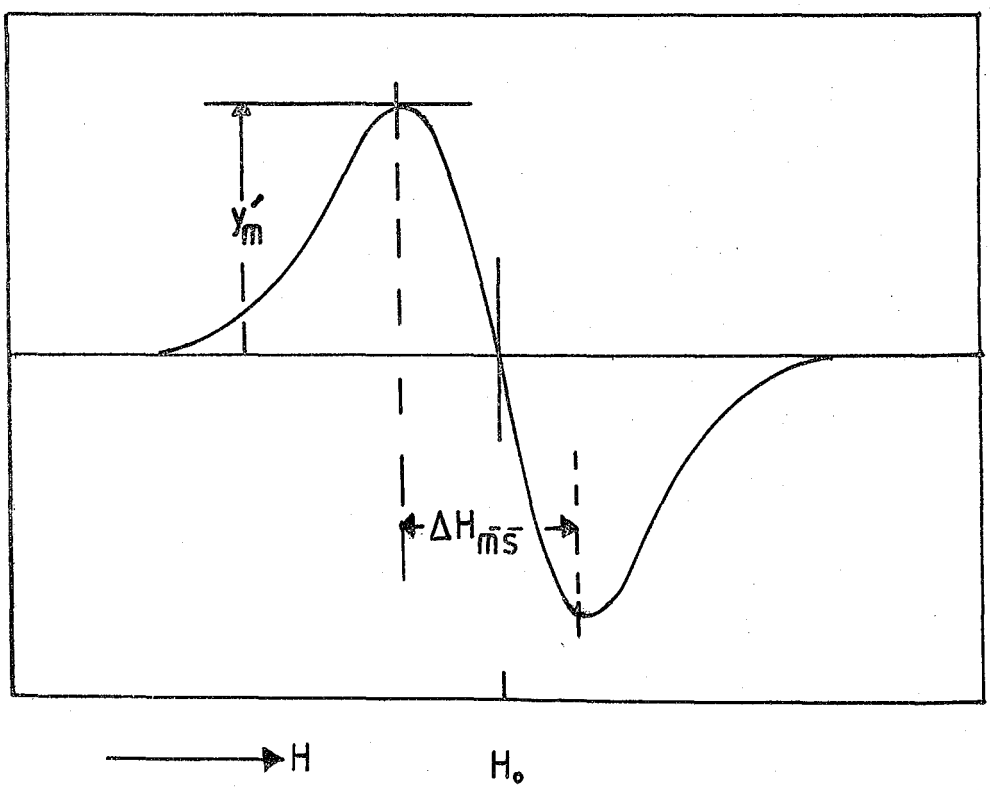

(b)

FIG. 2,7 DERIVATIVE LINESHAPES (a) LORENTZIAN AND (b) GAUSSIAN.

linewidth $\Delta H_{\frac{1}{2}}$ in the following manner :

$$\Delta H^{G}_{\frac{1}{2}} = (2 \ln 2)^{\frac{1}{2}} . \Delta H^{G}_{ms} = 1.1776 \Delta H^{G}_{ms} \qquad (2.26)$$

The corresponding expressions for the Lorentzian case are

$$y'^{L}_{m} = \frac{3}{4} y_{m} (\Delta H_{ms})^{-1} \qquad (2.27)$$

and

$$\Delta H^{L}_{\frac{1}{2}} = 3^{\frac{1}{2}} . \Delta H^{L}_{ms} = 1.7321 \Delta H^{L}_{ms} \qquad (2.28)$$

The Lorentzian shape is slightly sharper in the centre and decreases much more slowly in the wings beyond the half-amplitude or first derivative points. The two shape functions may be compared in the manner shown in Figure 2.8, where the two absorption curves are drawn with the same half-amplitude linewidths $\Delta H_{\frac{1}{2}}$, and two first derivative curves are plotted with the same peak-to-peak linewidths ΔH_{ms}. Figure 2.9 shows the dramatic difference between the two lineshapes when the absorption curves are matched at their inflection points and when the first derivative curves are matched at the half-amplitude points. The ratio $\Delta H_{ms} / \Delta H_{\frac{1}{2}}$ is defined as the 'lineshape factor'. From equation 2.26 this factor for a Gaussian line is 0.846, i.e.

$$\frac{\Delta H^{G}_{ms}}{\Delta H^{G}_{\frac{1}{2}}} = 0.846 \qquad (2.29)$$

and from equation 2.28, for a Lorentzian line

$$\frac{\Delta H^{L}_{ms}}{\Delta H^{L}_{\frac{1}{2}}} = 0.577 \qquad (2.30)$$

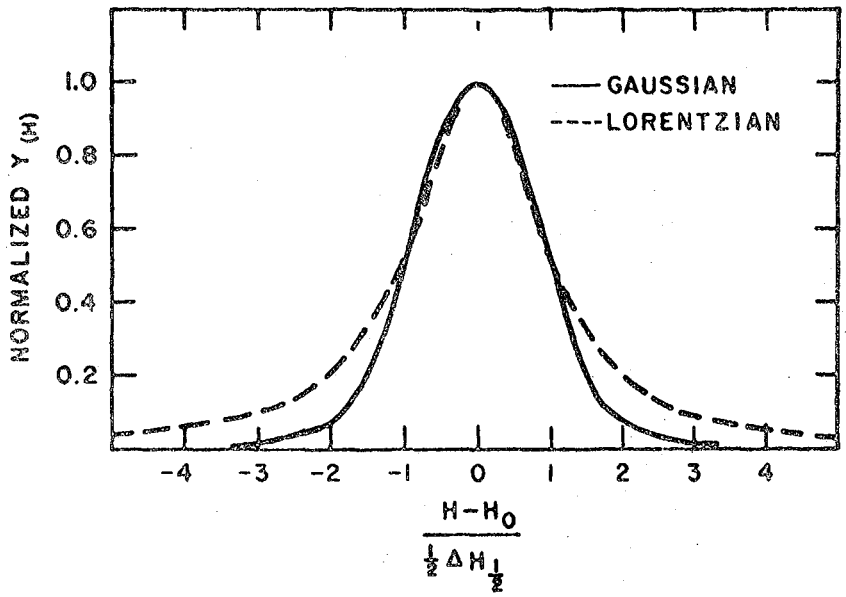

(a)

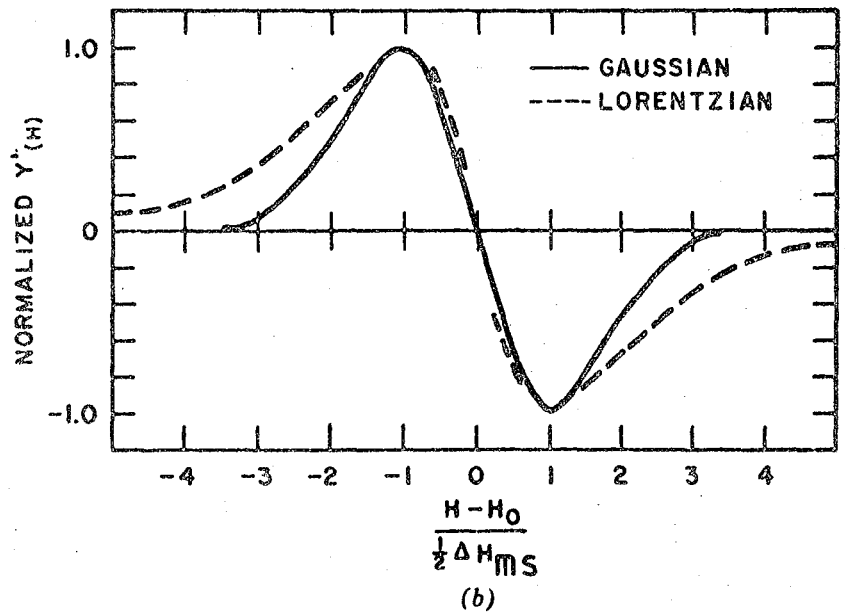

(b)

Fig. 2,8 (*a*) Lorentzian and Gaussian absorption curves with the same half amplitude line-width. (*b*) Lorentzian and Gaussian absorption first derivative curves with the same peak-to-peak line-width.

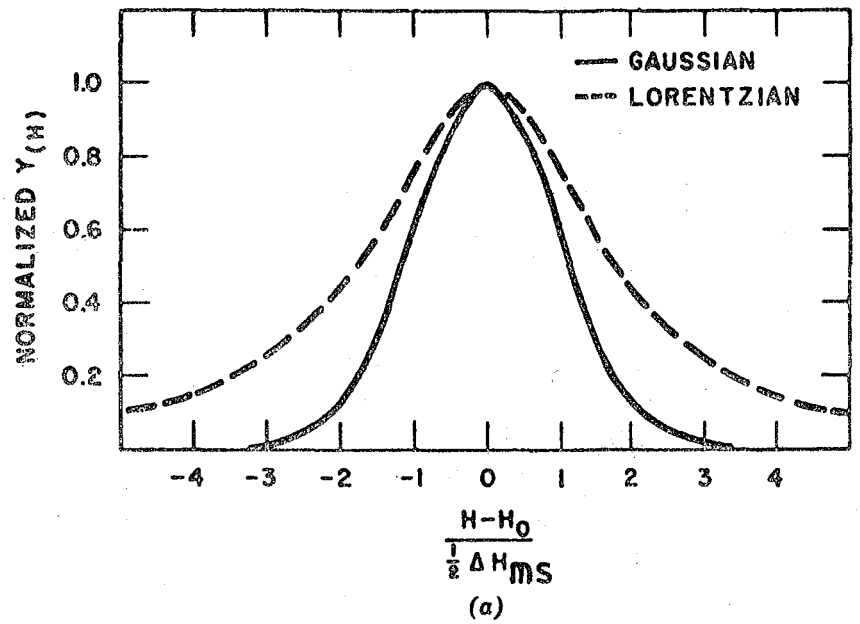

(a)

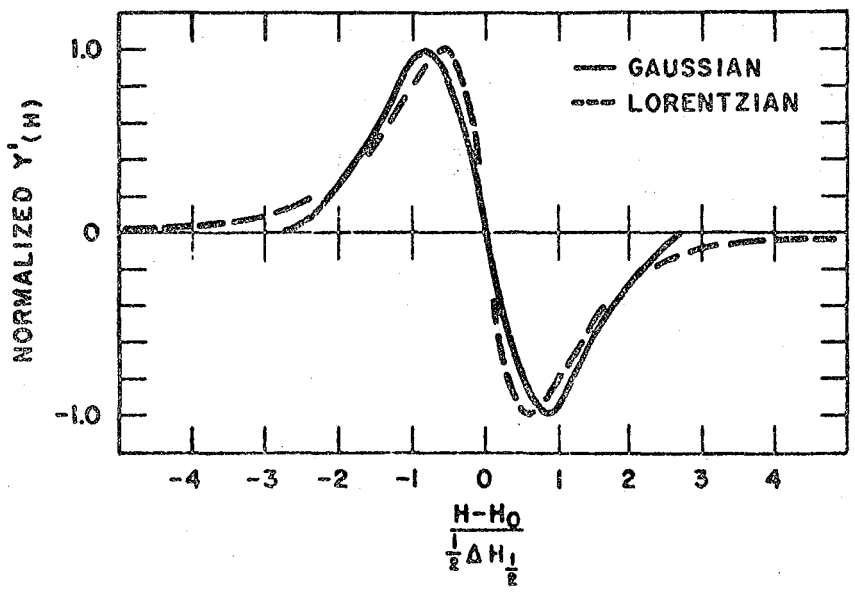

(b)

Fig. 2, 9 (*a*) Lorentzian and Gaussian absorption curves with the same peak-to-peak line-width. ΔH_{ms} (*b*) Lorentzian and Gaussian absorption first derivative curves with the same half amplitude line-width $\Delta H_{1/2}$.

By knowing the 'shape factor' one can estimate the lineshapes and consequently the sources of line broadening. The shape of the inhomogeneously broadened line has been predicted by Stoneham in 1969 (2.24). His results are summarized as follows :

	Source of Inhomogeneous Broadening	Predicted Shape of the Absorption Line
(i)	Broadening from hyperfine structure	Gaussian shape
(ii)	Broadening by random electric field	Intermediate between Lorentzian and Gaussian shape
(iii)	Strain broadening by dislocations	Lorentzian along [100] and nearly Gaussian along [111]
(iv)	Broadening by field gradient (due to charge effect)	Nearly Lorentzian
(v)	Strain broadening by point defects	At low concentrations (less than 0.1%) the shape is Gaussian and at high concentration the line becomes progressively Lorentzian

It can also be mentioned that for homogeneously broadened lines for dipolar interaction, the lineshape will be Gaussian and for exchange interaction the line shape will be Lorentzian.

2.3.3 Moments Ratio

The method that was used by Van Vleck (2.7) for the analysis of the shape of a paramagnetic resonance absorption line was 'the method of moments'. Poole (2.23) has described the method of calculation of moments from the first derivative (absorption) line. If the narrow band amplifier and phase sensitive detector are tuned to the modulation frequency, and the modulation amplitude H_m is much less than the linewidth (which will be the experimental case), then the recorded lineshape becomes the first derivative Y' of the absorption line Y as shown in Figure 2.7. The area A under the first derivative absorption curve y', as shown in Figure 2.10 is given by (2.23) as

$$A = (H_j - H_{j-1})^2 \sum_{j=1}^{m} \sum_{i=j}^{m} y'_j \qquad (2.31)$$

where y'_j is the amplitude of the first derivative absorption line at the magnetic field H_j and m is the number of intervals $(H_j - H_{j-1})$ as shown in Figure 2.10. The precision of the area determination is increased by increasing m and decreasing the interval $(H_j - H_{j-1})$. The second and fourth moments of the absorption lines expressed in terms of the parameter of the first derivative curves are given as

$$\text{Second moment, } \langle M_2 \rangle = \frac{(H_j - H_{j-1})^2}{A} \sum_{j=1}^{m} \sum_{i=j}^{m} (H_j - H_o)^2 \, y'_i \qquad (2.32)$$

$$\text{Fourth moment, } \langle M_4 \rangle = \frac{(H_j - H_{j-1})^2}{A} \sum_{j=1}^{m} \sum_{i=j}^{m} (H_j - H_o)^4 \, y'_i \qquad (2.33)$$

Detailed computational procedures for deriving moments from the

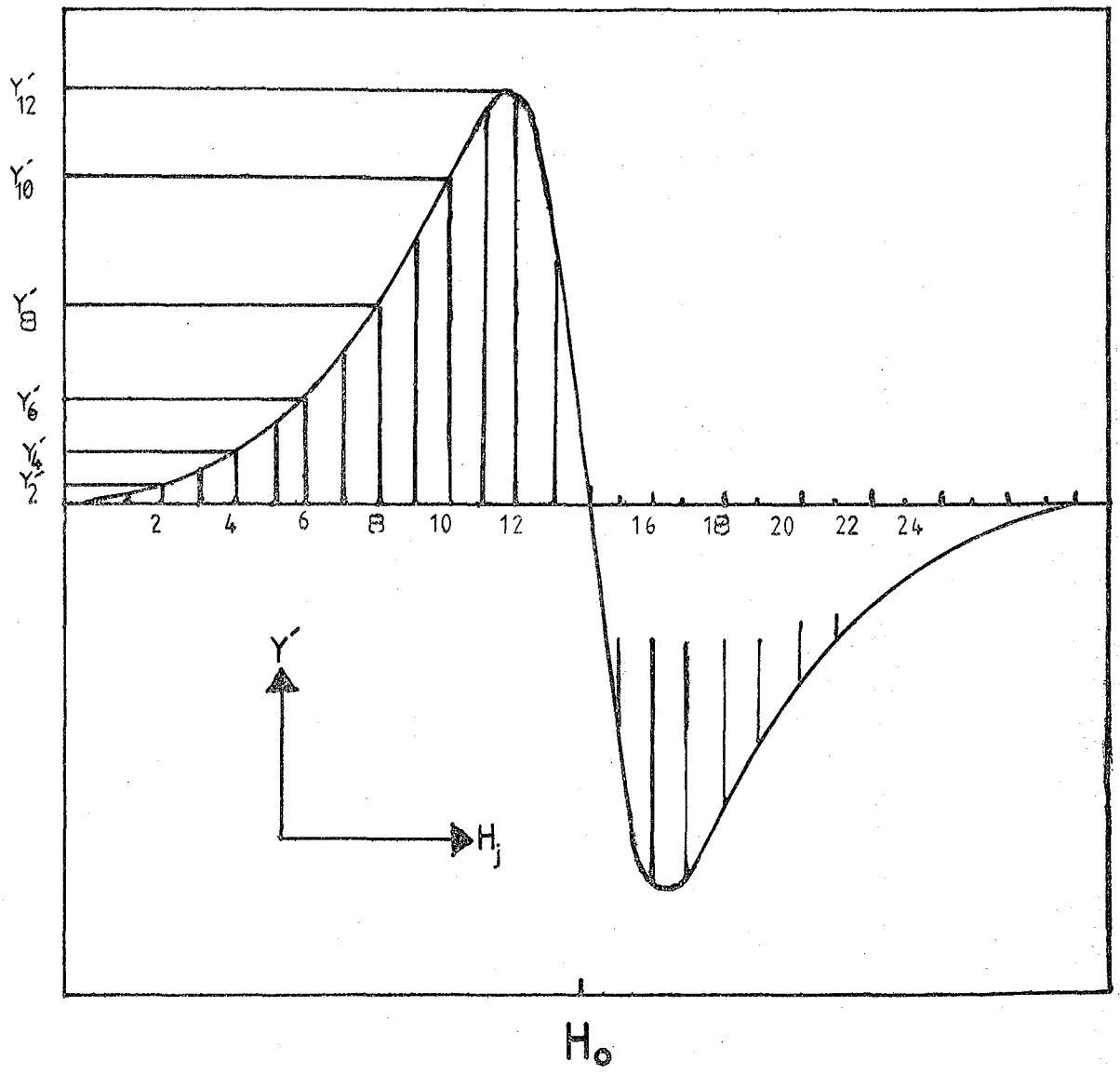

FIG. 2.10 METHOD OF MOMENT CALCULATION.

derivative curves by using the above two equations have been described in the reference (2.23). It has been shown by Van Vleck (2.6) that in the case of pure dipolar interactions the ratio of the moments is close to the value obtained for a Gaussian function, i.e.

$$M_4^{\frac{1}{4}} \Big/ M_2^{\frac{1}{2}} = 1.32 \qquad (2.34)$$

Al'tshuler and Kozyrev (2.25) reported that if exchange interactions are stronger than the dipolar interactions, then

$$M_4^{\frac{1}{4}} \Big/ M_2^{\frac{1}{2}} >> 1 \qquad (2.35)$$

and consequently the line acquires a Lorentzian shape.

REFERENCES

CHAPTER TWO

2.1 W.Low, Solid State Physics, Suppl.2,page 9, Acad.Press,London,1960.

2.2 A.Abragam and B.Bleaney, 'E.P.R. of Transition Ions', Clarendon Press, Oxford, (1970).

2.3 J.E.Wertz and J.Bolton, 'Electron Spin Resonance', McGraw Hill, New Yorm (1972).

2.4 W.Low, Phys. Rev. 105 (1957) 801.

2.5 A.M.Portis, Phys.Rev.91 (1953) 1071.

2.6 J.H.Van Vleck, Nuvo.cim,Suppl.No.3, 6 (1957) 993.

2.7 J.H.Van Vleck, Phys.Rev.74 (1948) 1168.

2.8 G.Brown, C.J.Krikby, and J.S.Thorp, J.Mat.Sci.9 (1974) 65.

2.9 J.S.Thorp, R.A.Vasquez, C.Adcock and W.Hutton, J.Mat.Sci. 11 (1976) 89.

2.10 D.C.Mattis, 'The Theory of Magnetism', Harper and Row,N.Y.(1965).

2.11 R.A.Vasquez, M.Sc.Thesis,Durham University,(1975),(unpublished).

2.12(a) W.Low, Phys.Rev.109 (1958) 247.

2.12(b) W.Low, Phys.Rev.109 (1958) 256.

2.13 J.W.Orton, P.Auzins and J.E.Wertz, Phys.Rev.Lett. 4 (1960) 128.

2.14 M.M.Abraham, L.A.Boatner,Y.Chen and J.L.Kolpus,Phys.Rev. B4 (1971) 2853.

2.15 P.Swarup, C and J.of Phys., 37 (1959) 848.

2.16 W.J.C.Grant and M.W.Strandberg, Phys.Rev.135A (1964) 724.

2.17 J.S.Thorp, G.Brown and H.P.Buckley, J.Mat.Sc.9 (1974) 1337.

2.18 J.S.Thorp and H.P.Buckley, J.Mat.Sc.9 (1974) 1499.

2.19 C.J.Gorter and J.H.Van Vleck, Phys.Rev.72 (1947)1128.

2.20 P.A.M.Dirac,'The Principle of Quantum Mechanics', Chapter 10, 4th ed., Clarendon Press, (1958).

2.21 P.W.Anderson and P.R.Weiss, Rev.Mod.Phys.25 (1953) 269.

2.22 R.Kubo and K.Tomita, J.Phys.Soc.Japan, 9 (1954) 888.

2.23 C.P.Poole, 'Electron Spin Resonance', p.775, Inter Science Publication, N.Y. (1967).

2.24 A.M.Stoneham, Rev.Mod.Phys. 41 (1969) 82.

2.25 S.A. Al'tshuler and B.M.Kozyrev, 'Electron Paramagnetic Resonance', Acad.Press, N.Y. (1964), p.120.

CHAPTER THREE

EXPERIMENTAL TECHNIQUES

3.1 THE X-BAND SPECTROMETER

In order to carry out a specific experiment using E.S.R., the basic pieces of apparatus listed below are necessary ; a microwave source, a means of storing energy in the form of a cavity resonator, a detector, an amplifier and recording device, and a source of steady magnetic field. For linewidth measurement one must add to these parts a system for modulation of the steady magnetic field which, together with a phase sensitive detection, enables one to obtain derivative output and correspondingly greater sensitivities. To carry out this measurement an X-band spectrometer (reflection cavity type) has been constructed ; the block diagram of which is shown in Figure 3.1.

The microwave power, which is to excite the electronic transitions, is provided by a type KS9-20A Mullard Klystron. A magic Tee splits this power equally into two of the arms of a bridge, one of which includes an E-H tuner, whilst the other leads to the resonant cavity which contains the sample under study. At the extreme of the third arm a diode is placed as a detector of the output of the bridge. By suitable adjustment of the E-H tuner the crystal output may be made proportional to the absorption by the sample at resonance. Additionally, a high Q wavemeter is included to measure the operating frequency and also an attenuator is inserted so that the power incident in the cavity may be adjusted and kept such as not to saturate the transitions. The bridge is balanced by adjusting the E-H pistons using the method suggested by Cullen in 1965 (3.1). When the bridge is balanced perfectly by the E-H tuner, no radiation falls on the

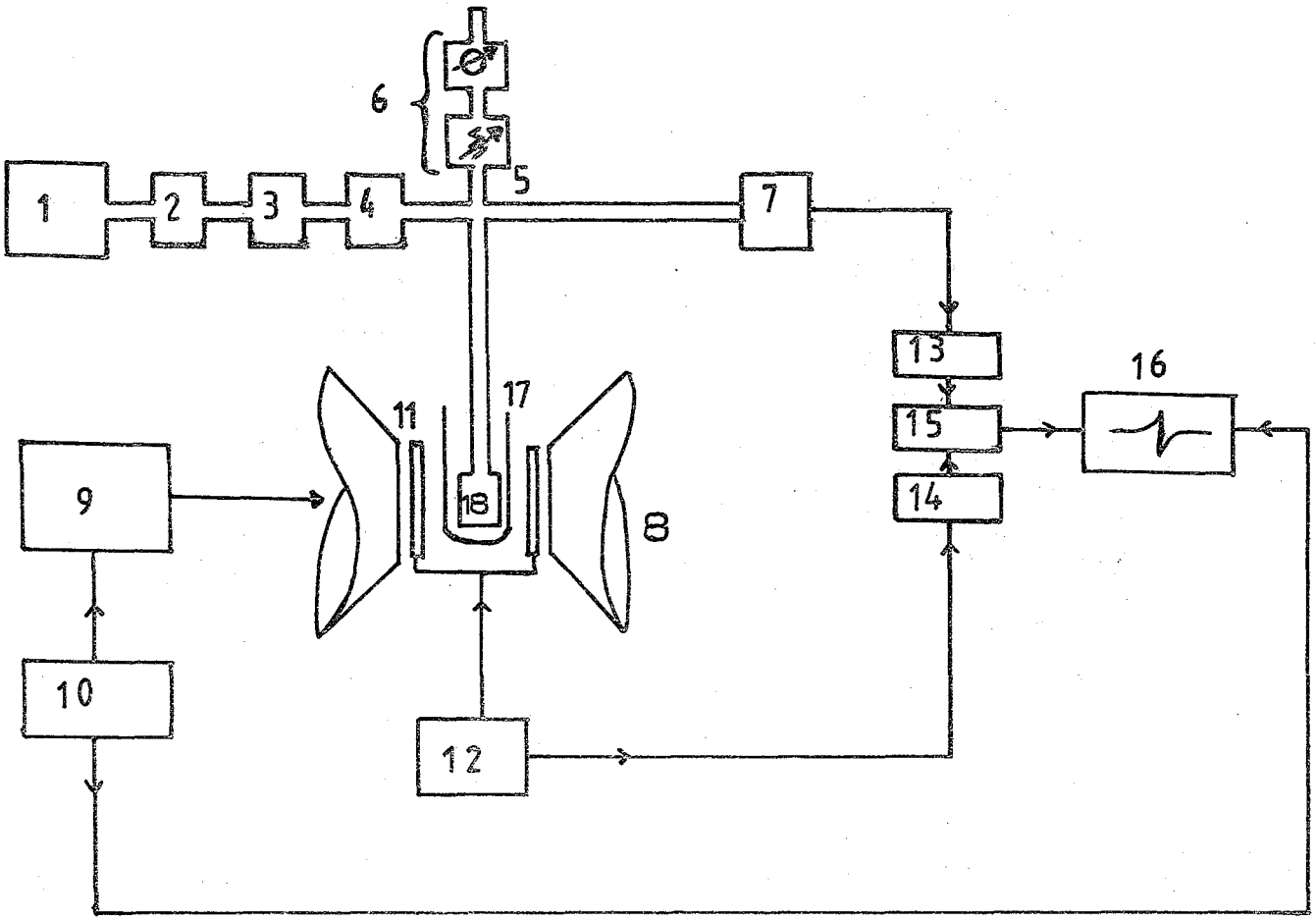

1 Klystron
2 Isolator
3 Wavemeter
4 Attenuator
5 Magic Tee
6 E-H Tuner
7 Detector
8 Magnet
9 D.C. Power Supply
10 Sweep Unit
11 Modulation Unit
12 A.F. Oscilator
13 Low Noise Amplifier
14 Phase Shifter
15 Phase Sensetive Detector
16 Recoder
17 Cryogenics
18 Cavity

FIG. 3.1 BLOCK DIAGRAM OF THE X- BAND E.S.R. SPECTROMETER.

detector diode in arm 2. The bridge is then unbalanced slightly so that when the sample absorbs microwave energy, the output signal incident on the detector is proportional to the amount of microwave energy absorbed by the sample.

The rectangular cavity is made of brass silver-plated to increase the Q factor and has dimensions 2.28 cm x 1.04 cm x 4.56 cm. It works in the TE_{102} mode and it is iris-coupled to a Cu/Ni waveguide. A diagram of the cavity is shown in Figure 3.2 which shows the selected location of the sample also. A continuously adjustable matching device has been used (3.2), for low temperature operation ; with this the sample could be matched by remote control from outside the cryostat.

The source of the necessary steady magnetic field is an electromagnet (Newport Instruments - Type AE), which is capable of being rotated to enable polar plots to be made. Using the technique of proton resonance measurement, it was found that the homogeneity of the field is of few parts in 10^4 over a volume of one cubic centimetre, i.e. sufficiently uniform over a volume greater than that of the sample. The rate of change of the field is controlled by means of a sweep unit which drives the power supply (Newport Instrument - Type D104) of the magnet, the minimum rate employed being five gauss per second. The magnet is also provided with two Helmholtz coils attached to the pole pieces, which connected to an audio power oscillator (Dawe Instrument - Type 440B), will in turn sweep the magnetic field. This method of field modulation is to increase the overall sensitivity of the spectrometer as discussed by Poole (3.3).

An arrangement of a phase sensitive detector, a phase shifter and a low noise amplifier tuned at the modulation frequency (115 Hz in this case) completed the system used to 'process' the signal from the detector output. The Y-axis of a pen recorder is fed with the output of the phase

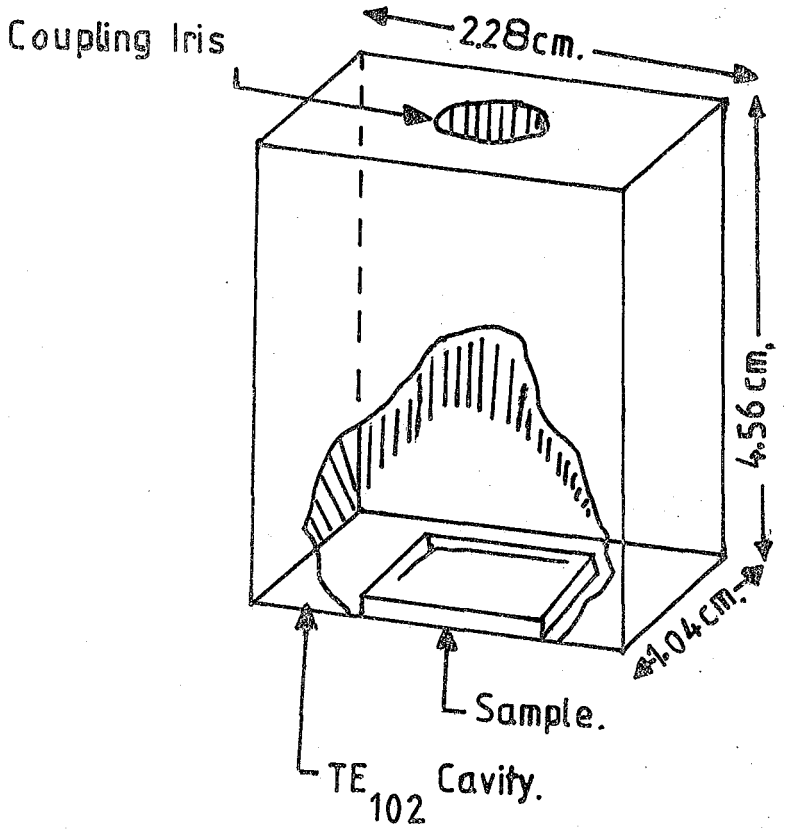

FIG. 3.2 POSITION OF THE SAMPLE IN THE MICROWAVE CAVITY.

sensitive detector, whilst the X-axis is connected to the output of the sweep unit so that a plot of the derivative of the resonance line versus magnetic field is obtained. To reduce the amount of noise coupled with the microwave output the heater of the klystron tube was connected to a d.c. battery (rather than to the a.c. supply in the valve power pack).

In order to measure the linewidth, the whole spectrum was recorded by scanning the main magnetic field over a 0.1 Tesla wide range and from this the transitions were identified. To ensure better accuracy in the measurement the rate of scan of the magnetic field through the transition was reduced to usually 50 mT in 4 minutes (about 0.2 mT per second) for the sample Co^{2+}/MgO and Ni^{2+}/MgO, whilst for the samples Cr^{3+}/MgO, Fe^{3+}/MgO and Gd^{3+}/MgO the rate of scanning was 10 mT in 32 seconds (about 0.4 mT per second). The modulating audio frequency field was kept at a level such that no artificial broadening of the line due to saturation effect was observed. This level was determined experimentally. Both the initial and the final points of the magnetic field scanned were measured using proton resonance and it was found (as expected from the manufacturer's data) that the sweep was linear in the region under consideration. From the calibrated scale, the peak-to-peak linewidth ΔH_{ms}, was measured as the separation, in units of magnetic field,of the two turning points of the derivative curve as shown in Figure 3.3 (a). Calculation of $\Delta H_{\frac{1}{2}}$ (the linewidth between the points of half-amplitude) was carried out by numerical integration of the derivative trace, as shown in Figure 3.3 (b).

3.2 CRYOGENIC TECHNIQUES

In order to observe the effect of temperature on the linewidths and to observe the signals from Co^{2+}/MgO, the spectrometer was equipped with a helium cryostat (Model MD4A - Oxford Instruments Ltd). A complete diagram of the system is given in Figure 3.4. Intermediate temperatures

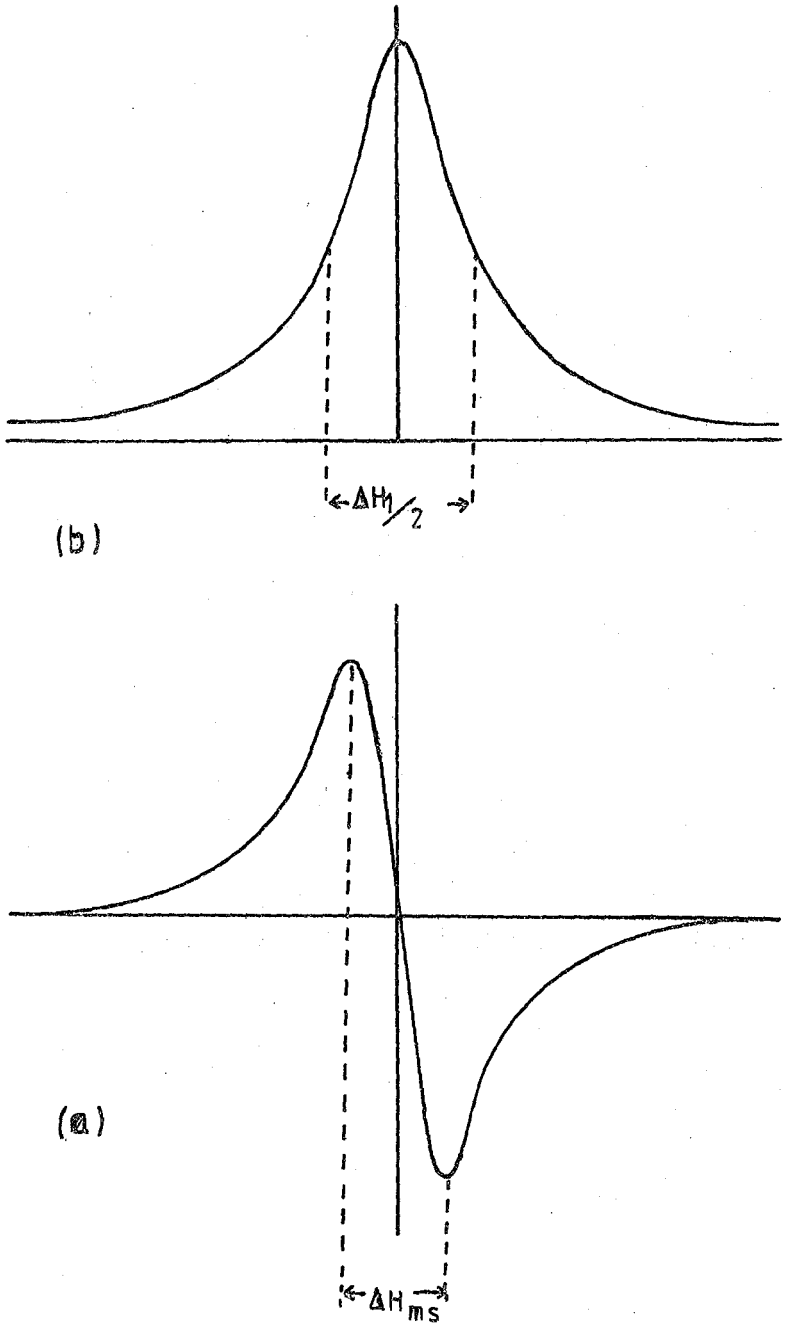

FIG, 3,3 DEFINITION OF LINEWIDTH

(a) DERIVATIVE PEAK-TO-PEAK WIDTH ΔH_{ms}.

(b) HALF AMPLITUDES WIDTH $\Delta H_{1/2}$

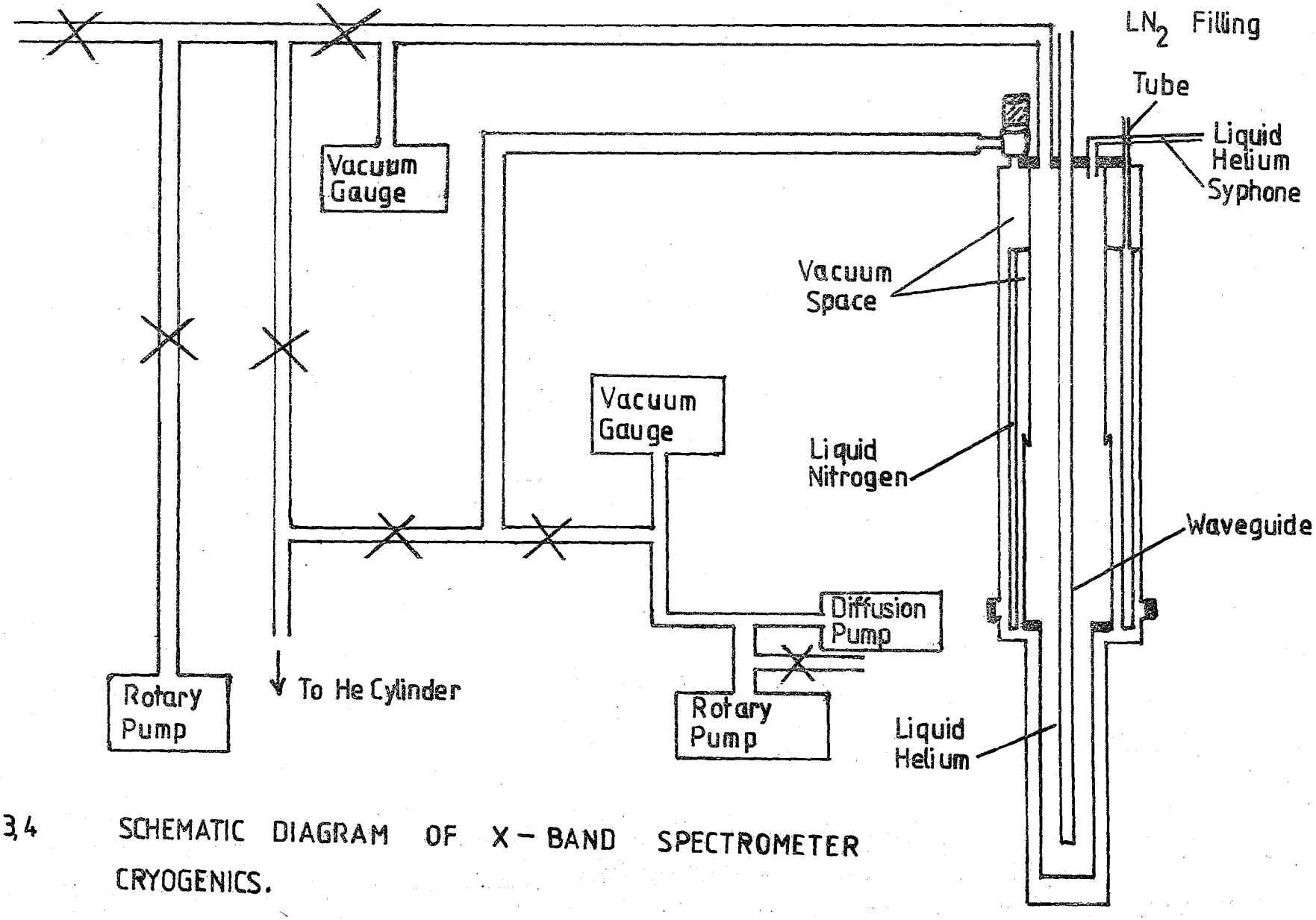

FIG, 3.4 SCHEMATIC DIAGRAM OF X-BAND SPECTROMETER CRYOGENICS.

between 293 K to 77 K could be obtained by establishing a heat contact between the liquid nitrogen chamber and the sample chamber with low pressure helium gas in the interspace. Alternatively they could be obtained by introducing small amounts of liquid nitrogen in the sample chamber which was subsequently pumped out. This step was followed by evacuating the interspace with a good backing pump to about 10^{-3} mm Hg. By adjusting the amount of liquid nitrogen pumped out, the desired temperature was obtained and kept constant to within 2 K for sufficient time to allow recordings of the spectrum. In this way cooling,to liquid nitrogen temperature, took less than two hours. The temperature of the specimen was measured by means of a copper-copper/constantan thermocouple strapped to the outside of the cavity.

The technique of transferring liquid helium into the cryostat was quite straight forward. The procedures were as follows :

(i) Evacuate the interspace to about 10^{-3} mm Hg.

(ii) Fill up the screening jacket with liquid nitrogen.

(iii) Flush out the sample chamber by helium gas ; when it reaches 77 K make sure that there is no liquid nitrogen left in the sample chamber.

(iv) Transfer liquid helium by metal syphon from the travelling dewar. This takes about ½ hour.

Once the liquid helium had been transferred, a temperature of 4.2 K could be maintained for several hours. The 'spot check' of the liquid helium in the cryostat was done by a low wattage carbon resistor.

3.3 THE VARIAN SPECTROMETER

In order to compare the spectra (obtained from the constructed X-band spectrometer, described in Section 3.1) with the spectra obtained from a commercial spectrometer (which has greater sensitivity, better homogeneity of magnetic field, and greater resolution of both magnetic

field and temperature) the X-band Varian equipment, V-4502-15 was used. It was operating at about 9.5 GHz. It has a rectangular TE_{102} cavity, the sample being mounted on a P.T.F.E . rod inserted through the cavity base for room temperature work. A block diagram of the Varian spectrometer is given in Figure 3.5. The magnet was a Varian 12" electromagnet controlled by a VFR 5203 field regulated power supply, which is capable of setting the desired field to 0.1 mT with one part in 10^5 repeatability, at 0.002 mT resolution. To check this measurements of field were also made using a proton magnetometer. The detailed procedure for observation of spectra has been described in the Varian literature (3.4).

For work below room temperature an Oxford Instruments continuous flow cryostat was used. This has a low liquid helium consumption rate, and will provide temperatures from about 2 K up to room temperature at a resolution of 0.1 K. When the cryostat was used it was found necessary to flood the wave guide with dry nitrogen to prevent water condensing in the microwave cavity.

No differences were observed in the spectra obtained from the constructed X-band spectrometer and the commercial Varian spectrometer, except in so far as the higher sensitivity of the latter made the recording of spectra easier. This comparison of spectra proved that the constructed X-band spectrometer had a high standard of performance and that the spectra recorded with it were valid and reliable.

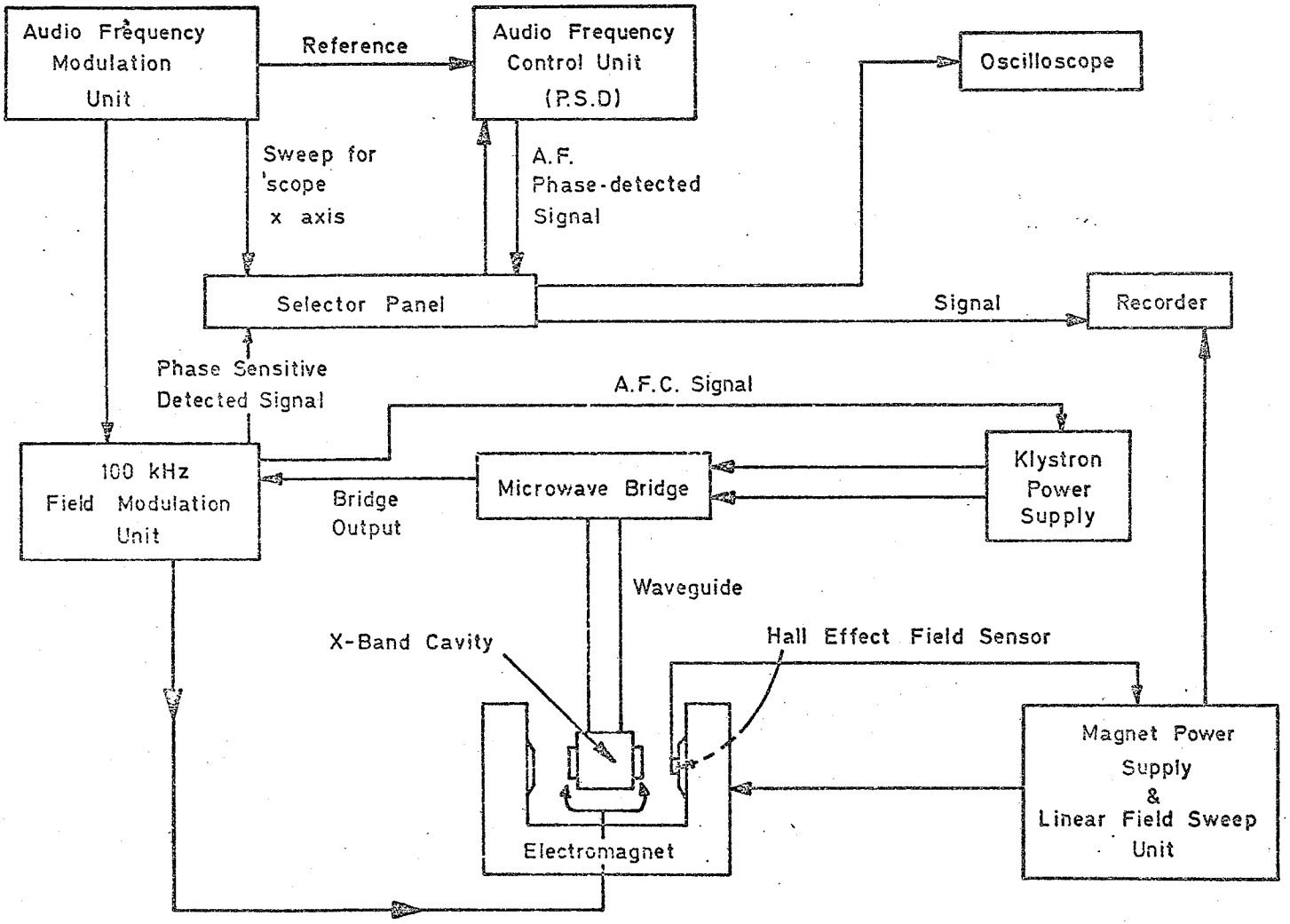

FIG. 3.5 BLOCK DIAGRAM OF VARIAN SPECTROMETER

REFERENCES

CHAPTER THREE

3.1 A.L.Cullen, Electron. letters. 1 (1965) 55.

3.2 R.A.Vasquez, M.Sc. Thesis. Durham University (1975) (unpublished).

3.3 C.P.Poole, 'Electron Spin Resonance', Inter Science, N.Y. 1967.

3.4 Varian V 4502 E.P.R. Spectrometer Manual.

CHAPTER FOUR

STUDIES ON Cr^{3+}/MgO

In this Chapter the electron spin resonance linewidths of Cr^{3+} in single crystal MgO at 9 GHz were examined experimentally and theoretically for a range of Cr^{3+} concentrations. In contrast to the behaviour expected from dipolar broadening the experimental peak-to-peak linewidth for the $\frac{1}{2}$ to $-\frac{1}{2}$ transition, which had a value of about 0.5 mT at 293 K, was independent of both polar angle and concentration over the range from 800 ppm Cr to 15,100 ppm Cr. The calculated dipolar linewidths exceeded those observed by factors of over one hundred ; the ratio of moments $M_4^{\frac{1}{2}} / M_2^{\frac{1}{2}}$ derived from the experimental data lay between 1.33 and 1.39 and the lineshapes were markedly Lorentzian. The data suggested that Cr^{3+} entered the lattice substitutionally, occupying magnesium sites, that the linewidths were determined by exchange narrowing over the whole concentration range examined and that the exchange energy, whose values lay between 4 GHz and 100 GHz, varied linearly with concentration.

4.1 INTRODUCTION

Trivalent chromium has three d electrons and a ground state of $^4F_{3/2}$. A cubic crystalline field splits the sevenfold-degenerate level into a low singlet and two higher triplets. The ground state responsible for the paramagnetic resonance absorption acts like a ^4S state, as the next highest triplet is separated by a large value 10 Dq (4.1). Spin-orbit coupling does not remove the fourfold -spin degeneracy of the ground state. Some electron spin resonance work on chromium doped magnesia (Cr^{3+}/MgO) has been reported in the literature (4.1-4.3) and the characteristic parameters of the spin Hamiltonian calculated for cubic crystalline fields. There is, however, little detailed information available either on the question of the sites actually occupied by the dopant atoms or on the nature of the interactions between the latter. Information of this nature has recently been obtained in several materials, including doped calcium tungstate (4.4, 4.5), alumina (4.6, 4.7) and magnesia (4.8), by making a comparison between the observed e.s.r. linewidths and those predicted from dipolar broadening. It was decided to adopt an approach similar to that used with iron doped magnesia. This Chapter presents the results of the linewidth comparison made for the $\frac{1}{2} \leftrightarrow \frac{1}{2}$ transition of Cr^{3+} in MgO in the temperature range 293 K to 77 K.

4.2 EXPERIMENTAL RESULTS

The chromium concentrations in the specimens examined ranged from 800 ppm to 15,100 ppm. Initial measurements were made at 9 GHz to establish the form of the spectrum in each specimen when H// (100) plane i.e. $\phi_H = 0^o$. An example of this is shown in Figure 4.1 which refers to a specimen containing 800 ppm Cr examined at 293 K. The spectrum at $\theta_H = 0^o$ shows a single strong isotropic line at about g = 1.98, accompanied by four hyperfine lines with a separation between the components of about

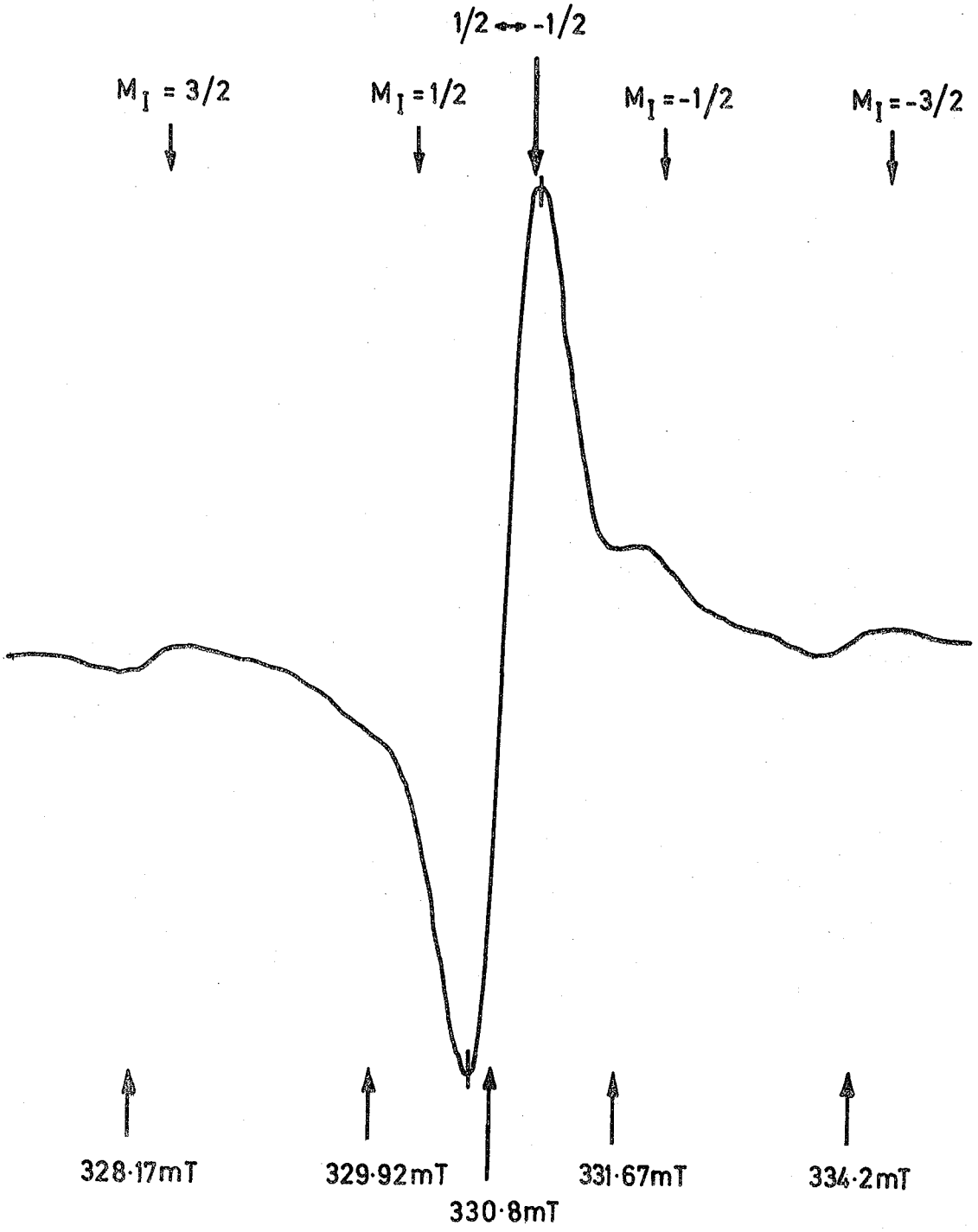

FIG.4.1 ESR spectra of Cr^{3+}/MgO; 293K, $\Theta_H = 0^\circ$, 9·167 GHz, 800 ppm Cr.

17.5 Gauss. The field values at which the transitions occurred were compared with the values expected for Cr^{3+} in an octahedral site. There was close agreement and on this basis and in view of the similarity between Figure 4.1 and the spectrum reported by Low (4.1), it was felt justifiable to attribute the spectrum to Cr^{3+} in octahedral sites. The hyperfine lines are due to the isotope ^{53}Cr ($I = {}^{3}/2$) which has an abundance of 9.5% ; the $A = 16.16 \times 10^{-4}$ cm^{-1}, deduced from the component separation agrees very closely with published values. The resonance field value for the $\frac{1}{2} \leftrightarrow -\frac{1}{2}$ transition was the same for all specimens even at the highest concentration, (15,100 ppm). Some weak additional lines were observed which were attributed to impurities, but these were well removed from the main Cr^{3+} line examined. Measurements of the magnetic field values at resonance for the $\frac{1}{2} \leftrightarrow -\frac{1}{2}$ transition and linewidth determinations were made at $\theta_H = 0^{o}$. There was no change in either the resonance field or the linewidth with polar angle at temperatures down to 77 K. The $\frac{1}{2} \leftrightarrow -\frac{1}{2}$ transition was used for detailed linewidth studies. The linewidth, defined as the width between points of maximum slope, ΔH_{ms}, was obtained directly from the derivative plots. At room temperature $\Delta H_{ms} \simeq 0.5$ mT. This is comparable to values reported in the literature. In order to check whether there was any appreciable contribution to linewidth due to spin lattice relaxation, the spectra were recorded at 77 K. The linewidths measured were only slightly larger than those at 293 K, e.g. 0.53 mT compared with 0.50 mT, suggesting that any contribution was very small.

4.3 THEORETICAL (DIPOLAR) LINEWIDTHS

The second moment, $\langle \Delta\omega^2 \rangle$, of the linewidth caused by dipolar interaction between Cr^{3+} ions in the magnesium oxide lattice has been shown in

Chapter 2 (Equation 2.14) to be

$$\langle \Delta\omega^2 \rangle_{Cr^{3+}/MgO} = 2.8757 \times 10^{20}.n.\left[15.9184-5.175\ Y^{*}_{4,0}(\theta_H,\theta_H) - 6.218\ Y^{*}_{4,4}(\theta_H,\theta_H)\right] \qquad (4.1)$$

For $\phi_H = 0^o$ the equation is totally real and by substituting the experimental values of concentration, n and polar angle, θ_H curves of dipolar broadening as a function of polar angle can be derived. Using the transformation of Equation 2.12, ΔH_{ms} can then be calculated and compared with experimental values. The theoretical curves for the variation of dipolar linewidth with polar angle are given by the full lines in Figure 4,2, which also includes the experimental data shown by the broken line. The predicted concentration dependence of linewidth is compared with the experimental data obtained at 293 K in Figure 4.3 in which the concentration is expressed as the percentage number of sites occupied.

4.4 DISCUSSION

Three salient features emerge from an initial comparison between the experimental results for the as-grown crystals and those predicted on the basis of dipolar broadening. In the first place the predicted linewidths are about 160 times larger than the observed linewidths ; secondly, the linewidth appears to be almost concentration independent, in marked contrast to the (concentration)$^{\frac{1}{2}}$ variation expected ; thirdly, the observed linewidth appears independent of polar angle in contrast to the angular dependence predicted, which shows a maximum near $\theta = 45^o$.

The discrepancy in the magnitude of the linewidth is far greater than those encountered in other materials in which similar comparisons have been made (Table 4.1).

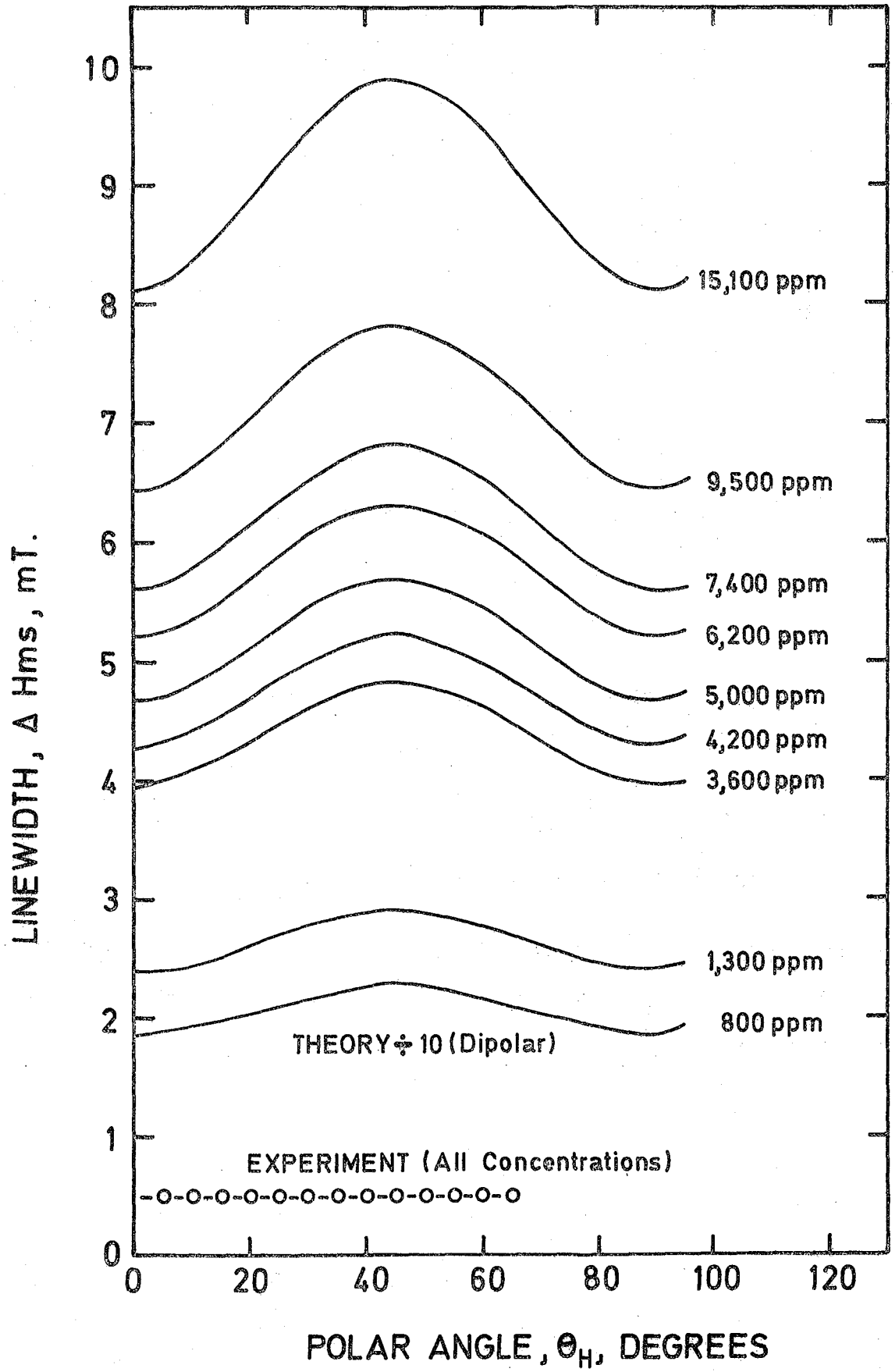

FIG. 42 Comparison of predicted and observed variation of linewidth with polar angle; full lines, dipolar broadening theory; broken line, experimental.

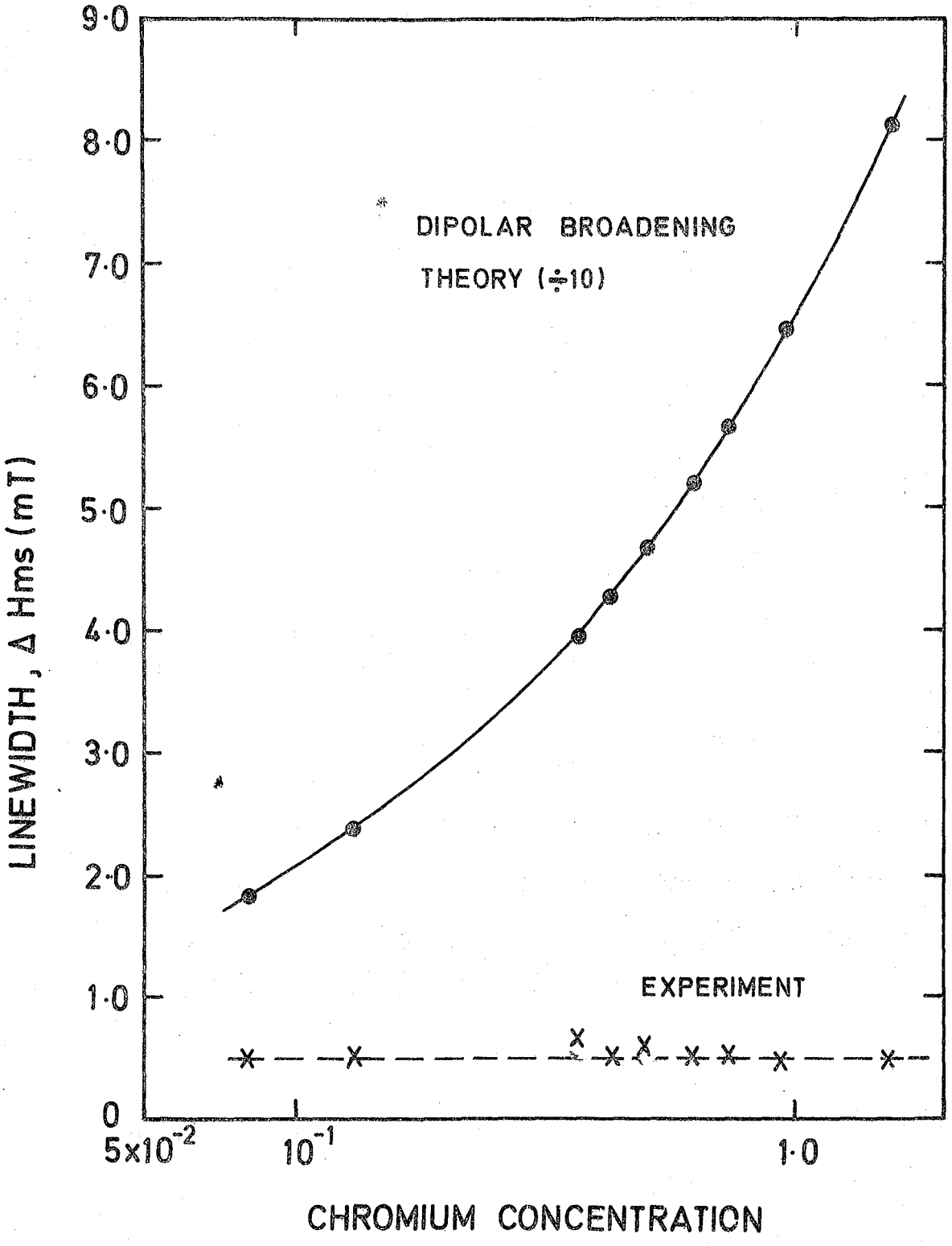

FIG. 4.3 Comparison of predicted and observed variation of linewidth with concentration; full line, dipolar broadening theory; broken line, experimental, $\Theta_H = 0^\circ$, 293K

Material	Predicted Linewidth (Dipolar Model)	References
Cr^{3+}/Al_2O_3 (Ruby)	5 times larger than observed	Grant et al (4.6)
$Nd^{3+}/CaWO_4$	Agreed closely with that observed	Brown et al (4.4)
$Gd^{3+}/CaWO_4$	7 times larger than observed	Thorp et al (4.5)
Double doped $Cr/Ti/Al_2O_3$	7 times larger than observed	Thorp et al (4.7)
Fe^{3+}/MgO	100 times larger than observed	Thorp et al (4.8)

TABLE 4.1 : Comparison of predicted dipolar linewidth with observed linewidth in different materials.

In the examples of Table 4.1 there was a reasonably good fit between the forms of the predicted and observed angular variation of the linewidth and also between the predicted and observed linewidth versus concentration variation except for Fe^{3+}/MgO which gave exchange narrowed linewidths. The large numerical disparity in Cr^{3+}/MgO suggested that a strong narrowing mechanism was involved and to substantiate the possibility of exchange narrowing the following evidence, shown in Table 4.2, was deduced from analysis of the lineshapes.

Exchange narrowing line mechanisms have been examined by Van Vleck (4.9). Experimental evidence for exchange narrowing is usually obtained from analysis of lineshapes and especially by comparison of moments. A review of Alt'Shuler (4.10) gives

$$\frac{M_4^{\frac{1}{4}}}{M_2^{\frac{1}{2}}} \gg 1$$

where M_2 and M_4 are respectively the second and fourth moments of the line as a criterion for exchange narrowing. An analysis of this type has been attempted as in (4.8) and the results are given in column three. The values of the ratio are similar to the figures quoted in the literature (4.8) for materials in which exchange narrowing occurs. This suggests that exchange narrowing is important, even at the lowest concentration (800 ppm Cr).

It has been calculated (4.11) that the ratio of peak-to-peak derivative linewidth, ΔH_{ms}, to the width at half-height, $\Delta H_{\frac{1}{2}}$, of the absorption curve for Gaussian lineshape is 0.846 and for the Lorentzian lineshape is 0.577. (Detailed derivation of these factors has been shown in Chapter 2 of Equations 2.29 and 2.30). Exchange narrowing would make the line adopt a Lorentzian shape. To confirm this, the spectra were

Chromium Concentration in p.p.m.	ΔH_{ms} (Obs) (mT)	$\frac{M_4^{\frac{1}{2}}}{M_2^{\frac{1}{2}}}$	$\frac{\Delta H_{ms}(Obs)}{\Delta H_{\frac{1}{2}}(Obs)}$	Exchange Energy J (GHz)	Weiss Constant θ (K)
800	0.47	1.38	0.425	4.39	3.15
1300	0.51	1.37	0.544	8.39	6.04
3600	0.73	1.39	0.642	19.13	13.78
4200	0.48	1.34	0.480	25.40	18.30
5000	0.65	1.33			
6200	0.51	1.38	0.563	41.80	30.2
7400	0.51	1.37	0.532	46.40	33.48
9500	0.40	1.35	0.479	69.00	49.72
15,100	0.42	1.36	0.470	102.60	73.70

TABLE 4.2 Lineshape data for a range of chromium concentration together with the derived values of J and θ ; 9.1 GHz, 293 K.

integrated numerically giving the integrated lineshapes some of which are shown in Figure 4.4. From these the widths at half-height $\Delta H_{\frac{1}{2}}$ have been calculated and the ratio of $\frac{\Delta H_{ms}}{\Delta H_{\frac{1}{2}}}$ derived ; the values are tabulated in column four. The results substantiate that the observed lineshapes are much more akin to Lorentzian than Gaussian.

The assumption, on the above basis, of an exchange-narrowed model enables evaluation of the exchange integral J to be made by adapting the Anderson-Weiss formula (4.12) to give

$$J \cong \frac{\frac{1}{6}\hbar.\langle\Delta\omega^2\rangle \quad \text{dipolar}}{\Delta\omega} \qquad (4.2)$$

where $\Delta\omega$ is the absorption line half-width at half-height in frequency unit (i.e. $\Delta\omega = \frac{2\pi g\beta}{h} \cdot \frac{1}{2} \Delta H_{\frac{1}{2}}$) obtained from the experimental spectrum. By using equation 4.2 values for $\langle\Delta\omega^2\rangle$ were obtained and thus the approximate J values for the specimens have been evaluated. Further, a plot of J against concentration gives a straight line as shown by the solid line in Figure 4.5 where again the concentration is expressed as the percentage number of sites occupied. If this line is extrapolated to 66.6% of available sites occupied by Cr^{3+}, (i.e. to the point corresponding to Cr_2O_3), an exchange energy of 4.38×10^{12} Hz is obtained ; this compares well with the values of 3.75×10^{12} Hz for Cr^{3+} in Cr_2O_3 (which has the Al_2O_3 crystallographic structure) (4.13) and of 2.49×10^{12} Hz for Cr^{3+} in MgO (4.14), both of which estimates were obtained from intensity measurements of e.s.r. pair spectra. The values of Weiss constant, θ, have also been calculated from the Weiss molecular field equation

$$3k\theta = 2Jz \; S\,(S + 1) \qquad (4.3)$$

where z is the number of nearest neighbours and k is the Boltzmann constant ;

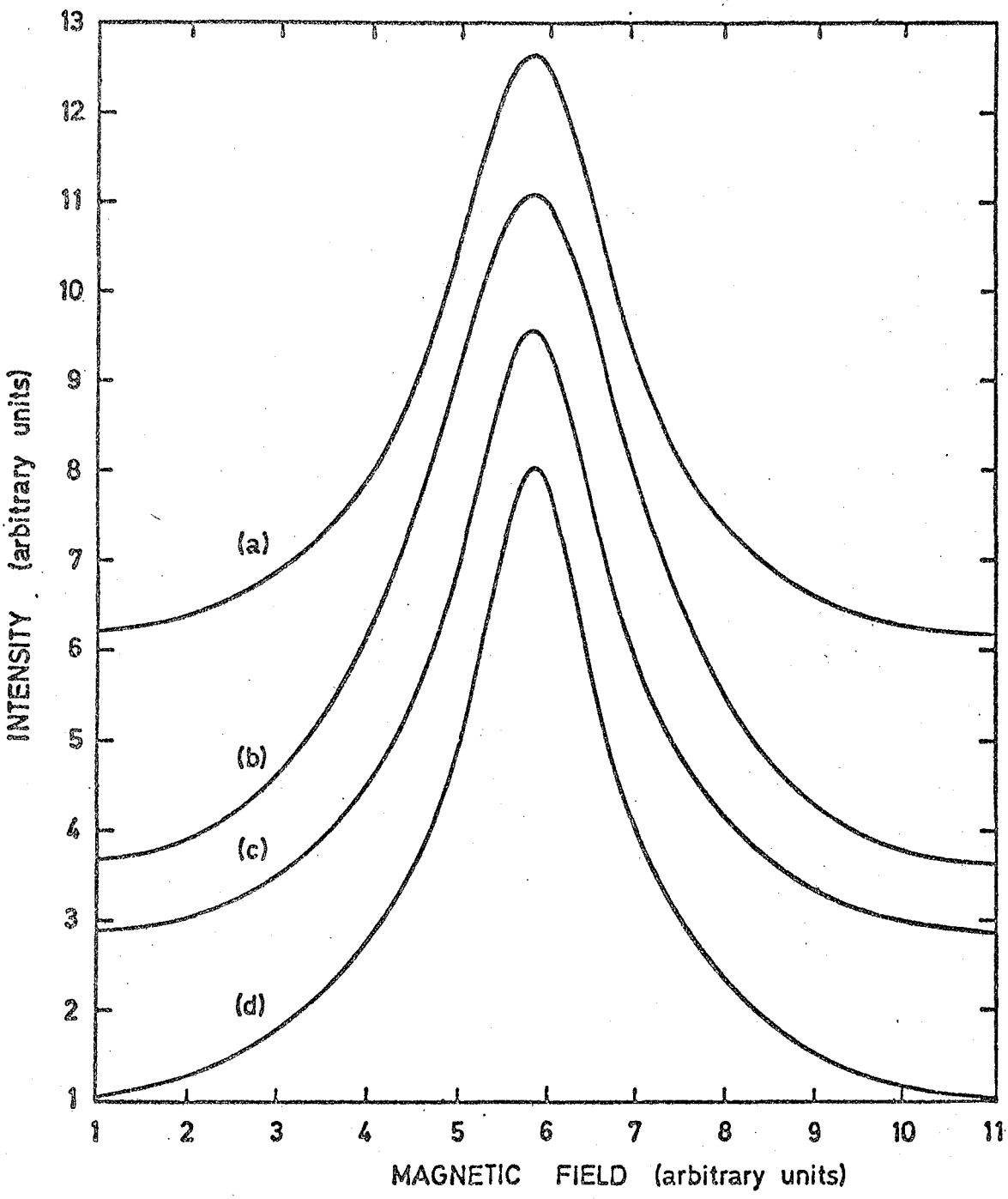

FIG. 4.4 Integrated lineshapes for (a) 1300 ppm Cr, (b) 3600 ppm Cr, (c) 6200 ppm Cr and (d) 15,100 ppm Cr.

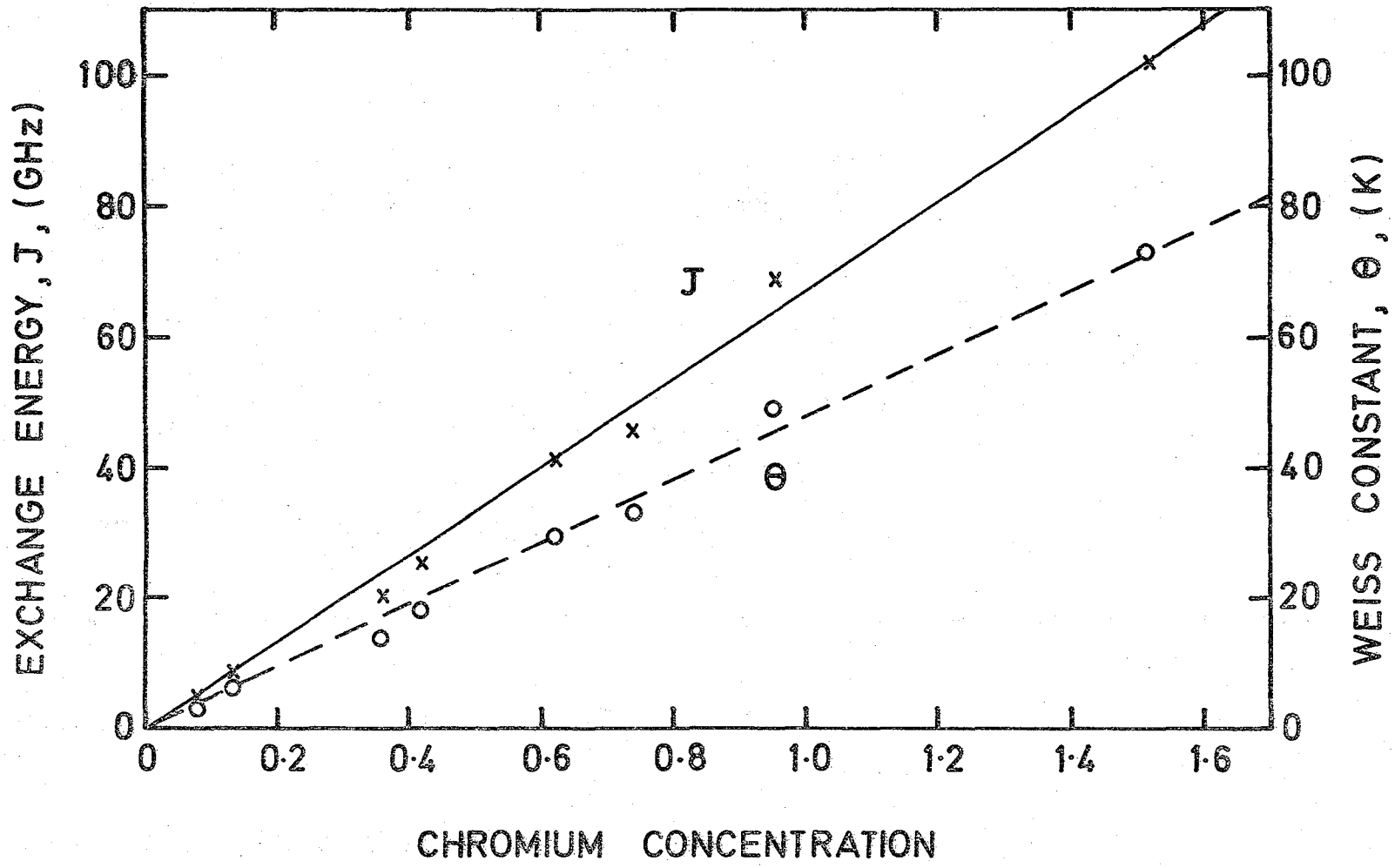

FIG. 4.5 The variation of J and Θ with Chromium Concentration.

in the MgO lattice z = 6. The values of θ are tabulated in column six. A plot of θ against concentration also gives a straight line as shown by the broken line in Figure 4.5. This indicates that the θ value is linearly dependent on the dopant concentration over the range examined. The slight increase in linewidth as the temperature decreases towards 77 K may be due to the unresolved superhyperfine interaction with the ^{25}Mg nuclide (I = 5/2) at nearest neighbour cation positions. Such a superhyperfine line has been found experimentally (4.15) (linewidth 0.017 mT, A_s = 0.13 mT) in the temperature range 77 K to 220 K.

It is concluded from the linewidth studies as a whole that chromium enters the magnesium oxide lattice substitutionally occupying magnesium sites at concentrations of up to at least 15,000 ppm ; that even at low concentrations 800 ppm, there is strong exchange narrowing of the e.s.r. lines and that the exchange energy varies linearly with the chromium concentration over the range examined.

REFERENCES

CHAPTER FOUR

4.1 W.Low, Phys. Review 105 (1957) 801.

4.2 J.S.Van Weiringen and J.G Renson, 'Paramagnetic Resonance' Vol.1 Edit.W.Low. Academic Press, N.Y. 1963, p 105.

4.3 J.E.Wretz and P.Auzins, Phys. Rev. 106 (1957) 484.

4.4 G.Brown, C.J.Krikby and J.S.Thorp, J.Mat.Sci. 9 (1974) 65.

4.5 J.S.Thorp, G.Brown and H.P.Buckley, J.Mat.Sci.9 (1974) 1337.

4.6 W.J.C. Grant and M.W.W.Strandberg. Phys.Rev. 135A (1964) 727.

4.7 J.S.Thorp and H.P.Buckley, J.Mat.Sci.9 (1974) 1499.

4.8 J.S.Thorp, R.A.Vasquez, C. Adcock and W.Hutton, J.Mat.Sci.11 (1976) 89.

4.9 J.H. Van Vleck, Nuovo Cimento.Supp. 6 (1956) 993.

4.10 S.A.Al'tshuler and B.M. Kozyrev, 'Electron Paramagnetic Resonance' Academic Press, N.Y. 1964, p 120.

4.11 C.P. Poole, 'Electron Spin Resonance', John Wiley & Sons, N.Y. 1967, p 775.

4.12 P.W.Anderson and P.R.Weiss, Rev.Mod.Phys. 25 (1953) 269.

4.13 P.W.Anderson, Solid State Physics. Edts.F.Seitz & D.Turnbull, 14 (1963) 99.

4.14 J. Marguglio and Yong Moo Kim, J.Chem.Phys. 62 (1975)1497.

4.15 J.C.M.Henning and J.H.Denboef. Phys.Letts.59A (1970) 241.

CHAPTER FIVE

E.S.R. LINEWIDTHS IN Co^{2+}/MgO

In this Chapter the electron spin resonance linewidths of Co^{2+} in single crystal MgO at 9 GHz were examined experimentally and theoretically for a range of Co^{2+} concentration from 310 ppm to 9900 ppm. In contrast to the behaviour expected from dipolar broadening the experimental peak-to-peak linewidth for the octed hyperfine lines were about twelve to fifty times less than the calculated dipolar linewidths according to temperature and concentrations. The peak-to-peak linewidths as determined experimentally increase from .8 mT at 310 ppm Co^{2+} to 4.0 mT at 9900 ppm Co^{2+} at a polar angle $\theta_H = 0^o$ and at 20 K. Peak-to-peak linewidth independnet of polar angle but strongly dependent on temperature and slightly dependent on concentrations were observed. The ratio of moments $M_4^{\frac{1}{4}} / M_2^{\frac{1}{2}}$ derived from the experimental data lay between 1.35 to 1.44 and the lineshapes were markedly Lorentzian in the range of temperature measured. The data suggested that Co^{2+} entered the lattice substitutionally, occupying magnesium sites, that the linewidths were determined, after exchange energy, over the whole concentration range examined and that the exchange energy whose values lay between 6 GHz to 77 GHz, varied linearly with concentration. Part of the work described in this Chapter was undertaken in collaboration with L. J.C. Bluck and T. G. Bushell.

5.1 INTRODUCTION

The electron spin resonance (e.s.r.) linewidth results of Cr^{3+} in magnesium oxide have been discussed in Chapter 4. As part of further studies on different ions a similar investigation has been made of the cobalt doped magnesia (Co^{2+}/MgO) in an attempt to provide specimens of known structural characteristics on which electrical conductivity and dielectric loss measurements might subsequently be made. The e.s.r. spectra of Co^{2+}/MgO was first observed by Low in 1958 (5.1) and then by Fry and Llewellyn in 1962 (5.2), where the characteristic parameters of the spin Hamiltonian were calculated for cubic crystalline field. There is, however, little detailed information available either on the question of the sites actually occupied by the dopant atoms or on the nature of the interactions between the latter. Information of this nature has been obtained for Cr^{3+}/MgO (as described in Chapter 4) by making a comparison between observed e.s.r. linewidths and those predicted from dipolar broadening. It was decided to adopt a similar approach with Co^{2+}/MgO. The divalent ion of cobalt has electronic configuration of 3 d^7 ($^4F_{9/2}$). In the MgO lattice the ^4F level splits into three and these are further split by spin orbit interaction (5.1) and the lowest level is a Kramers doublet. Since the only natural isotope of cobalt is ^{59}Co, which has a nuclear spin $I = {}^7/_2$, considerable hyperfine interaction is expected. This Chapter presents the results of the linewidth comparison made for the hyperfine transitions in the ground doublet of Co^{2+} in the temperature range from 4.2 K to 65 K. Above 65 K the cobalt spectrum in MgO is not observable.

5.2 EXPERIMENTAL RESULTS

The cobalt concentrations in the specimens examined ranged from 310 to 9900 ppm. Initial measurements were made to establish the form of the spectrum in each specimen at various temperatures. An example of

this is shown in Figure 5.1, which refers to a specimen containing 310 ppm Co examined at temperatures between 4.2 K and 65 K. The spectrum, which is isotropic, shows a total of eight hyperfine line with g value about 4.278 and with hyperfine constant about $A = 98.0 \times 10^{-4}$ cm^{-1}. The values at which the transitions occurred were compared with the values expected from the energy level diagram (5.3). There was close agreement and on this basis, and in view of the similarity between Fig 5.1 and the features of the liquid helium temperature spectra reported for the 1 cm and 3 cm regions respectively in references (5.1) and (5.4), it was felt justifiable to attribute the spectrum to Co^{2+} in the octahedral sites. A conspicuous difference in the intensity and the hyperfine line energy separation A was observed between the low and high magnetic field sides. Even at high gain the crystals showed only the lines due to Co^{2+} and a weak line due to iron, which suggests that these crystals are of higher degree of perfection than the corresponding Cr^{3+}/MgO sample. This is possibly due to the fact that, since the Co^{2+} ion is doubly charged, a direct substitution for Mg^{2+} is possible in the MgO lattice without the need for charge compensating vacancies.

The linewidth determinations were made at $\theta_H = 0^o$. The linewidths of the eight hyperfine lines were equal to each other and were independent of polar angle θ_H, but strongly dependent on temperature (Fig 5.2). There is some difficulty in ascertaining the linewidth at high temperatures and, above 50 K, the points marked on Fig 5.2 have been derived from the separation of points of inflection on the derivative plots. The linewidths were also slightly dependent on concentration but not by as much as the (concentration)$^{\frac{1}{2}}$ behaviour expected from dipolar theory. Increases in resonance linewidth for higher dopant concentrations have been reported by Fry and Llewellyn (5.2) in the endor experiments. There was no change in either the resonance field or the hyperfine constant A with polar angle at temperatures in the range measured. The peak-to-peak linewidth, defined

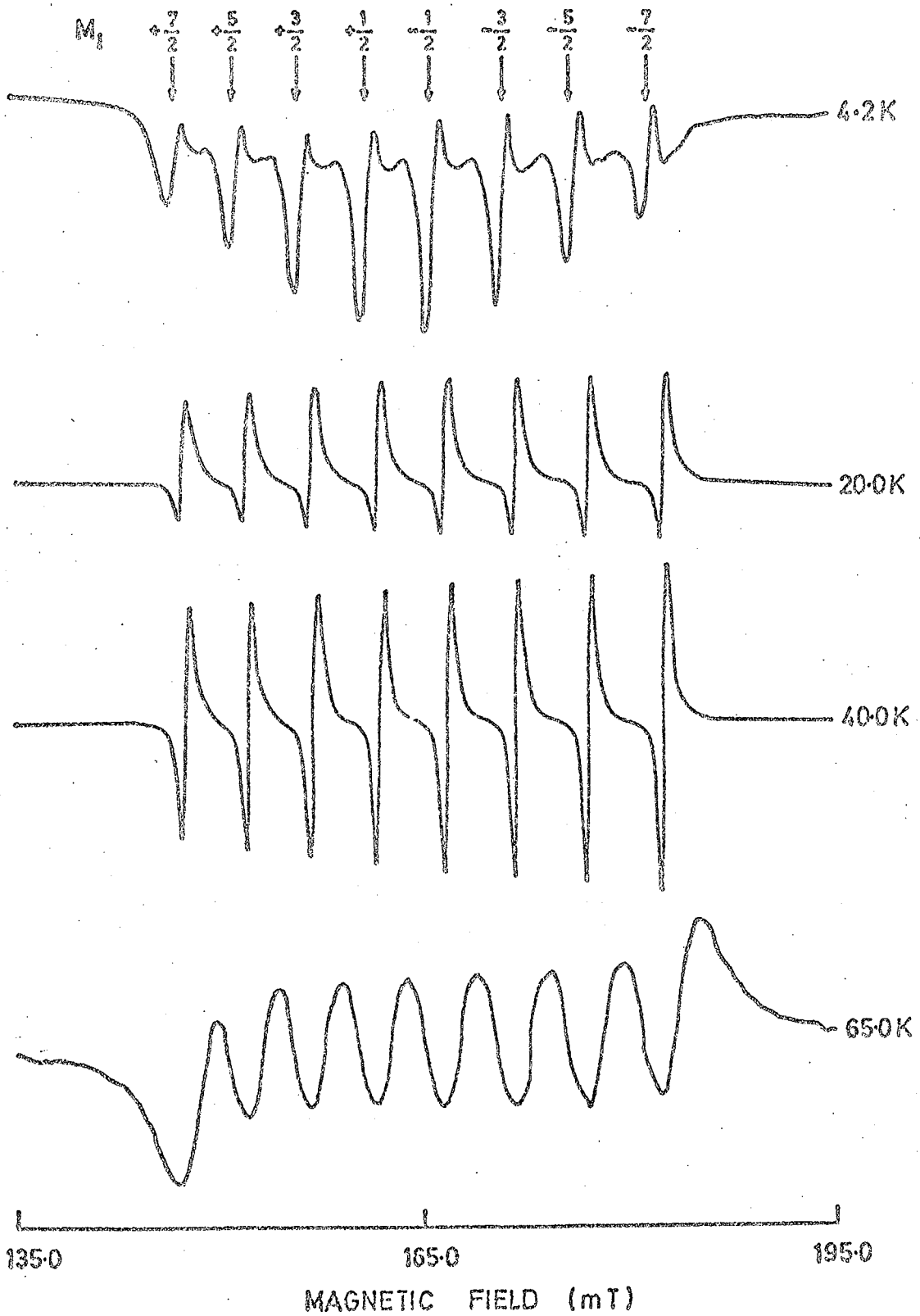

FIG. 5.1 VARIATION OF LINESHAPE WITH TEMPERATURE

Co^{2+}/ MgO (310ppm.) ; 9·515 GHz ; $\Theta_H = 0°$.

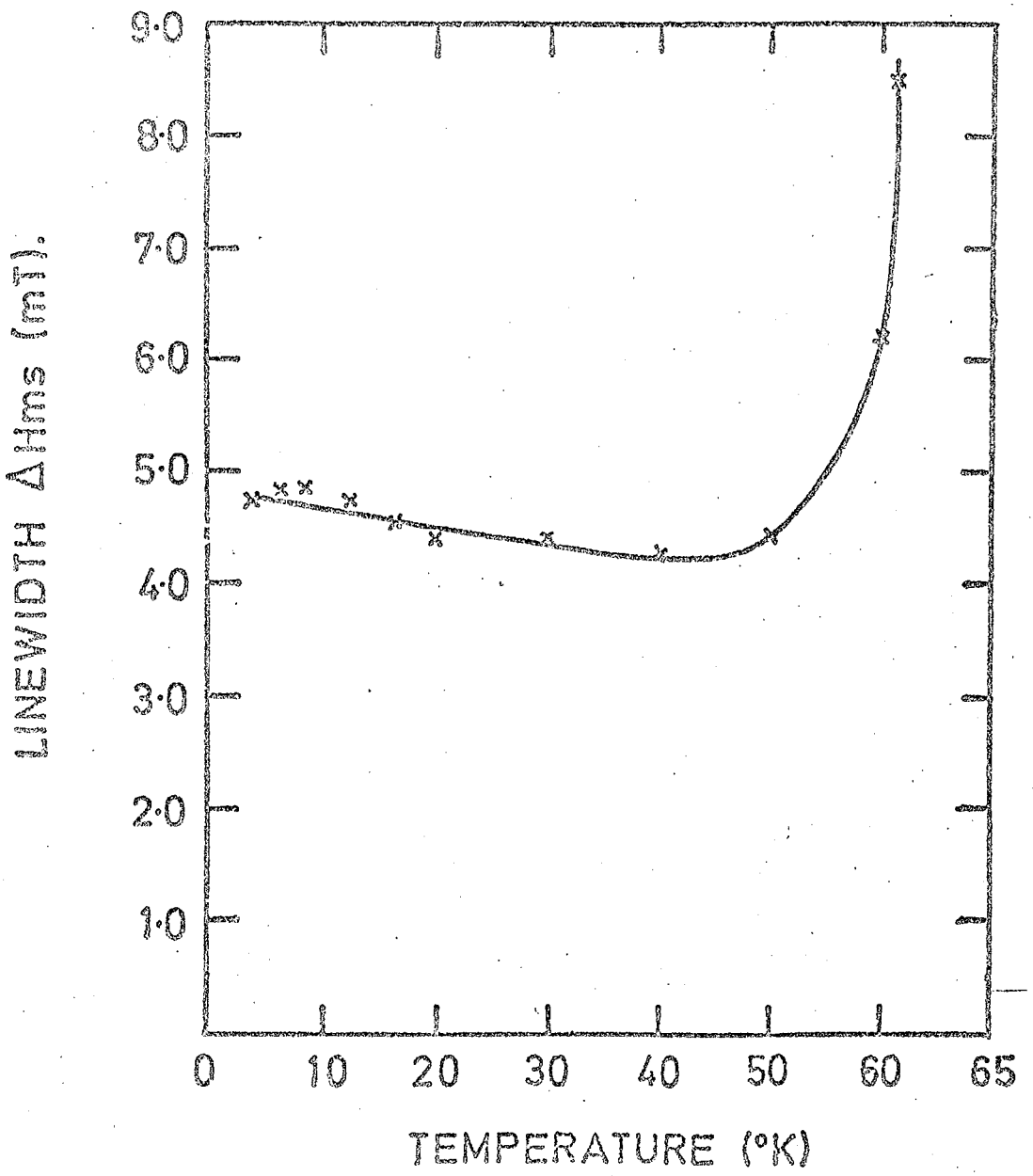

FIG. 5.2 THE TEMPERATURE DEPENDENCE OF THE LINEWIDTH FOR Co^{2+}/MgO (8200ppm).
9·515 GHz. $\theta_H = 0°$.

as the width between points of maximum slope, ΔHms, was obtained directly from the derivative plots. As the temperature decreased from 65 K the linewidth first decreased to a minimum at about 40 K and then increased from 20 K down to 4.2 K. For all the specimens, the linewidths ΔHms at 4.2 K were less than the linewidths at 60 K. For the low concentration specimen (310 ppm Co) at temperatures of 20 K, 4.2 K and 60 K the linewidths ΔHms were 0.8 mT, 1.7 mT and 2.4 mT respectively, while for the high concentration specimen (9900 ppm Co) the values of ΔHms for the corresponding temperatures were 4 mT, 4.9 mT and 4.9 mT respectively.

5.3 THEORETICAL (DIPOLAR) LINEWIDTHS

The second moment, $\langle \Delta\omega^2 \rangle$ of the linewidth caused by dipolar interaction between Co^{2+} ions in the magnesium oxide lattice has been shown in Chapter 2 (Equation 2.15) to be

$$\langle \Delta\omega^2 \rangle_{Co^{2+}/MgO} = 6.2644 \times 10^{21}.n.\left[15.9184 - 5.175\, Y^{*}_{4,0}(\Theta_H,\Theta_H) - 6.218\, Y^{*}_{4,4}(\Theta_H,\Theta_H) \right] \qquad (5.1)$$

Using the transformation equation and considering $\phi_H = 0^o$, the peak-to-peak derivative linewidths ΔHms can be evaluated and compared with experimental values. The general curves for the variation of linewidth with polar angle are given in Figure 5.3, which also shows the experimental values of linewidth. The predicted concentration dependence of linewidth at $\Theta_H = 0^o$ (obtained from Fig 5.3) is shown in Figure 5.4, which also gives the experimental points.

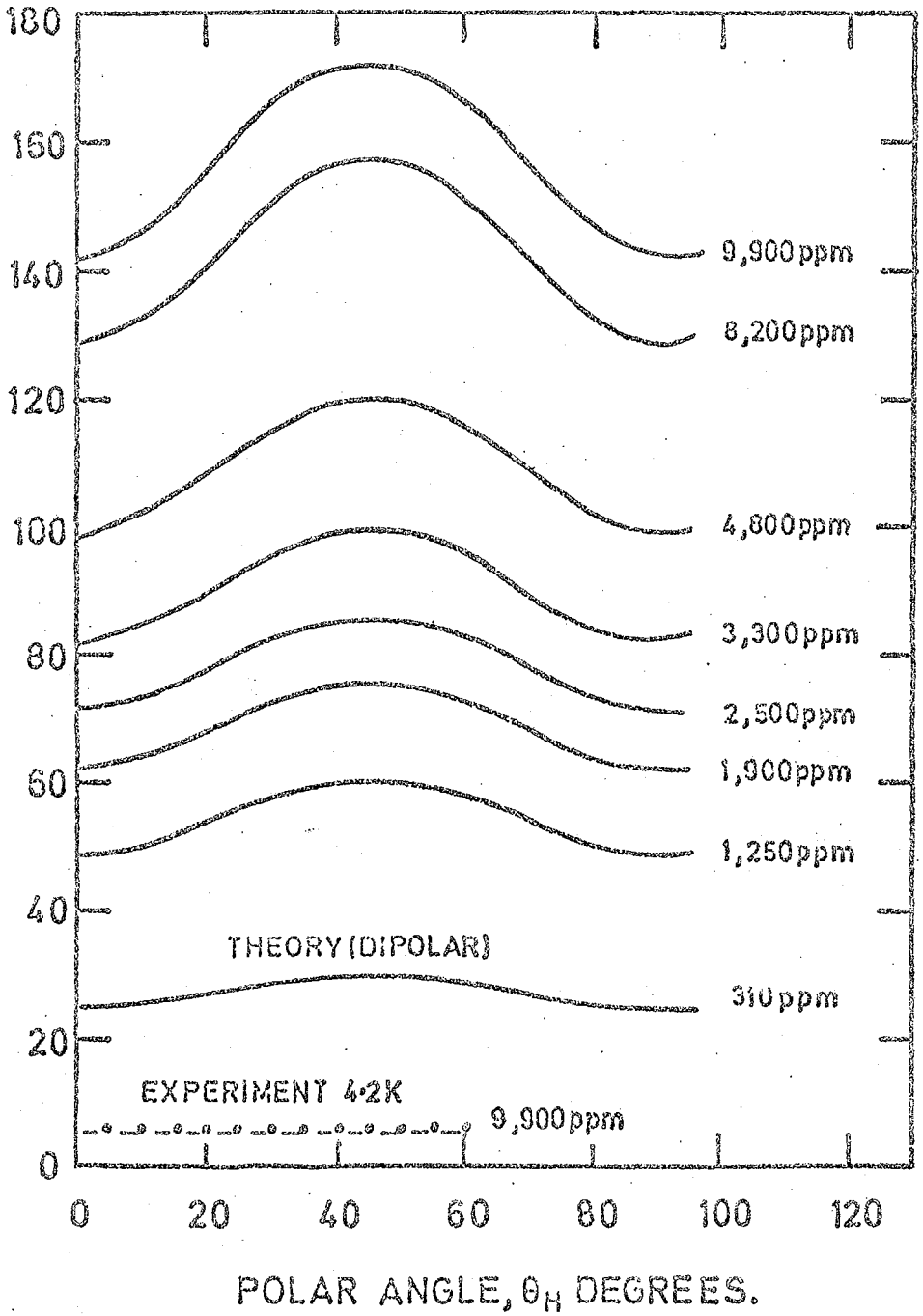

6.5.3. COMPARISON OF PREDICTED AND OBSERVED VARIATION OF LINEWIDTH WITH POLAR ANGLE.

5.4 DISCUSSION

Two salient features emerge from initial comparison between the experimental results for the as-grown crystals and dipolar theory. Firstly, the predicted linewidths are about fifty times larger than the observed linewidths ; secondly, the linewidth appears to be independent of polar angle in contrast to the maximum linewidth at 45^{o} expected for dipolar broadening. The former discrepancy was similar to that encountered with both Fe^{3+}/MgO (5.5) and Cr^{3+}/MgO (5.6). These both showed linewidths of about one hundred times less than the predicted dipolar widths, an effect attributed to exchange narrowing ; the independence of width on polar angle has also been observed in Cr^{3+}/MgO. In Co^{2+}/MgO, the measured linewidth varied from between twelve and fifty times less than predicted by dipolar broadening theory (Table 5.1). This large numerical disparity in Co^{2+}/MgO suggested that there was a strong narrowing mechanism such as had previously been found in both Fe^{3+}/MgO and Cr^{3+}/MgO.

To substantiate the possibility of exchange narrowing within the range of measured concentrations and temperature, additional evidence based on lineshape analysis has been obtained and this data is also given in Table 5.1. To obtain the data,it was considered that in all cases an undistorted lineshape could be obtained from the leading (or trailing) half of the first (or last) line of the octet ; this, when integrated, gave one side of the absorption line. It was also assumed that the line was symmetrical about the mid point. The ratio $M_4^{\frac{1}{4}} / M_2^{\frac{1}{2}}$ (where M_2 and M_4 are respectively the second and fourth moments) was then derived and the results are tabulated in column five of Table 5.1. The values of the ratio are similar to the figures quoted for Fe^{3+}/MgO and Cr^{3+}/MgO (Chapter 4). This suggests that at temperatures between 60 K to 4.2 K exchange narrowing is important, even at the lowest cobalt concentration (310 ppm).

(1) Cobalt concentration in ppm	(2) ΔHms (Dipolar) $\theta_H = 45^\circ$ (mT)	(3) Temperature (k)	(4) ΔHms (obs) (mT)	(5) $\frac{M_4^{\frac{1}{2}}}{M_2^{\frac{1}{2}}}$	(6) $\frac{\Delta Hms\ (obs)}{\Delta H_{\frac{1}{2}}\ (obs)}$
310	30.1	4.2	1.7	1.44	0.57
		20	0.8	1.39	0.57
		60	2.4	1.396	0.61
1,250	60.1	4.2	2.9	1.358	0.58
		20	2.1	1.41	0.55
2,500	86.7	4.2	2.9	1.365	0.48
		20	2.1	1.41	0.64
3,300	99.7	4.2	2.9	1.39	0.47
		20	2.0	1.39	0.51
4,800	120.2	4.2	3.6	1.36	0.50
		20	2.4	1.38	0.57
		60	3.9	1.37	0.55
8,200	157.1	4.2	4.7	1.37	0.69
		20	4.4	1.43	0.65
		60	6.3	1.41	0.58
9,900	172.6	4.2	4.9	1.35	0.63
		20	4.0	1.37	0.54
		60	4.9	1.39	0.67

TABLE 5.1 Lineshape data for a range of cobalt concentration at temperatures of 4.2 K, 20 K and 60 K ; 9.515 GHz, $\theta_H = 0^\circ$

The lineshape factor is defined as the ratio of the peak-to-peak derivative linewidth, ΔHms, to the width of half-height, $\Delta H_{\frac{1}{2}}$, of the absorption curve. The values of this factor for Lorentzian and Gaussian lines are respectively 0.577 and 0.846 (5.7). Exchange narrowing would make the line adopt a Lorentzian shape. To confirm this, the widths at half-height, $\Delta H_{\frac{1}{2}}$, have been calculated from the observed integrated lineshapes and the ratio of $\frac{\Delta Hms}{\Delta H_{\frac{1}{2}}}$ derived ; the values are tabulated in column six of Table 5.1 and show that the lineshapes are more Lorentzian than Gaussian in the range of concentration and temperature used.

The assumption, on the above basis, of an exchange-narrowed model enables evaluation of the exchange energy J to be made by adopting the method used in Chapter 4. The values of J for the different specimens at 4.2 K have been tabulated in column two of Table 5.2. Further, a plot of J against concentration gives a straight line as shown in Fig 5.5. If this line is extrapolated to 50% of the available sites occupied by Co^{2+}, i.e. to the point corresponding to CoO, an exchange energy of 32×10^{11} Hz is obtained. This may be compared with the value for CoO of 1.43×10^{11} Hz obtained from the temperature dependence of susceptibility (5.8) and also with the reported value of $J = 6.298 \times 10^{11}$ Hz as measured from the intensity of pair spectra in Co^{2+}/MgO (5.9).

The values of Weiss constant θ have been calculated from the Weiss molecular field equation

$$3 \; K \; \theta \; = 2 \; J \; z \; S(S + 1) \qquad (5.2)$$

where z is the number of nearest neighbours and K is the Boltzmann constant ; in the MgO lattice z = 6.

Even though the actual spin of Co^{2+} is 3/2, it was observed only the octet of hyperfine lines due to the interaction between an effective spin

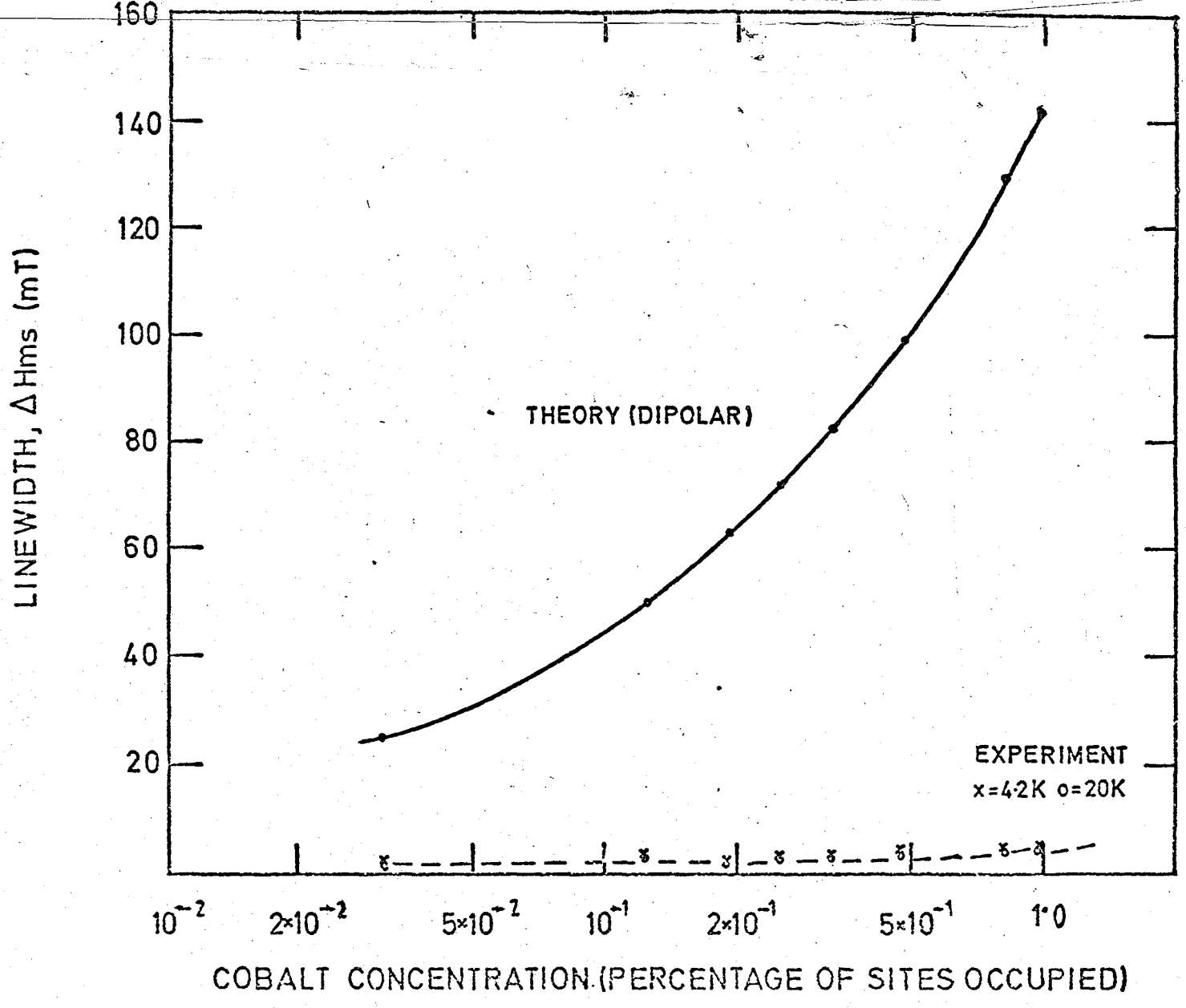

FIG. 5.4 COMPARISON OF PREDICTED AND OBSERVED VARIATION OF LINEWIDTH WITH CONCENTRATION; $\theta_H = 0^\circ$, 9·51 GHz.

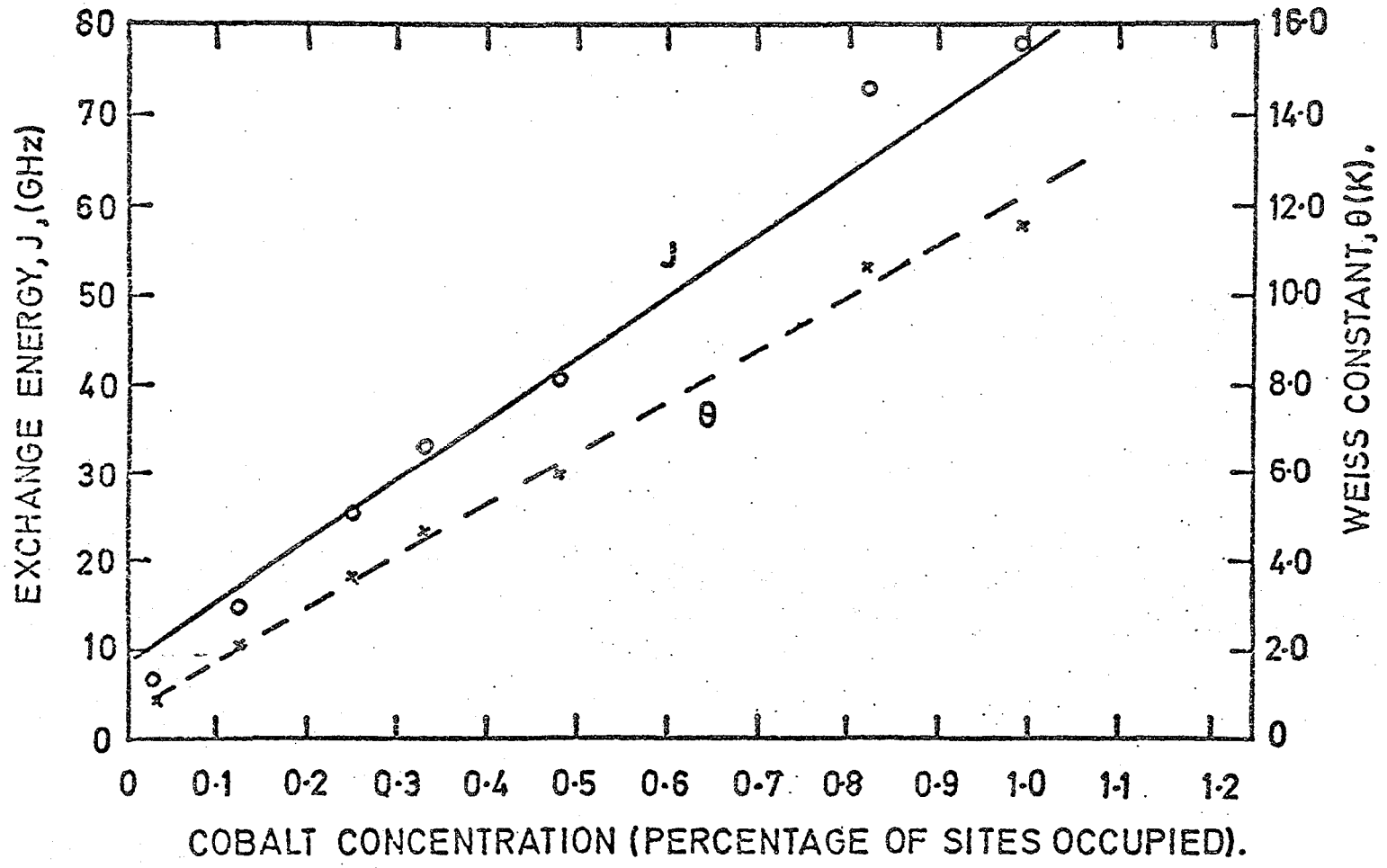

FIG.5.5 THE VARIATION OF J AND θ WITH COBALT CONCENTRATION, 4·2K.

Sample Concentration (ppm)	Exchange Energy (GHz)	Weiss Constant θ (K)
310	6.11	0.88
1250	14.67	2.10
2500	25.48	3.66
3300	33.00	4.75
4800	40.76	5.87
8200	73.74	10.61
9900	77.60	11.17

TABLE 5.2 Evaluation of Exchange Energy and Weiss Constant, for various concentrations of cobalt, 4.2 K.

of $\frac{1}{2}$ and the nuclear spin I = 7/2. Thus taking S = $\frac{1}{2}$, the values of θ have been evaluated from equation 5.2 and tabulated in column three of Table 5.2. Similar effective spin value considerations have been reported in the literature (5.9, 5.10). A plot of θ against concentration also gives a straight line, (Fig 5.5). If this line is extrapolated to the point representing pure CoO, a value of Weiss constant θ = 550 K is obtained. This is comparable to the literature value CoO of 330 K (5.11) and thus supports the validity of assuming S = $\frac{1}{2}$.

The differences in both the intensity and hyperfine energy separation A in the octet spectrum of Co^{2+}/MgO are the same at all temperatures. These effects may be due to cross-relaxation between cobalt ions, an interaction which also is temperature independent. Cross-relaxation would be expected to affect the population distribution in the components of the octet and hence their relative intensities. Cross-relaxation between cobalt ion in MgO has been reported by Pryce (5.3) for specimens containing less than 230 ppm Co, and so cross-relaxation would be very likely at the higher doping levels used in the present work. The increase of linewidth ΔHms in the range of temperature 20 K down to 4.2 K may be due to unresolved hyperfine interaction with the ^{25}Mg nuclide while the increase of linewidth above 40 K can be attributed to relaxation broadening.

REFERENCES

CHAPTER FIVE

5.1 W. Low, Phys. Rev. 109 (1958) 256.

5.2 D.J.I.Fry and P.M.Llewellyn, Proc. Roy. Soc.A 266 (1962) 84.

5.3 M.H.L. Pryce, Proc. Roy. Soc. London, A283 (1965) 433.

5.4 J.C.M. Henning and J.H.Den Boef, Phys. Rev. B14 (1976) 26.

5.5 J.S.Thorp, R.A. Vasquez, C. Adcock, and W. Hutton, J. Mat. Sci. 11 (1976) 89.

5.6 J.S.Thorp, M.D.Hossain and L.J.C.Bluck, J.Mat.Sci. 14 (1979) 2853.

5.7 C.P.Poole, 'Electron Spin Resonance', John Wiley & Sons, N.Y., (1967), p 775.

5.8 P.W.Anderson, Solid State Phys., V-14 (1963) 99.

5.9 S.Geschwind, 'Electron Paramagnetic Resonance', Plenum Press, N.Y. 1972.

5.10 E.B.Tucker, Phys. Rev. 143 (1966) 264.

5.11 C.R.C. Handbook, (Physics and Chemistry), 57th Edit. (1977-78). P.E. 120.

CHAPTER SIX

THE '10/3' EFFECT IN Fe/MgO

In this Chapter electron spin resonance linewidths of Fe^{3+} in single crystal MgO were examined at 9 GHz for crystals having iron concentrations of 2300 ppm and 4300 ppm over the temperature range 293 K to 4.2 K. For the $+\frac{1}{2} \rightarrow -\frac{1}{2}$ transition the linewidth remains constant from 293 K to about 15 K, below which line broadening occurs. From 15 K to 4.2 K the linewidth increases steadily without any change in the g value of the line. At 4.2 K the width of the line is about 3.7 times larger than at 77 K for each concentration. The lineshapes are Lorentzian over the whole temperature range examined and the data suggested that the effects observed below 15 K were due to non-secular line broadening mechanisms (the '10/3' effect) originally proposed by Anderson and Weiss.

6.1 INTRODUCTION

In a recent publication, Thorp et al (6.1) reported that the E.S.R. linewidths of Fe^{3+} in single crystal MgO at 9 GHz were determined by exchange narrowing throughout the temperature range from 293 K to 77 K. These linewidth measurements have now been extended to the liquid helium temperature range, using the same specimens on which high temperature data was available in an attempt to establish which linewidth mechanisms held at lower temperatures. There have been several previous studies of the low temperature E.S.R. behaviour of Fe^{3+}/MgO. Feher (6.2) observed the angular dependence of linewidth for the $+\frac{1}{2} \rightarrow -\frac{1}{2}$ transition of Fe^{3+} in MgO and reported that there was an increase in linewidth in going from 77 K to liquid helium temperatures. In a sample containing 200 ppm Fe^{3+} Feher found that, at 10 GHz, the linewidth at 1.2 K was about 2.5 times larger than that at 77 K, but gave no explanation. Stoneham et al (6.3) also reported that the E.S.R. linewidth of Fe^{3+} in single crystal MgO at 19.4 GHz was broadened as a function of decreasing temperature in the liquid helium range and suggested that this resulted from motional narrowing of the linewidth due to dipolar interaction with Fe^{2+} ions. In the present measurements any contribution to linewidth resulting from motional narrowing due to Fe^{2+} ions can be neglected for the following reasons. In the MgO crystals used by Stoneham et al the ratio of Fe^{2+} to Fe^{3+} ions was 4:1. Here, however the crystals (which contained a detectable amount of Fe^{2+} in the as-grown state (6.1)) were heat treated in air at 1200° C for about 30 hours. Evidence from the X-ray and E.S.R. measurements made by Cordischi et al (6.4) shows that heating to 700° C in air for about five hours is sufficient to oxidise Fe^{2+} completely to Fe^{3+} ; consequently, effects attributable to Fe^{2+} could be neglected.

Line broadening due to non-secular mechanisms, often called the 1O/3 effect, was first proposed by Anderson and Weiss in 1953 (6.5) in connection with the line broadening in some paramagnetic salts such as $Fe_2(SO_4)_3$, $Fe(NH_4)(SO_4)_2$, $MnSO_4$ and $MnCl_2$. A more detailed theoretical treatment was given by Kubo and Tomita in 1954 (6.6). Further experimental evidence was obtained by several workers including Abe et al (6.7, 6.8) in the single crystals of potassium cupric chloride ; ammonium cupric chloride and coppertrichloroacetate monohydrate, Rogers et al (6.9) in D.P.P.H. and Henderson et al (6.10) in potassium cupric chloride. The '$1O/3$' effect refers to the increase in magnetic resonance linewidth which occurs in an exchange narrowed situation when the Zeeman frequency becomes comparable to the effective exchange frequency ; in the theoretical treatments it is explained by the inclusion of non-secular spin-spin terms.

6.2 EXPERIMENTAL RESULTS

The iron concentrations in the crystals were 2300 ppm and 4300 ppm respectively. For both crystals, the linewidth observed for the $+\frac{1}{2} \leftrightarrow -\frac{1}{2}$ transition at any particular value of Θ_H remained constant throughout the temperature range 293 K to about 15 K. However, there is, as reported previously (6.1), a variation of linewidth with polar angle. Below 15 K the linewidth increases rapidly without any change in the g value of the line. The spectra of one of the samples is shown in Figure 6.1, which refers to a specimen containing 2300 ppm Fe^{3+} taken at $\Theta_H = 0^o$. In Figure 6.2 the observed peak-to-peak widths are plotted as a function of temperature. The linewidths, defined as the width between points of maximum slope (ΔH_{ms}), were obtained directly from the derivative plots. For each sample the width at 4.2 K was about 3.7 times larger than that observed at 77 K.

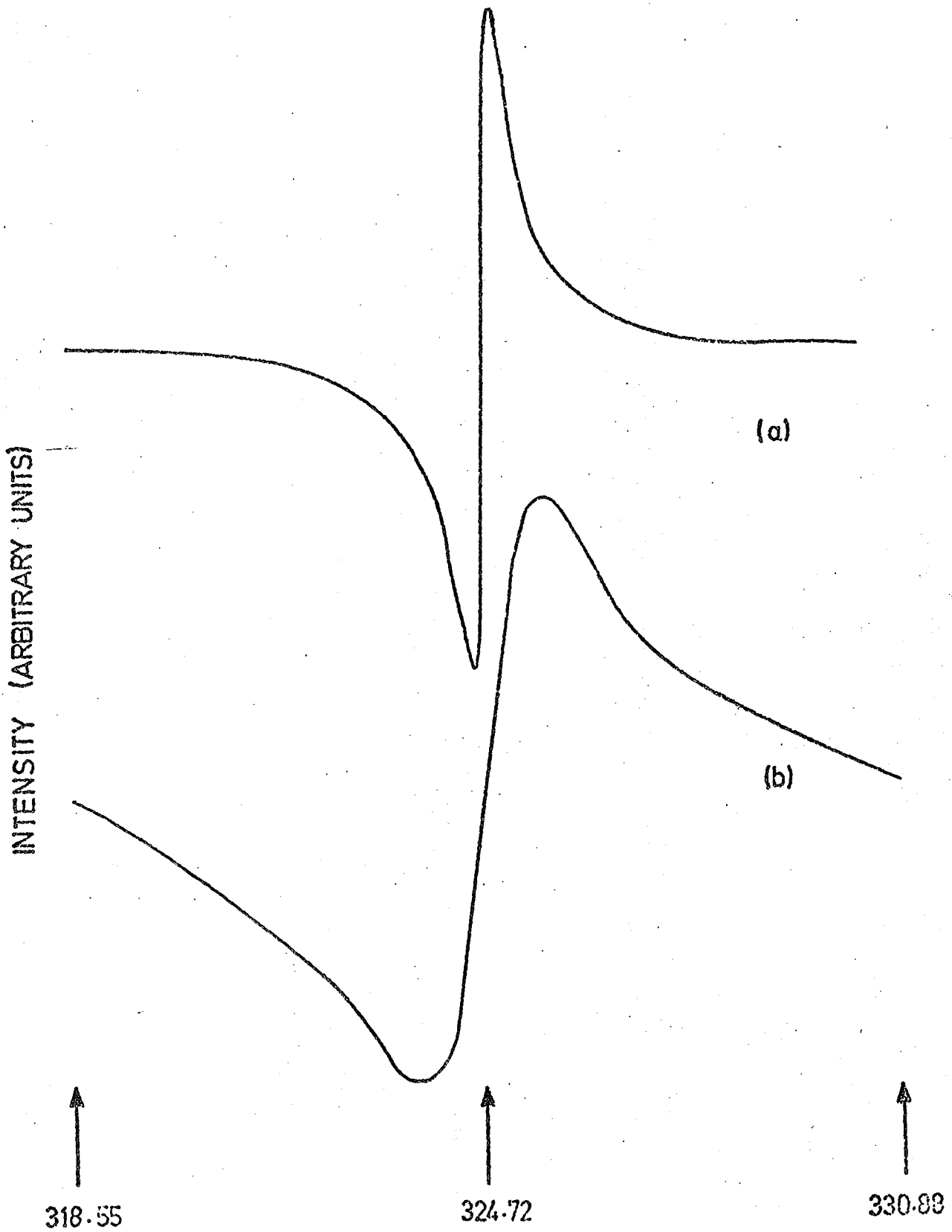

FIG. 6.1 DERIVATIVE LINESHAPE OF $-\frac{1}{2} \longleftrightarrow +\frac{1}{2}$ TRANSITION Fe^{3+}/MgO (2300ppm), (a) 77K, (b) 4·2 K; $\Theta_H = 0°$, 9·1 GHz.

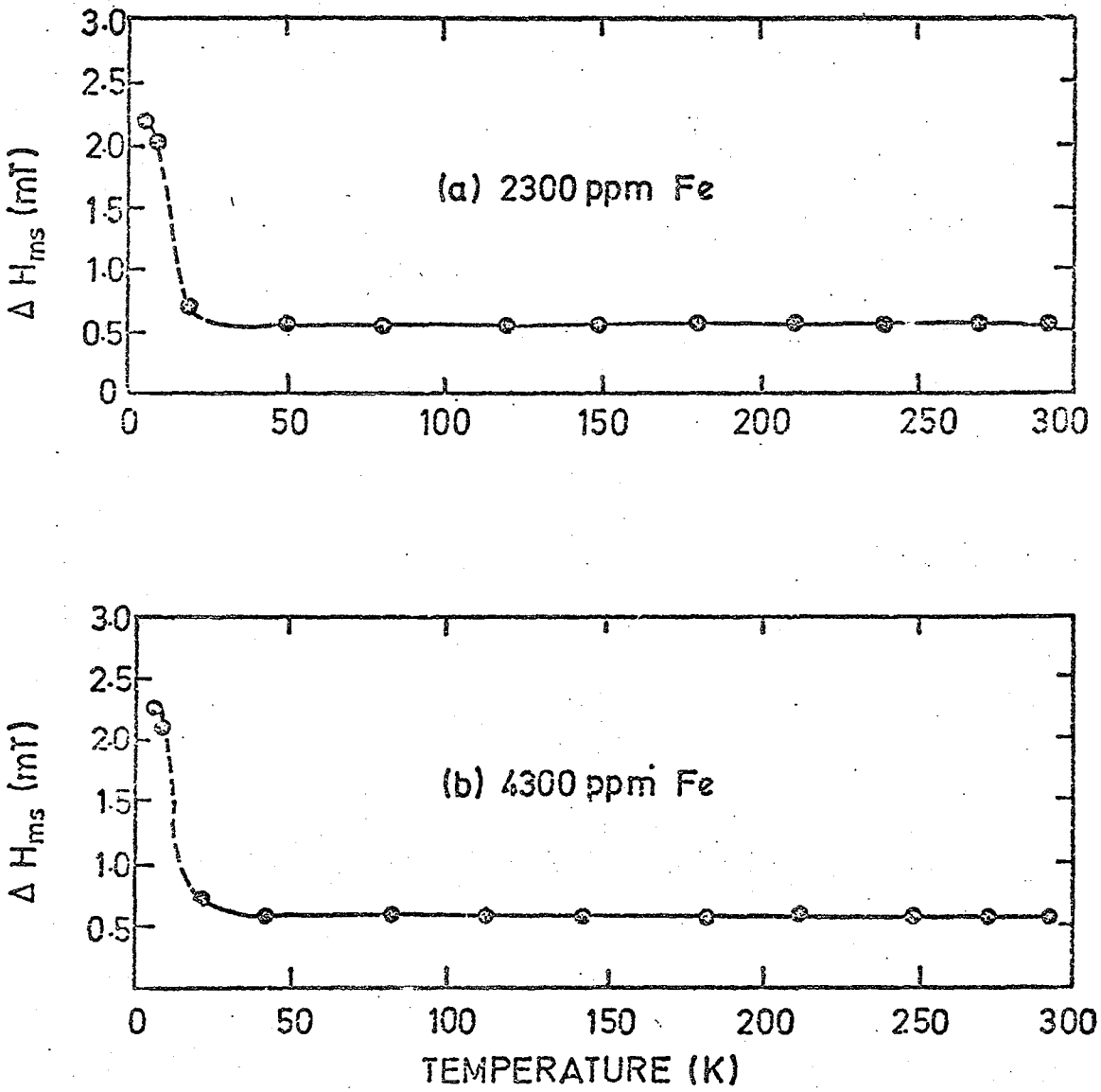

FIG. 6.2 TEMPERATURE DEPENDENCE OF THE LINE WIDTH; $\theta_H = 0°$
9.1 GHz $\frac{1}{2} \leftrightarrow -\frac{1}{2}$ TRANSITION.

6.3 DISCUSSION

To examine the nature of the interactions involved in the line broadening at low temperatures lineshape analysis and moment calculations were made, following the methods described in Chapter 4 ; the results are tabulated in Table 6.1.

The data of Table 6.1 showed that the observed linewidths at 4.2 K were about 3.7 times larger than that at 77 K. Even so, these broadened linewidths were still very much less than the values predicted on the basis of the known concentrations by dipolar theory which strongly suggested that they were not determined by dipolar interactions. Analysis of the lineshapes showed, firstly, that the values of the ratio $M_4^{\frac{1}{4}}/M_2^{\frac{1}{2}}$ (where M_2 and M_4 are respectively the second and fourth moments) at low temperatures were similar to the figures quoted elsewhere (6.1) for exchange narrowed E.S.R. lines and, secondly, that the values of the ratio $\Delta H_{ms}/\Delta H_{\frac{1}{2}}$ (where ΔH_{ms} is the derivative linewidth and $\Delta H_{\frac{1}{2}}$ is the width of the integrated line at half-height) were consistent with those expected for Lorentzian lineshapes. An example is shown in Figure 6.3, which refers to a crystal containing 2300 ppm Fe^{3+}. This evidence indicated that exchange narrowing mechanisms were present and were indeed the dominant factor affecting the linewidth at all temperature down to 4.2 K.

To establish whether the exchange energy was comparable to the Zeeman energy, values of J were derived from the spectra recorded at 4.2 K. The half linewidth ($\Delta\omega$) expressed in frequency units is related to $\Delta H_{\frac{1}{2}}$ by $\Delta\omega = \frac{2\pi g\beta}{h} \cdot \left[\frac{1}{2}.\Delta H_{\frac{1}{2}} \right]$ and the exchange energy (J) is related to $\Delta\omega$ by

$$\Delta\omega \qquad \frac{<\Delta\omega^2>\ \text{dipolar}}{J/\hbar}$$

in which $<\Delta\omega^2>$ is the second moment of the line and is dependent on con-

Iron concentration ppm.	Temperature (k)	Experimental linewidths (mT)	Calculated dipolar linewidth (mT) Ref-(6.1)	Moment Ratio $M_4^{\frac{1}{2}} / M_2^{\frac{1}{2}}$	ΔH_{ms} (obs) / $\Delta H_{\frac{1}{2}}$ (obs)
2300	77	0.58	42.58	1.40	0.452
	4.2	2.20	42.58	1.35	0.414
4300	77	0.63	58.44	1.41	0.570
	4.2	2.38	58.44	1.34	0.545

Table 6.1 : Lineshape Data of Fe^{3+}/MgO at 77k and 4.2k.

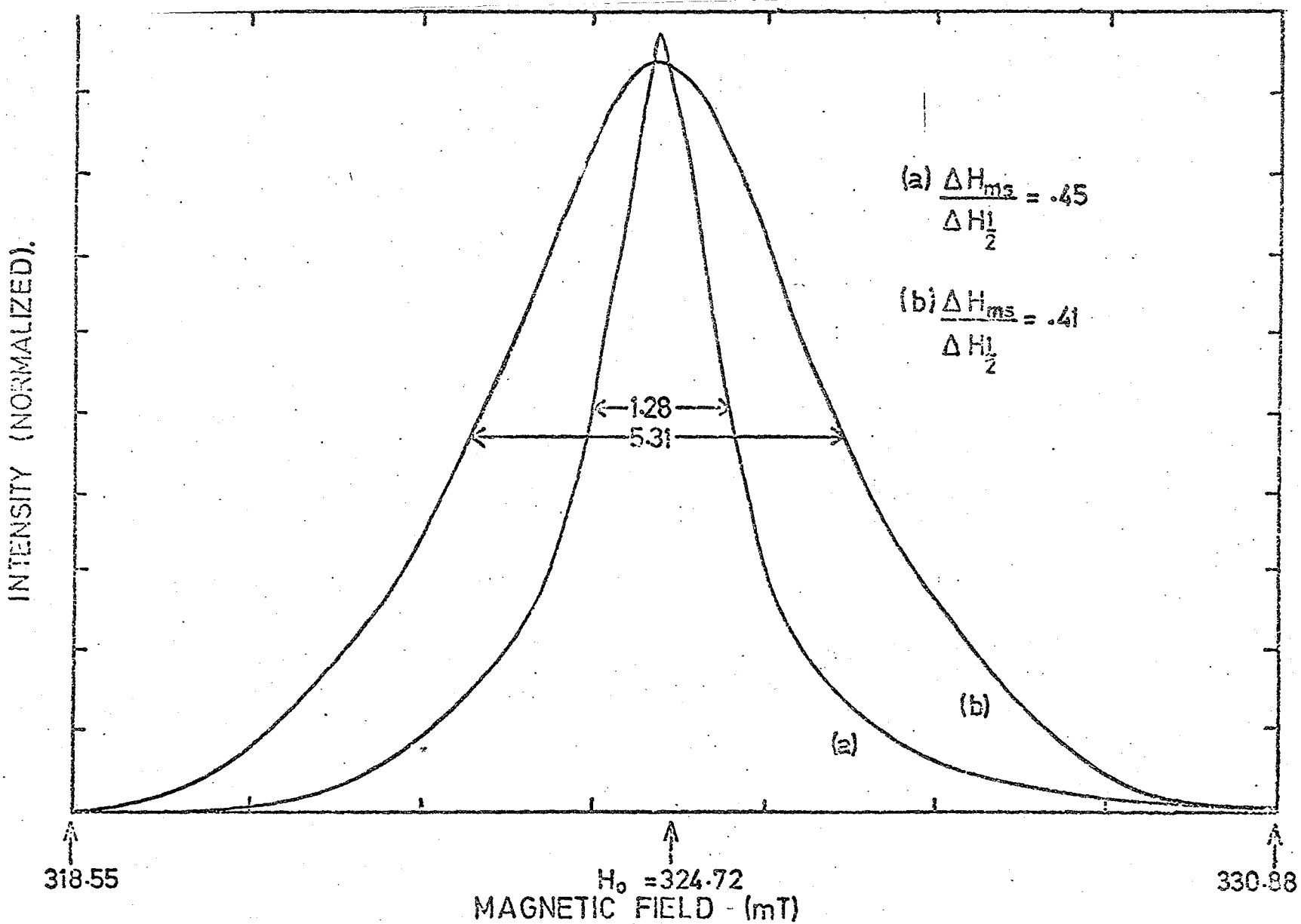

FIG. 6,3 INTEGRATED LINESHAPES FOR $-\frac{1}{2} \leftrightarrow +\frac{1}{2}$ TRANSITION, (2300 ppm Fe); (a) 77 K, (b) 4·2 K; $\Theta_H = 0°$, 9·1 GHz.

centration (6.1). The comparison is given in Table 6.2, which shows that, in particular for the lower concentration, the values are comparable.

Iron Concentration (ppm)	Temperature (K)	Exchange Energy (GHz)	Zeeman Energy (GHz)
2300	4.2	6.375	9.1
4300	4.2	14.56	9.1

TABLE 6.2 : Comparison between Exchange Energy and Zeeman Energy

It has been reported by Abe et al (6.8) in the crystal copper-trichloracetate that the '10/3 effect' was reduced and its onset shifted towards lower temperatures as the resonance frequency increased from 9 GHz to 23 GHz ; the observed lineshape remained Lorentzian throughout the temperature range from 293 K to 4.2 K. Kubo and Tomita (6.6) showed theoretically that the '10/3 effect' should become smaller at shorter wavelengths (i.e. $\omega_o >> \omega_{exch.}$) because of the disappearance of the non-secular broadening. Some Japanese experiments show that the 10/3 factor tends to disappear if one goes to high microwave frequencies ; for example, Ono et al (6.11) found in the crystal $CuK_2Cl_4:2H_2O$ that the '10/3 effect' which was pronounced at 9.96 GHz had completely disappeared at 38.9 GHz. This conclusion appears to be confirmed by the results of Ammer et al (6.12) and Vasquez (6.13) who did not report any line broadening at liquid helium temperatures and 35.5 GHz in the same Fe^{3+}/MgO specimens as used here.

There are several other possible sources of line broadening. These include broadening due to strain, described by Feher (6.2), and broadening due to point defects and dislocations ; discussed by Stoneham (6.14). However, Feher reported that the effect of strain broadening on the $+\frac{1}{2} \leftrightarrow -\frac{1}{2}$ transition of Fe^{3+}/MgO is negligible ;furthermore, the point defect broadening is not likely to be important because it arises from size difference effects and here the value of ionic radius of the Fe^{3+} (0.645 $\mathring{A}$) is less than that of Mg^{2+} (0.72 $\mathring{A}$) (6.15). A further possible source of broadening is an inhomogeneous distribution of dislocations which would produce a nearly Gaussian lineshape (6.14). It has also been shown theoretically by Sabirov (6.16) that the width of the resonance line of an exchanged narrowed line may be increased and its shape may become Gaussian at low temperature, when $\omega >> kT$, where ω is the Larmor spin frequency ; however, in this experimental situation $kT >> \omega$. It cannot rule out the possibility of some contributions to line broadening due to unresolved hyperfine lines of ^{57}Fe, $I = \frac{1}{2}$; which have been found experimentally (6.17, 6.18) at 20 K and have a hyperfine constant A = 10 Gauss. The broadening from unresolved hyperfine structure results in a Gaussian lineshape (6.14). In these crystals the observed lineshape is Lorentzian, so none of the mechanisms leading to a Gaussian lineshape can be important.

In summary, the present experiments confirm that exchange narrowing mechanisms dominate the linewidth over the whole temperature range from 77 K to 4.2 K. The observed linewidths at 4.2 K, under conditions where the exchange energy was comparable with the Zeeman energy, were 3.7 times larger than at 77 K ; this compares well with the value of 3.3 predicted by theory and the results show that the '$^{10}/_{3}$ effect' is operative in the liquid helium temperature range.

REFERENCES

CHAPTER SIX

6.1 J.S. Thorp, R.A. Vasquez, C.Adcock and W.Hutton, J.Mat.Sci.11 (1966) 89,

6.2 E.R.Feher, Phys. Rev. 136 (1964) A145.

6.3 A.M.Stoneham, K.A.Muller and W.Berlinger, Solid Stat.Com.10 (1972) 1,005.

6.4 D. Cordischi, D.Gazzahi and M.Valigi, J.Solid State Chem.24 (1978) 371.

6.5 P.W.Anderson and P.R.Weiss, Rev.Mod.Phys. 25 (1953) 269.

6.6 R.Kubo and K.Tomita, J.Phys. Soc. Japan 9 (1954) 888.

6.7 H.Abe, K.Ono, I.Hogashi, J.Shimada and K.I.Wanage, J.Phys.Soc. Japan, 9 (1954) 814.

6.8 H.Abe and H.Morigarlci, 'Paramagnetic Resonance , V.2', p.587. Edt. W. Low. Acad. Press, N.Y. 1963.

6.9 R.N. Rogers, M.E.Anderson and A.E.Parke, Bull.Amer. Phys. Soc. 6 (1959) 261.

6.10 A.J.Henderson, Jr. and R.N. Rogers, Phys. Rev. 152 (1966) 218.

6.11 K.Ono, H. Abe, J. Shimada, Phys. Rev. 92 (1953) 551.

6.12 E.A.E. Ammar and J.S.Thorp, J.Mat.Sci. 12(1977) 2,087.

6.13 R.A.Vasquez, M.Sc. Thesis, Durham University, (1975) (unpublished).

6.14 A.M.Stoneham, Rev.Mod.Phys. 41 (1969) 82.

6.15 R.D.Shannon and C.T.Prewitt, Acta, Cryst. B 25 (1969) 925.

6.16 R.Kh. Sabirov, Sov.J. Low Temp. Phys. 4 (1978) 169.

6.17 B. Henderson, J.E.Wertz, T.P.P.Hall and R.U.Dowsing, J.Phys. C4 (1971) 107.

6.18 P.R.Locker and S.Geschwind, Phys.Rev, 139 (1965) A991.

CHAPTER SEVEN

LINE BROADENING IN Cr^{3+}/MgO AT LIQUID HELIUM TEMPERATURES

In this Chapter line broadening has been observed at 9 GHz in the E.S.R. absorption spectrum of Cr^{3+} in MgO in the liquid helium temperature range, for a range of Cr^{3+} concentrations from 800 ppm to 7400 ppm. The broadened linewidths at 4.2 K are about two times larger than at 77 K and depend on polar angle. The lineshapes are Gaussian, in contrast to the Lorentzian lineshape between 293 K to 77 K. The broadening is interpreted by the combined effects of strain, due to the charge misfit of Cr^{3+} and the host cation, and temperature which causes both exchange striction and departure from the cubic symmetry to a lower symmetry. Analysis of the linewidth data gives $D = (5.25 \pm 0.40) \times 10^{-4}$ cm^{-1} and confirms that the total linewidth, ΔH_t, is given by

$$\Delta H_t = \Delta H_o + \left| \frac{2\Delta D}{g} \cos \Theta_H \right|$$

where ΔH_o is the linewidth independent of concentration, temperature and polar angle Θ_H.

7.1 INTRODUCTION

The electron spin resonance (E.S.R.) linewidths for transition metal ions in diamagnetic host crystals can arise from various mechanism. Firstly, there is homogeneous broadening which includes effects due to interaction of the spin system with lattice vibrations, dipole-dipole interactions between like and unlike spins, fluctuations in the microwave frequency and variations in the relative slope of Zeeman split energy levels. Secondly, inhomogeneous broadening processes must be considered and these include the effects of unresolved nuclear hyperfine structure, thermal fluctuations in the crystalline field parameters and local strain produced in the vicinity of the impurity ion by defects which arise in effecting charge compensation if the impurity ion has a valency differing from that of the host cation. In addition, other mechanisms may occur in special circumstances as, for example, broadening due to the '$10_{/3}$ effect' (7.1).

The present work has examined the linewidths of Cr^{3+} occurring as substitutional ions in MgO (7.2,7.3) in the liquid helium temperature range ; previous studies (3) had shown that the linewidth was determined by exchange narrowing at temperatures down to 77 K.

Chromium doped MgO in which Cr^{3+} is in cubic symmetry has been studied extensively by means of E.S.R. (7.2-7.8). The Cr^{3+} ion has the $3d^3$ electronic configuration. In a crystal field of cubic (octahedral) symmetry the ground state is an orbitally non-degenerate $^4A_2$ (^4F) state with spin $S = \frac{3}{2}$. Since zero field splitting is absent (7.2,7.3) at perfectly cubic sites, the allowed E.S.R. transitions $\left(+\frac{3}{2} \nrightarrow +\frac{1}{2}\right)$, $\left(+\frac{1}{2} \nrightarrow -\frac{1}{2}\right)$ and $\left(-\frac{1}{2} \nrightarrow -\frac{3}{2}\right)$ coincide and a single E.S.R. line should result ; however, a fourfold hyperfine spectrum due to the isotope $^{53}Cr\left(I = \frac{3}{2}\right)$ and having a separation of about 16.3×10^{-4} cm^{-1} between

successive components has been observed (7.2,7.3,7.9) ; super hyperfine lines due to neighbouring ^{25}Mg nuclides have also been reported (7.10). The temperature dependence of the axial field splitting D of charge compensated Cr^{3+} ions in MgO and the isotopic shift in the crystalline field energy between ^{52}Cr and ^{53}Cr has been reported both experimentally (7.12) and theoretically (7.13) to be maximum at low temperature ; the pressure dependence of the isotopic g shift has also been reported (7.14). However, the hyperfine splitting constant A has been found to be independent of temperature. Dipolar coupling to paramagnetic impurities other than cubic Cr^{3+} and anisotropic hyperfine coupling to Mg^{25} were considered (7.15) as a source of inhomogeneous broadening at liquid helium temperatures.

The linewidths of Cr^{3+} in cubic sites of MgO in the range of temperature 293 K to 77 K measured by the author (as described in Chapter 4) were determined by exchange narrowing and the linewidth was independent of both temperature and concentration. Here, by contrast, the observed linewidths at liquid helium temperatures increase with decreasing temperature.

7.2 EXPERIMENTAL RESULTS

The chromium concentrations in the specimens examined ranged from 800 ppm to 7400 ppm ; these samples had been used in the previous study (as described in Chapter 4).

Initial measurements were taken to establish the form of the spectrum at 4.2 K in each specimen. An example of this is shown in Figure 7.1, which refers to a specimen containing 800 ppm Cr^{3+} examined at 4.2 K and 77 K. Other low and medium concentration samples similarly showed a broader linewidth at 4.2 K than at 77 K. For concentrations up to 7400 ppm Cr^{3+} the 4.2 K linewidth was rather more than two times the 77 K linewidth. There was no change in resonance field with temperature down to 4.2 K. The variation of linewidth with polar angle θ_H has also

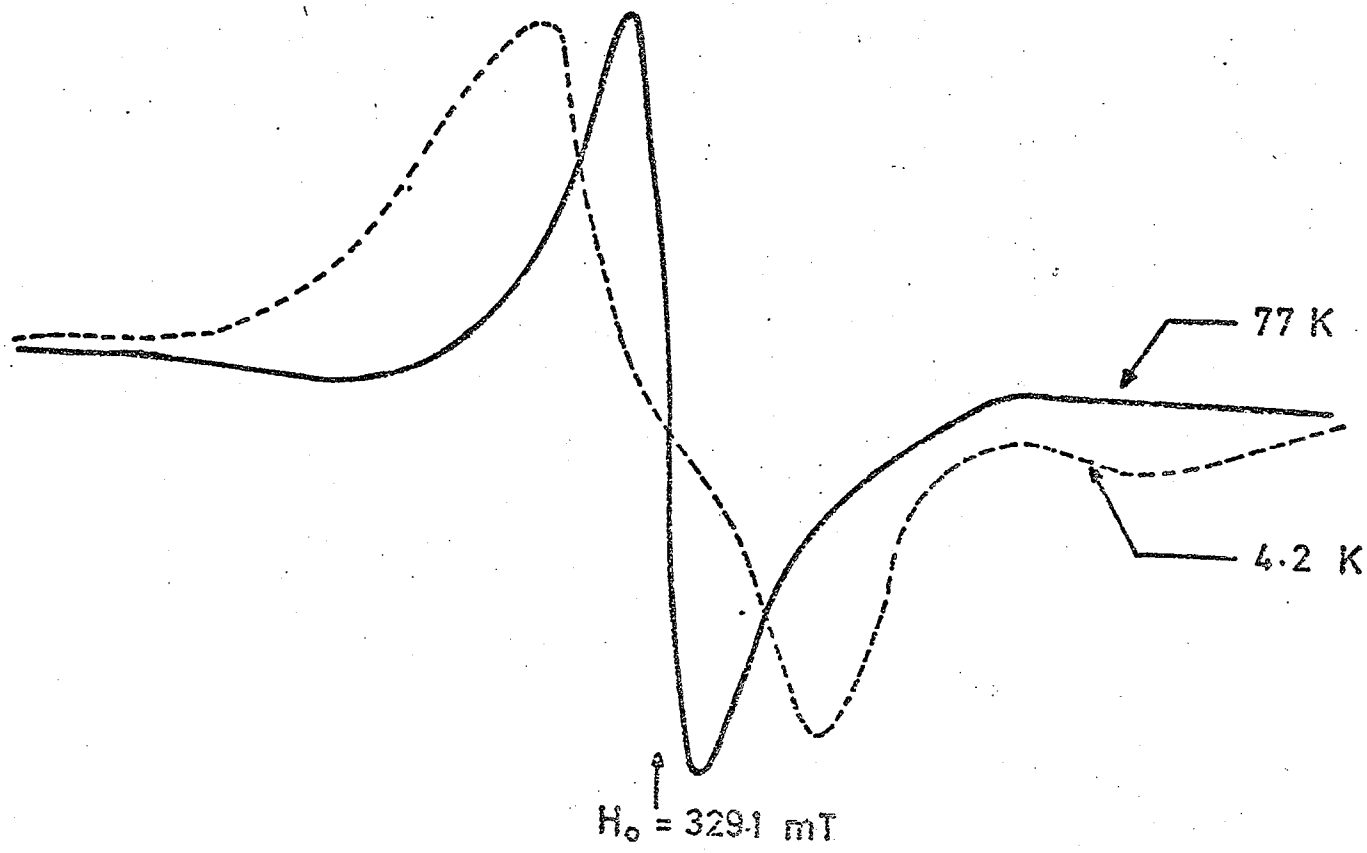

FIG. 7.1 LINE BROADENING OF $\frac{1}{2}$ TO $-\frac{1}{2}$ TRANSITION OF Cr^{3+}/MgO: 77 K & 4.2 K, $\theta_H = 0°$, 9.12 GHz, 800 ppm Cr.

been found in the liquid helium temperature range and for a specimen containing 800 ppm Cr^{3+}, is shown in Figure 7.2. The maximum linewidths were observed at $\theta_H = 0^o$. A linewidth variation with temperature has been found only below about 15 K and above 15 K the width of the resonance line was independent of temperature as shown in Figure 7.3.

7.3 DISCUSSION

Three salient features emerge from an initial comparison between the experimental 4.2 K results for the as-grown crystals and those described for temperatures above 77 K (in Chapter 4). In the first place, the observed linewidths are about two times larger than the observed 77 K values (Chapter 4). Secondly, the linewidths are dependent on polar angle. Thirdly, the lineshapes are Gaussian in contrast to the Lorentzian lineshape (Chapter 4) found between 293 K and 77 K.

Though the line is broadened at liquid helium temperature, yet the observed linewidth is about 50 times less than that predicted from the dipolar broadening theory (Chapter 4). The ratios $M_4^{\frac{1}{4}}/M_2^{\frac{1}{2}}$ (where M_2 and M_4 are respectively the second and fourth moments) were greater than unity, as shown in Table 7.1, which indicated that exchange narrowing is still present at low temperature. In Fe^{3+}/MgO broadening due to the '10/3' effect under exchange narrowing conditions at liquid helium temperatures has been described in Chapter 6. The '10/3' effect predicts a Lorentzian lineshape, unlike the lineshape observed here in Cr^{3+}/MgO ; details of the lineshape analysis are given in Figure 7.4 and Table 7.1. A close examination of the absorption lineshapes, shown in Figure 4, reveals a pair of shoulders. These are indicative of the fact that in a slightly distorted octahedral field, the $\pm\frac{3}{2} \leftrightarrow \pm\frac{1}{2}$ transitions occur at field values slightly different from that of the $\pm\frac{1}{2}$ transition. Similar shoulders on the absorption line of Cr^{3+}/MgO have been reported (7.17). The possible broadening mechanisms are considered now.

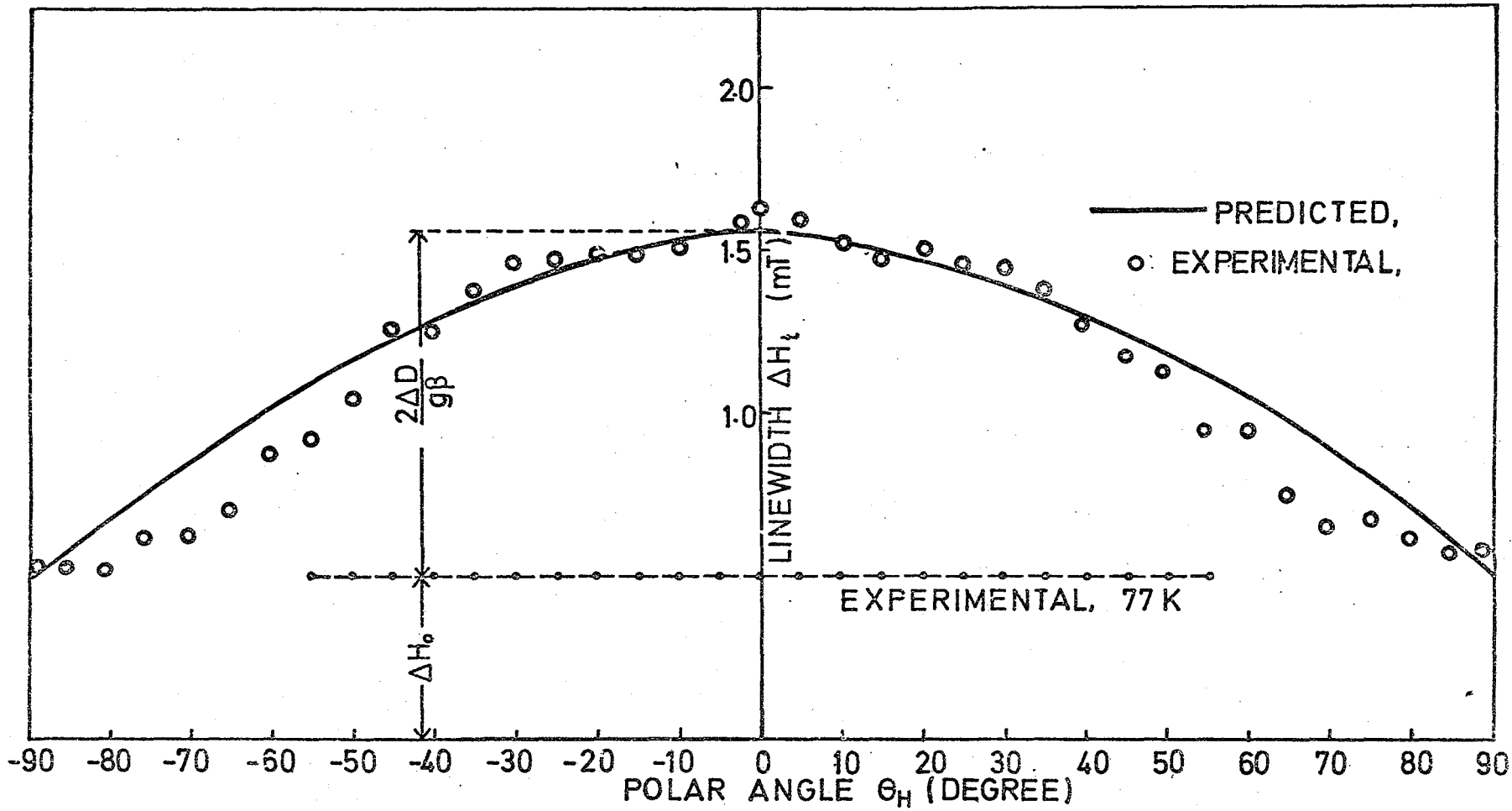

FIG, 7.2 LINEWIDTH VARIATION WITH POLAR ANGLE θ_H, Cr^{3+}/MgO (800ppm), 4·2 K, 9·12 GHz.

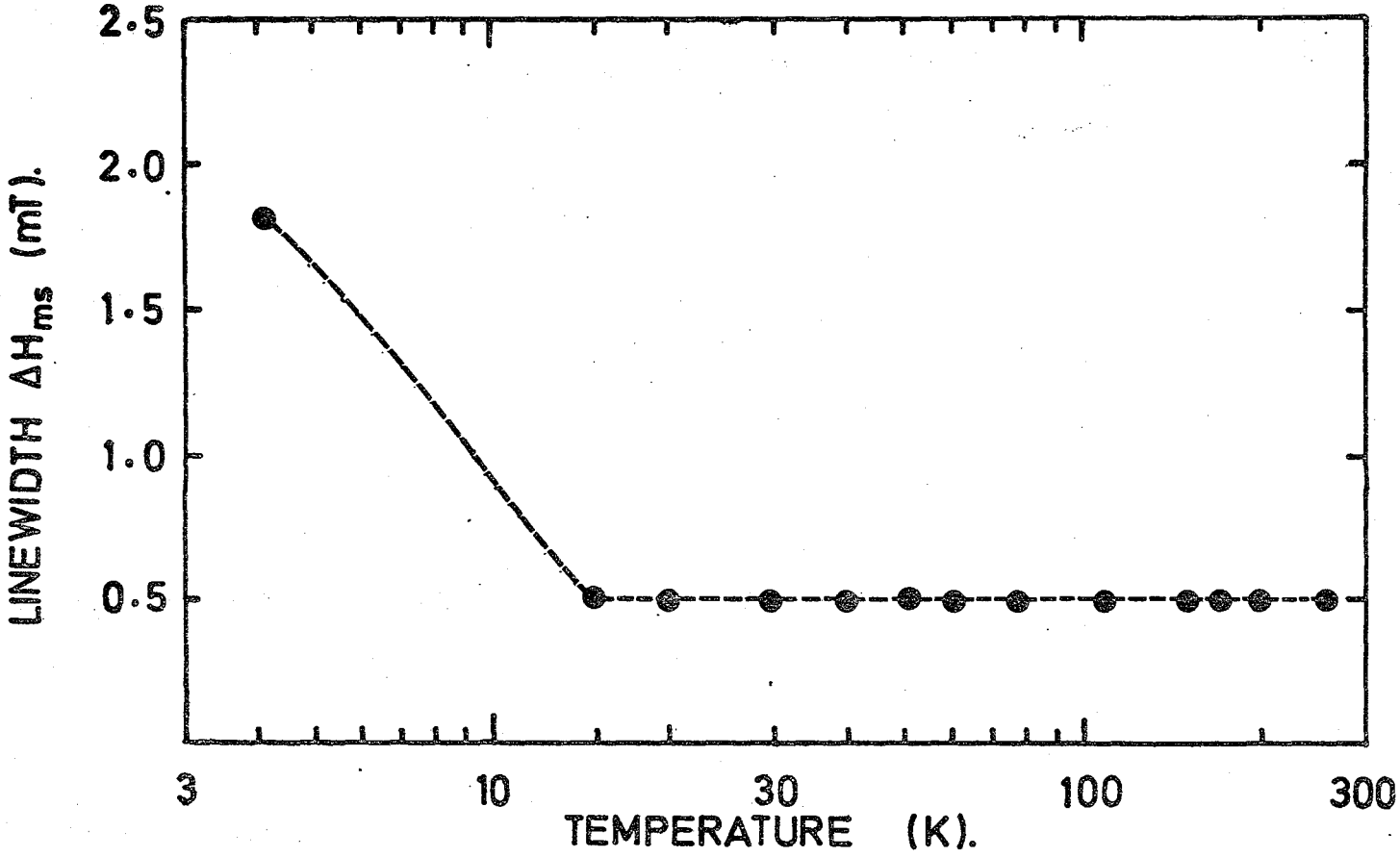

FIG. 7.3 VARIATION OF LINEWIDTH VS. TEMPERATURE; 9.1 GHz, $\theta_H = 0^\circ$, Cr^{3+}/MgO (800 ppm).

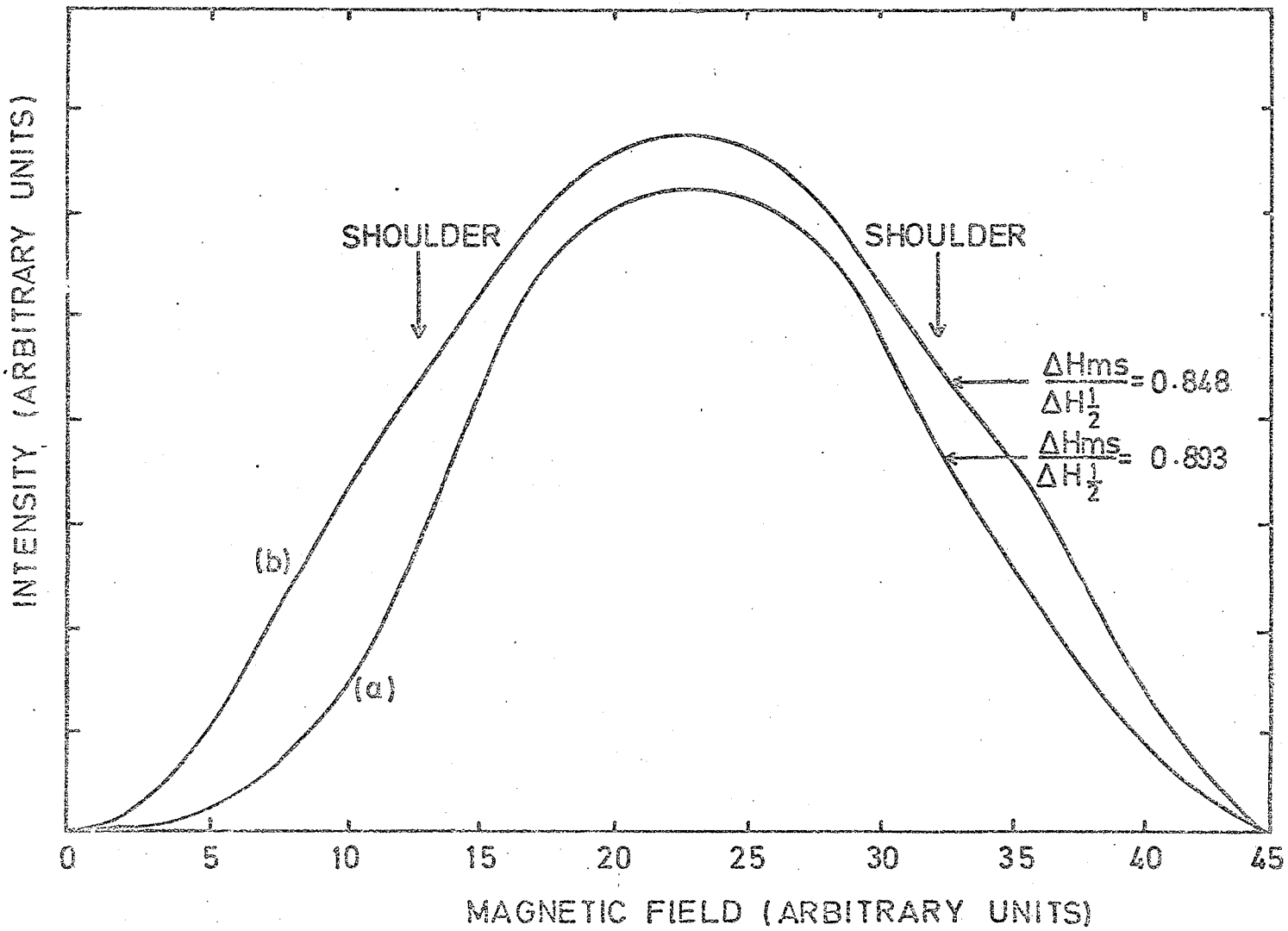

FIG.7.4. COMPARISON OF INTEGRATED LINESHAPES FOR (a) 7400 ppm AND (b) 800 ppm Cr AT 4.2 K, 9.1 GHz, $\theta_H = 0°$.

Chromium Concentration (ppm)	ΔHms (Obs) at 77K (mT)	ΔHms (Obs) at 4.2K	$\frac{M_4^{\frac{1}{2}}}{M_2^{\frac{1}{2}}}$ * at 4.2K	$\frac{\Delta Hms\,(Obs)}{\Delta H_{\frac{1}{2}}\,(Obs)}$ * at 4.2K	Lineshape	ΔD (cm^{-1})
800	0.50	1.60	1.226	0.848	Gaussian	5.08×10^{-4}
1300	0.60	1.82	1.259	0.776	Nearer to Gaussian	5.17×10^{-4}
3600	0.80	2.06	1.251	0.960	Gaussian	5.72×10^{-4}
4200	0.60	1.58	1.26	0.821	Nearer to Gaussian	4.53×10^{-4}
5000	0.70	1.86	1.28	0.839	Nearer to Gaussian	5.36×10^{-4}
6200	0.60	1.84	1.345	1.02	Gaussian	5.82×10^{-4}
7400	0.60	1.70	1.274	0.948	Gaussian	5.08×10^{-4}

TABLE 7.1 Lineshape data for a range of chromium concentration together with derived values of ΔD ; 9.1 GHz; 4.2K ; $\theta_H = 0^\circ$.

*Figures in column 4 and 5 have been obtained by using the procedure described in Chapter 4.

The Cr^{3+} ions occupy the Mg^{2+} sites substitutionally (7.2,7.3). The extra positive charge on the trivalent Cr^{3+} must be compensated for to ensure stability. It has been reported that in Cr^{3+}/MgO (7.5) and Fe^{3+}/MgO (7.18) charge compensation is affected by Mg^{2+} vacancies located along one of the cube axes. One would expect that these vacancies are distributed throughout the crystal at random. The uneven localized charge distribution of the vacancies probably causes Cr^{3+} to be slightly displaced from the original crystal lattice positions. The temperature dependence of the crystal field splitting due to thermal expansion of the host crystal has been reported (7.11). Presumably, due to the combined effect of temperature and displacements, a distortion from octahedral symmetry will result ; this will cause some zero field splitting, which would explain the splitting of the resonance line to $M = \pm \frac{3}{2} \leftrightarrow \pm\frac{1}{2}$ at low temperatures. Similar splitting of the spectrum of Cr^{3+} in chrom alum in isomorphous aluminium alum has been reported at about 160 K (7.19),although a single line was observed at room temperature. In addition, these distortions in the crystal may play a role in exchange striction (7.20), the phenomenon whereby the lattice tends to distort so as to lower the exchange energy until it is balanced by elastic forces. So, the broadening observed here at low temperature may be strain broadening, due to a charge misfit of Cr^{3+} from the host cation. The strain model has been used to explain the anisotropic broadening of Mn^{2+}, Fe^{3+} and Cr^{3+} E.S.R. absorption lines in MgO (7.21, 7.22) and optical absorption lines of Cr^{3+}/MgO at low temperatures (7.23).

Another possible source of line broadening, described by Stoneham (7.24) is due to point defects. The point defect model arises essentially from a size difference effect and is not likely to make an important contribution here because the ionic radius of the doping ion

(Cr^{3+}, 0.615 Å) is less than that of the cation (Mg^{2+}, 0.72 Å), (7.25).

To explain the spectrum at low temperature, one could use the spin Hamiltonian (neglecting hyperfine interaction).

$$H_s = g\beta H.S_z + D\left(S^2_z - \frac{5}{4}\right) \qquad (7.1)$$

Since Cr^{3+} has $S = \frac{3}{2}$, and three lines would be observed representing the transitions

$$\left.\begin{aligned} W \pm \tfrac{3}{2} &\rightarrow W \pm \tfrac{1}{2} = g\beta H \pm 2D \\ W + \tfrac{1}{2} &\rightarrow W - \tfrac{1}{2} = g\beta H \end{aligned}\right\} \qquad (7.2)$$

But it did not show three resolved lines, rather a single broad line. Because of this, it was not possible to measure the value of D exactly, but the change in D was determined by taking the difference in the positions of the peaks of the derivative lines observed at 77 K and 4.2 K. The shift of peak along the magnetic field axis due to the internal strain is $\frac{\Delta D}{g\beta}$ and the best estimate of ΔD, as shown in column 7 of Table 7.1, is $(5.25 \pm 0.40) \times 10^{-4}$ cm^{-1}. This is comparable to the value of $\Delta D = (1.2 \pm 0.2) \times 10^{-4}$ cm^{-1} derived by Serway et al (7.22) assuming strain and tetragonal symmetry, from measurements on the $M = \frac{3}{2} \rightarrow \pm\frac{1}{2}$ transition in a Cr^{3+}/MgO sample containing 10 ppm Cr^{3+}. It has been reported by Van Wieringen et al (7.4) that the linewidth of the $\pm \frac{3}{2} \rightarrow \pm \frac{1}{2}$ transition in Cr/MgO was twice as wide as that of the $\frac{1}{2} \leftrightarrow -\frac{1}{2}$ transition, with H parallel to the (100) direction. On this basis and taking the reported linewidth value of 0.5 mT (7.3) for the $\pm \frac{1}{2}$ transition, one could observe the three resolved lines separately if the value of $\frac{\Delta D}{g\beta}$ is greater than

2.5 mT (i.e. 24 x 10^{-4} cm^{-1}).

The observed total linewidth ΔH_t when H lies in a (100) plane can be written as

$$\Delta H_t = \Delta H_o + \left| \frac{2\Delta D}{g\beta} \cos \Theta_H \right| \qquad (7.3)$$

where ΔH_o represents a linewidth independent of polar angle Θ_H, temperature and concentration and is taken to be the width of the $M = \pm\frac{1}{2}$ transition, when the zero field splitting energy D = 0 and the Zeeman field is along a cube axis. This can be considered to be the intrinsic linewidth in the absence of internal strain. The comparisons between the observed linewidth at 4.2K and the linewidth according to Equation (7.3) are shown in Figure 7.2. The line broadening was maximum at $\Theta_H = 0^o$, which indicates the direction of strain in the crystal lattice. Thus it can be assumed that the Cr^{3+}/MgO crystal lattice acquires strain at low temperature - due to vacancies (caused by charge misfit), along one of the cube axes. Strain effects due to poor annealing have been reported for Ni^{2+} in magnesium oxide (7.26) and Cr^{3+} in yttrium aluminium garnet (7.27). To examine the effect of heat treatment in removing strain two of the as received Cr^{3+}/MgO specimens (800 ppm and 3600 ppm) were heated at 1000° C for 12 hours in air and cooled slowly down to room temperature, (4 hours). The linewidths of these samples at 4.2K fell from 1.6 mT to 0.91 mT and from 2.06 mT to 0.81 mT respectively. The resulting values are close to the linewidths at 77K and were independent of polar angle Θ_H. The 800 ppm Cr specimen (for which the room temperature linewidth was .7 mT) was then heated in air at 1000° C for 12 hours and cooled down to room temperature much more quickly (1 hour). The linewidth at room temperature increased to 1.2 mT and became polar angle dependent showing a similar variation to that observed before at 4.2K, and indicating the presence of considerable strain. The reactions between

vacancies and Cr^{3+} ions in MgO crystal as a function of temperature have been discussed by Glass (7.28) ; where the valency of the Cr^{3+} ion is unchanged the vacancies are essentially immobile up to 900^{o} C . The heat treatment of the specimens in air at 1000^{o} C for 12 hours followed by a slow cool down to room temperature creates this mechanism of charge compensation of the Cr^{3+} ion whereas quick cooling creates strain in the specimen.

Using E.S.R. techniques, Watkins and Feher (7.29) found that the strain coupling coefficients for Cr^{3+} in cubic sites of MgO were $G_{11} = 0.6 \pm 0.6$ and $G_{44} = 4.2 \pm 0.6$ (with dimensions of cm^{-1}/unit strain). The stress coefficient C_{ii} is related to the strain coupling coefficient G_{ii} through the elastic stiffness coefficient (7.21). Using the value of coefficient quoted by Watkins and Feher, the stress coefficients were calculated by Serway et al (7.22) and have values $C_{11} = (2.8 \pm 2.8) \times 10^{-13}$ cm/dyne. It has been reported by Feher (7.21) that the change in crystal field splitting parameter D in MgO due to pressure p along the (100) axis is given by

$$\Delta D = \frac{3}{2} C_{11} P \qquad (7.4)$$

Using the quoted values (7.22) for C_{11} and taking $\Delta D = (5.25 \pm 0.40) \times 10^{-4}$ cm^{-1}, the pressure P experienced in the crystal at low temperature along (100) is $(6.25 \pm 0.8) \times 10^{8}$ dyne cm^{-2}. Walsh (7.14) measured the shift of the 'g' factor as a function of hydrostatic pressure and found that a 'g' shift of + 0.00025 corresponds to a pressure of 10^{10} dyne cm^{-2}. The derived pressure is about sixteen times less than Walsh's value, so it is not surprising that there was not any g-shift at low temperature.

REFERENCES

CHAPTER SEVEN

7.1 P W Anderson and P R Weiss, Rev. Mod. Phys. 25 (1953) 269.

7.2 W Low, Phys. Rev. 105 (1957) 801.

7.3 J S Thorp, M D Hossain and L J C Bluck, J.Mat.Sci. 14 (1979) 2853.

7.4 J S Van Wieringen and J G Renson, -Paramagnetic Resonance' V-I, p 105, Ed. W Low, Academic Press, N.Y. 1963.

7.5 J E Wertz and P Auzins, Phys. Rev. 196 (1957) 484.

7.6 J E Wertz and P Auzins, J.Chem. Sol. 28 (1967) 1557.

7.7 J P Larkin, G F Imbusch and F B Yauricks, Phys. Rev. B7 (1973) 495.

7.8 J C M Henning and J H den Boef, Phys.Lett.A 59 (1976) 241.

7.9 G A Woonton and G L Dyer, Can.J.Phys. 45 (1967) 2265.

7.10 J C M Henning and J H den Boef, Phys. Rev. B18 (1978) 60.

7.11 W M Walsh, J Jener and N Bloembergen, Phys.Rev. 139 (1965) A1338.

7.12 S A Marshall, J A Hodges and R A Serway, Phys. Rev.136 (1964) A1024.

7.13 K N Shrivastava, Phys.Letts. 42A (1973) 385.

7.14 W M Walsh, Phys.Rev. 122 (1961) 762.

7.15 J G Castle Jr. and D W Feldman, Phys.Rev. 121 (1961) 1349.

7.16 J S Thorp, R A Vasquez, C Adcock and W Hutton, J.Mat.Sci.4 (1976) 89.

7.17 B Henderson and J E Wertz, Advances Phys. 17 (1968) 749.

7.18 B Henderson, J E Wertz, T P P Halls and R D Dowsin, J.Phys. C4 (1971) 107.

7.19 K J Standley and A D Tooke, J.Phys. C1 (1968) 149.

7.20 Electron paramagnetic resonance, Ed. by S Gesehwind, Plenum N.Y. 1974.

7.21 E R Feher, Phys. Rev, 136 (1964) 145.

7.22 R A Serway, S A Marshall and R B Robinson, Phys. Stat.Sol.B56 (1973) 319.

7.23 A L Schowlow, Phys. Rev. 122 (1961) 1469.

7.24 A M Stoneham, Rev.Mod. Phys. 41 (1969) 82.

7.25 R D Shannon and C T Prewitt, Acta Cryst. B 25 (1969) 925.

7.26 S R P Smith, F Dravnicks and J E Wertz, Phys.Rev.179 (1969) 471.

7.27 R A Serwey, F H Yangand and S A Marshall, Phys. Stat.Sol.(b) 89 (1978) 267.

7.28 A M Glass, J.Chem.Phys. 46 (1967) 2080.

7.29 G D Watkins and E R Feher, Bull.Amer.Phys.Soc. 7 (1962) 29.

CHAPTER EIGHT

E.S.R. BEHAVIOUR OF Gd^{3+}/MgO

In this chapter the electron spin resonance linewidth of Gd^{3+} in single cyrstal MgO at 9 GHz was examined experimentally and theoretically for Gd^{3+} concentration of 310 ppm. In contrast to the behaviour expected from dipolar broadening the experimental peak-to-peak linewidth had a value of about 0.3 mT at 293K and was independent of polar angle. The calculated dipolar linewidth exceeded that observed by a factor of about one hundred ; the ratio of moments $M_4^{\frac{1}{4}} / M_2^{\frac{1}{2}}$ derived from experimental data was 1.33 and the lineshape was Lorentzian. The data suggested that Gd^{3+} entered the lattice substitutionally, occupying magnesium sites, and that the linewidth was determined by exchange narrowing over the temperature range 293K to 4.2K.

8.1 INTRODUCTION

In the last four chapters, the E.S.R. studies of some iron group ions (Cr^{3+}, Co^{2+} and Fe^{3+}) substituted as impurities in single crystal of MgO have been described. A few of the E.S.R. results for rare-earth group ions doped in MgO have been reported recently ; such as Er^{3+} in 1964 (8.1), Eu^{2+} and Gd^{3+} in 1971 (8.2), Dy^{3+} and Yb^{3+} in 1974 (8.3) where the spectra corresponded to a site of cubic symmetry. The trivalent gadolinium ion has seven unpaired electrons in the 4f unfilled shell which make it half-filled and give rise to a ground state $4f^7$, $^8S_{7/2}$; in a cubic field it can split into two doublets and a quadruplet and the lowest level is a Kramers doublet. As an S-state ion gadolinium should exhibit no first order crystal field splitting, a feature discussed in (8.4). However, ground state splittings of Gd^{3+} were observed in CaO (8.5), SrO (8.6) and MgO (8.2) ; the observed splitting mechanisms were more complex than a simple linear dependence on the crystal potential. Van-Vleck and Penny (8.7) have suggested that the splitting arising from the combined action of the cubic field and spin-orbit interaction will be very small. The ionic radius of Gd^{3+} in octahedral coordination is 0.938 Å (8.8). In the single crystal MgO, gadolinium is expected to go into the lattice by the substitution at the octahedral site as,in the octahedral position, the ratio of cation radius lies between 0.732-0.414 (8.9). The ionic radius ratio between Gd^{3+} and O^{-2} (1.40 Å) is 0.670, which lies in the range of quoted values (8.9). In the host crystal MgO, the linewidth of iron group ions such as Cr^{3+} (Chapter 4), Co^{2+} (Chapter 5) and Fe^{3+} (Chapter 6) have been shown to be determined by exchange narrowing, while the linewidth of Gd^{3+} in $CaWO_4$ is determined by dipolar broadening mechanisms (8.10). It is worthwhile testing which one of these mechanisms holds true for Gd^{3+} in MgO. This work was undertaken in an attempt to give information

on the question of the sites actually occupied by the dopant atoms and on the nature of the interactions between the latter in the temperature range 293K to 4.2K.

8.2 EXPERIMENTAL RESULTS

The gadolinium concentration in the specimen which was the only sample available was 310 ppm. The crystal which had dimensions 9.8 mm x 5 mm x 2.2 mm was cloudy-white ; the same colour for MgO single crystal doped with Gd^{3+} has been reported by Abraham et al (8.11). The E.S.R. spectrum of gadolinium in MgO has been recorded at 9 GHz. Only one isotropic line was observed where the seven transitions coincide at $h\nu = g\beta H$. The single line transition corresponding to an effective spin $S' = \frac{1}{2}$, of Cr^{3+} in MgO (8.12 and 8.13), Co^{2+} in MgO (8.14) and Dy^{3+} in MgO and SrO (8.3) have been observed instead of transitions corresponding to the spin value S >1. The typical spectrum of the single line transition at $\Theta_H = 0^o$ at different temperatures has been shown in Figure 8.1. The g value of the line is about 1.991, which is the same as the reported value for the $\frac{1}{2} \rightarrow -\frac{1}{2}$ transition in (8.2). Measurements of the magnetic field values at resonance and linewidth determinations were made as functions of both polar angle and temperature. There is no change in resonance field with temperature. There is a small variation of resonance field with polar angle, which departs by up to 0.3 mT from its value at $\Theta_H = 0^o$, when the magnetic field is directed along the [100] plane. The variation of resonance field has also been reported elsewhere (8.2) where it was found for the case in which the magnetic field was directed along the [110] plane at T = 77 K, that the resonance magnetic field changed by up to 1.2 mT over a similar range of polar angle. On the basis of the very close agreement between the measured g value and the reported 'g' value in (8.2) it was felt justifiable to attribute the spectrum to Gd^{3+} in octahedral sites. Some very weak additional lines were observed, which were due to

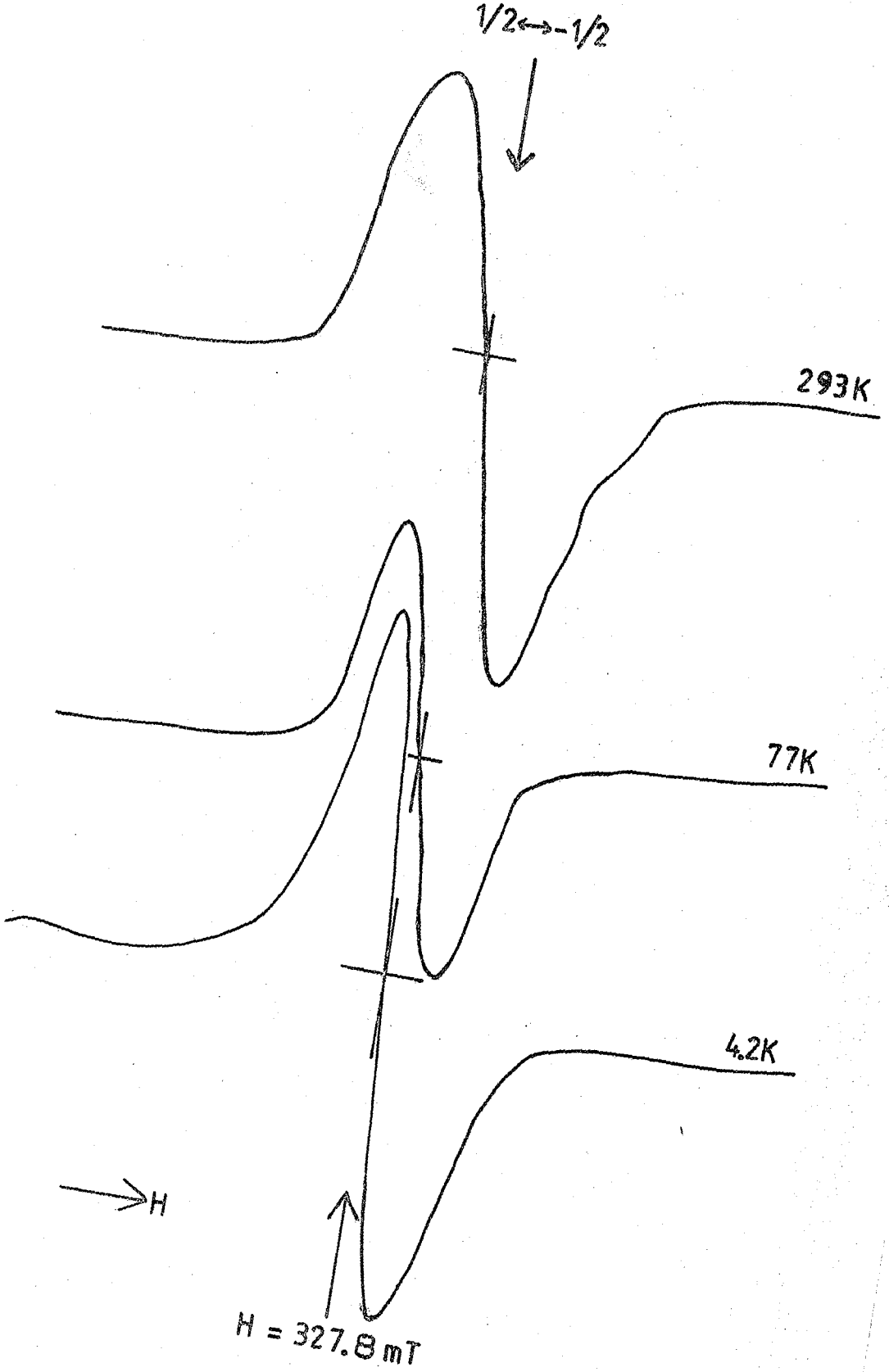

FIG. 8.1 DERIVATIVE LINE OF Gd^{3+}/MgO, $\theta_H = 0°$, 9.14GHz, 310 PPm Gd.

Fe^{3+} and Mn^{2+} as impurities. The linewidth defined as the width between points of maximum slope, ΔH_{ms}, was obtained directly from the derivative plots. The measured linewidth at room temperature was about 0.3 mT, which was independent of polar angle as shown in Figure 8.2. This behaviour of the rare earth group S-state ion Gd^{3+} is in marked contrast (in the MgO lattice) to the linewidth variation with polar angle θ_H of the iron group S-state ion Fe^{3+} [where ΔH_{ms} increased with the increasing value of θ_H (8.15)] . In order to check whether there was any appreciable contribution to linewidth due to spin-lattice relaxation, the spectra were recorded as a function of temperature from room temperature down to 4.2K ; the linewidths remained constant which shows the relaxation effect on linewidth is negligible.

8.3 DISCUSSION

One salient feature emerges from an initial comparison between the experimental results for the as grown crystal and those reported in the literature (8.2), in which a spectrum of seven lines was observed instead of the single transition found here. The observation of only one line indicates that the cubic field splitting is zero. Similar reduction of the cubic field splitting for Gd^{3+} in CaO and SrO (8.16) and Cr^{3+} in MgO (8.12,8.13) has been reported. The observed linewidth of Gd^{3+}/MgO was half that of the linewidth for the S-state ion Fe^{3+} in MgO (8.10) for the same concentration (310 ppm). Thus the narrow linewidth (ΔH_{ms} = 0.3 mT) and the general behaviour of the spectrum showed that the cubic symmetry was preserved to a high order, for the measured concentrations of gadolinium, despite the fact that gadolinium has a larger valency and ionic radius (0.97 Å) than the host lattice cation Mg^{2+} (ionic radius of 0.72 Å). In this case it is obviously necessary for a lattice to distort in order to accept the larger ion, i.e. the neighbours move away from their normal positions. Here the experimental result showed that if any distortion is

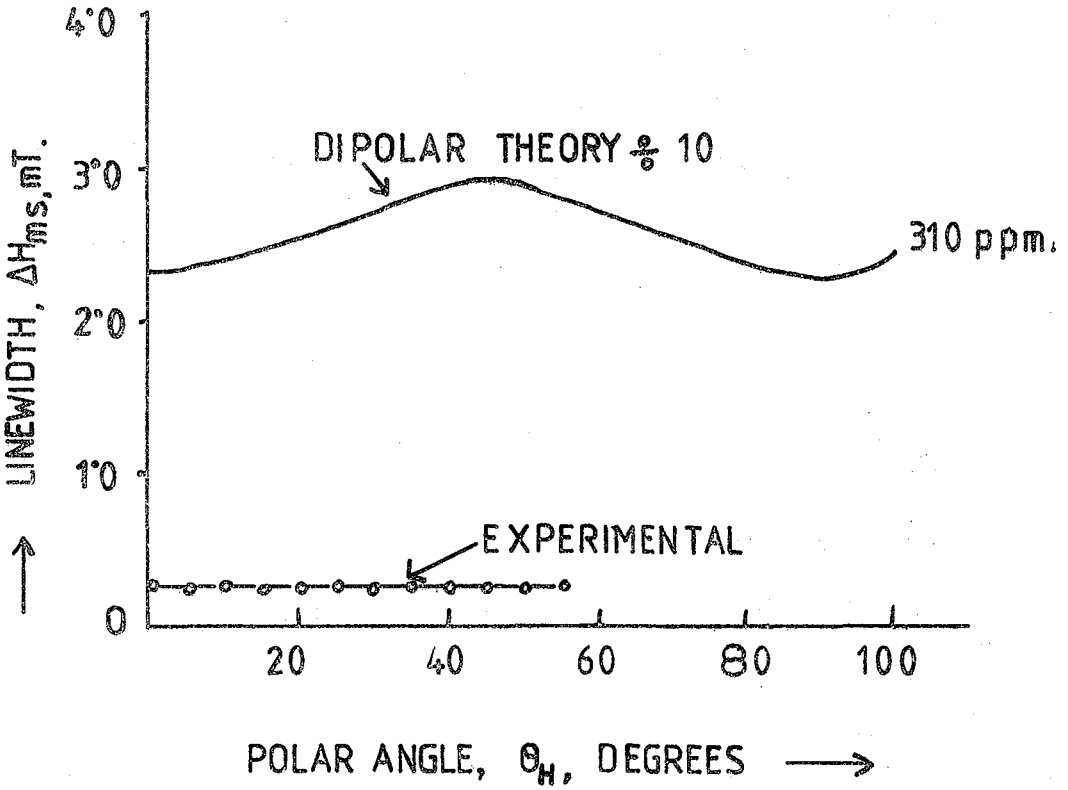

FIG, 8,2 Comparison of predicted and observed variation of linewidth with polar angle; Gd^{3+}/MgO (310 ppm). ±1/2 TRANSITION.

present, it would be uniform leaving the local symmetry completely unchanged. Substitution of trivalent ions for divalent cation, Mg^{2+}, without disturbing the octahedral cubic symmetry have been reported in (8.12 and 8.15). This was found also for an ion which had an effective S-state in the ground state (8.15).

A comparison of the reported results at X-band of the rare-earth ions doped in MgO and the present results is given in Table 8.1.

Ion	Ionic Radius (Å) Ref. (8.8)	Concentration (ppm)	Peak-to-peak linewidths ΔH_{ms} (mT)	g value	Spectrum corresponds to	Refs.
Er^{3+}	0.881	300	0.3	4.3	one octa- and the other tetra-hedral	(8.1)
Yb^{3+}	0.858	not mentioned	0.2 H// [111]	2.5662	cubic site	(8.3)
Dy^{3+}	0.908	"	0.2 H// [111]	6.5662	cubic site	(8.3)
Eu^{2+}	1.17	"	narrow H// [110]	1.9894	cubic site	(8.2)
Gd^{3+}	0.938	"	narrow H// [110]	1.992	cubic site	(8.2)
Gd^{3+}	0.938	310	0.3 H// [100]	1.991	octa-hedral cubic site	This work

TABLE 8.1 : Comparison of results of rare-earth ions in MgO, X-band.

The present ESR results and the reported results in Table 8.1 indicate the relative absences of strains in the MgO crystal lattice for substitutional rare-earth ions of larger ionic radius and valences than the cation Mg^{2+}. This is especially remarkable in MgO.

To consider the mechanism responsible for the ground state splitting of Gd^{3+} in the various crystals of O_h^5 space group lattice of cubic symmetry, a comparison of splitting parameters is given below.

Para-magnetic ion	Host Crystal	Lattice Space Group	Lattice Constant (Å)	Inter-ionic distance in crystals (Å)	g-values	Cubic field splitting C in 10^{-4} cm^{-1}	Refs
Gd^{3+}	SrO	O_h^5	5.10	2.54	1.9918	-21.6 ± .2	(8.6)
Gd^{3+}	CaO	O_h^5	4.797	2.40	1.9925	46.4 ± .4	(8.5)
Gd^{3+}	MgO	O_h^5	4.-112	2.10	1.9920	-139.8 ± .02	(8.2)
Gd^{3+}	MgO	O_h^5	4.2112	2.10	1.9920	0	This work

TABLE 8.2 : Cubic field splittings of Gd^{3+} in various oxide crystals in cubic symmetry.

Watanabe (8.17) in 1957 has extended the theoretical discussion of the crystal field splitting in the S-state ions beyond the treatment of Van-Vleck and Penny (8.7) and Pryce (8.18) and he concludes that the cubic field

splitting c would be of the form

$$c = (Dq)^2 \left[a - b\,(Dq)^2 \right] \qquad (8.1)$$

where Dq represents the usual measure of the cubic field strength, and 'a' and 'b' are constants depending on the detailed nature of the excited states. Since the potential (i.e. Dq) is presumably small for most rare earth ions and the spin-orbit interaction fairly large, Low (8.19) in 1959 considered that the splitting ought to be primarily proportional to the square of the potential or inversely to the tenth power of the interionic distance. From Table 8.2, the ratio of Ca-O and Mg-O distances is about 1.142 and the ratio of the Sr-O and Mg-O distances is about 1.209. Assuming that substituting the trivalent gadolinium ion does not change this ratio appreciably, one can calculate the ratio of cubic splittings. The ratio of cubic splittings

$$\frac{c_{MgO}}{c_{CaO}} : \frac{c_{CaO}}{c_{SrO}} : \frac{c_{SrO}}{c_{MgO}} \text{ are proportional to } 3.77 : 1.76 : 0.149.$$

If one puts the measured cubic field splitting value of c_{CaO} and c_{SrO} from Table 8.2 in the above relation, the two values of c_{MgO} will be 174.9×10^{-4} cm^{-1} and 144.9×10^{-4} cm^{-1}. The latter value of c_{MgO} is close to the measured value of c_{MgO} reported in (8.2). This shows that the mechanism responsible for the cubic field splitting follows the inverse tenth power of the inter-ionic distance. So from the observed spectrum of Gd^{3+} in MgO and the spectrum reported in the literature (8.2), it may be assumed that the cubic field splitting mechanism depends also on the crystal history. The result given here represents measurements on only one sample and is not necessarily applicable for all Gd^{3+} in MgO samples.

In order to get information about the nature of the interaction between the dopant atoms, a comparison was made between the measured line-

width and the predicted dipolar broadening linewidth. For Gd^{3+}, s = 7/2 and g = 1.991 in MgO lattice, the peak-to-peak dipolar linewidth as a function of polar angle θ_H was evaluated by the method described in Chapter 2, Section 2.2.1. The theoretical curve for the variation of dipolar linewidth with polar angle is given in Fig 8.2 by the full line. The measured linewidth is about 100 times narrower than the predicted dipolar linewidth at $\theta_H = 45^o$. The large numerical disparity suggested that there was a strong narrowing mechanism such as the exchange narrowing observed in Fe^{3+}/MgO (8.15), Cr^{3+}/MgO (Chapter 4) and Co^{2+}/MgO (Chapter 5). Experimental evidence for exchange narrowing is usually obtained from analysis of lineshapes and comparisons of moments. To find the lineshape factor, the observed derivative line was integrated, as shown in Fig 8.3 and the ratio of the peak-to-peak derivative linewidth to the integrated linewidth at half-height was found to be 0.591. Therefore, the observed lineshape factor is very close to the Lorentzian lineshape factor of 0.577 (8.20). This Lorentzian lineshape indicates exchange narrowing. The moment ratio $\frac{M_4^{\frac{1}{4}}}{M_2^{\frac{1}{2}}}$, where M_2 and M_4 are respectively the second and fourth moments, was derived as 1.33. This value is similar to the figures quoted in (8.12, 8.15) for examples of exchange narrowed ESR lines. This suggests that the observed spectrum of Gd^{3+}/MgO is also determined by'exchange narrowing'.

The exchange energy J has been derived, by adopting the same method as described in Chapter 4, and compared with the reported values for iron group ions in the MgO lattice (8.21) for the same concentration (Table 8.3).

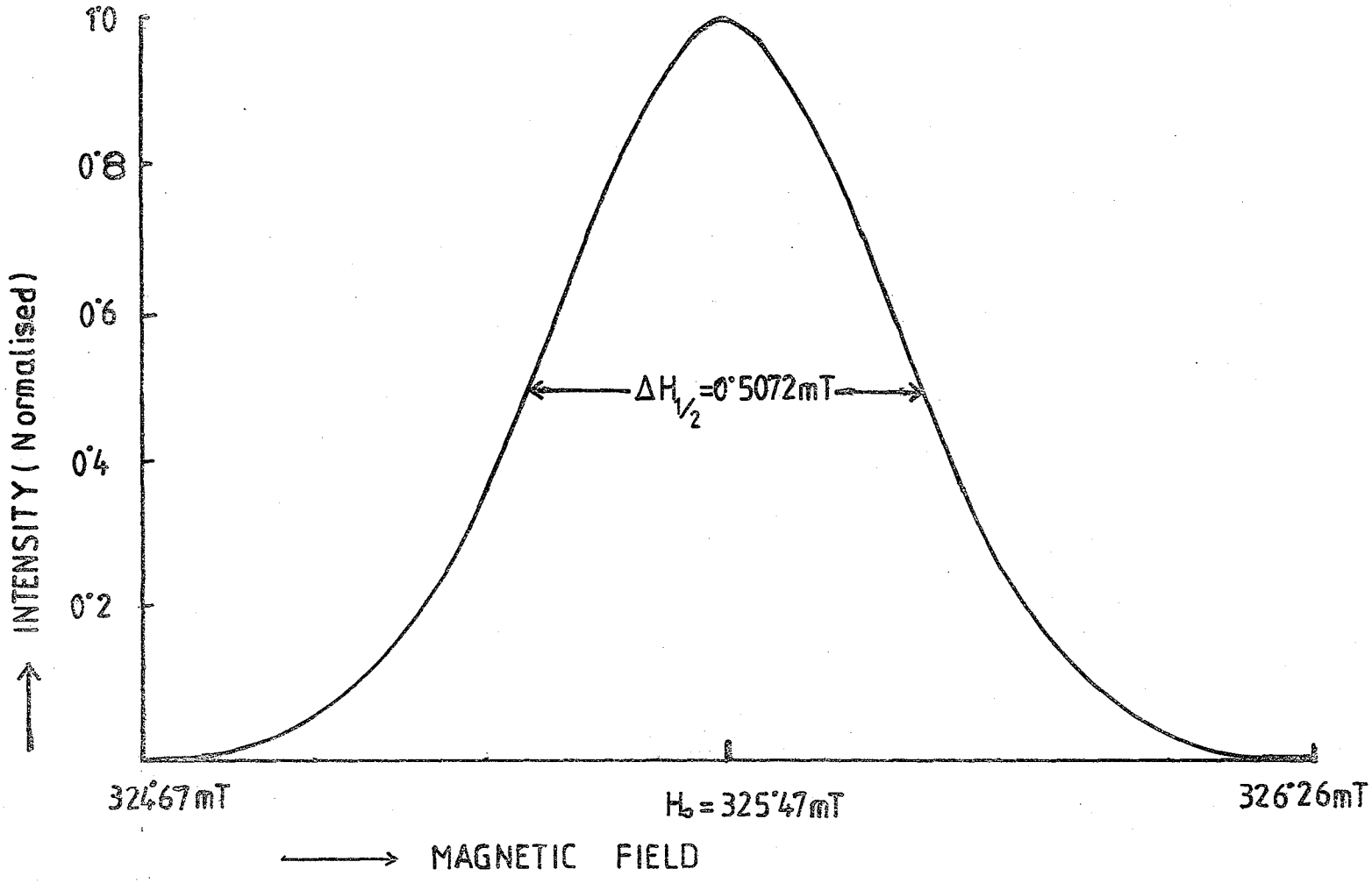

FIG, 8,3 INTEGRATED LINESHAPE FOR Gd^{3+}/MgO(310ppm), θ_H=0°, 9·069GHz, 293K.

ION	Ground State	Concentration (ppm)	Exchange Energy J (GHz)	References
Gd^{3+}	$^8S_{7/2}$	310	15.00	This work
Fe^{3+}	$^6S_{5/2}$	310	3.99	All these values have been calculated from the slope for J (8.21).
Cr^{3+}	$^4F_{3/2}$	310	2.03	
Co^{2+}	$^4F_{9/2}$	310	1.98	

TABLE 8.3 : Comparison of J values for different ions in MgO.

This table shows that in MgO, Gd^{3+} has a greater exchange energy since Gd^{3+} has a higher spin value and a greater ionic radius, which causes greater overlapping between paramagnetic impurity coordinating ions than the other iron group ions, which substantiates that S-state ions have greater exchange energy than F-state ions in the same host lattice MgO, irrespective of their periodic group.

In order to maintain the neutrality of the crystal, these have to be either some positive ion vacancies or negative ion interstitials. Since the spectrum can be fitted with a simple cubic spin-Hamiltonian, $h\nu = g\beta H$ and since only a single transition of narrow linewidth (0.3 mT independent of polar angle) with strong exchange energy was seen, the evidence seems to show that there are no interstitial ions in the neighbourhood. So vacancies may be one Mg^{2+} ion for every two Gd^{3+} ions in the magnesium sites. Similar vacancy rules for charge neutralizing due to trivalent S-state ion Fe^{3+} in MgO have been reported (8.15).

The linewidth mechanism of Gd^{3+} in the $CaWO_4$ lattice (substituted at calcium sites) has been shown to fit a dipolar broadening mechanism

(8.10), which is in contrast to the present observed linewidth mechanism of Gd^{3+} in MgO. The number of Mg^{2+} cationic sites close to that occupied by one substitutional Gd^{3+} ion (corresponding to the eight unit cells of MgO around the central Gd^{3+} ion) is 64. The sphere which contains these 64 sites has a radius of 7.294 Å (8.15), while the corresponding radius of a sphere which contains the 64 Ca^{2+} cationic sites in $CaWO_4$ lattice around the substitutional Gd^{3+} ion is 13.5794 Å (8.22). So the same S-state ion, Gd^{3+}, shows different linewidth mechanisms according to the radius of this sphere and the larger radius of sphere corresponds to the dipolar mechanism.

Thus it may be concluded that the observed spectrum for Gd^{3+}/MgO corresponds to a site of cubic symmetry and gadolinium enters the magnesium oxide lattice substitutionally for the measured concentration 310 ppm. The linewidth is determined by exchange narrowing throughout the temperature range between 293K to 4.2K.

REFERENCES

CHAPTER EIGHT

8.1 D. Descamps and Y.M.D. Aubigne, Phys. Lett. 8 (1964) 5.

8.2 M.M. Abraham, L.A.Boatner, Y. Chen, J.L. Kolpus and R.W.Reynolds, Phys. Rev.B 4 (1971) 2853.

8.3 R.W.Reynolds, L.A. Boatner, Y.Chen and M.M.Abraham, J.Chem.Physics, 60 (1974) 1593.

8.4 B. Bleaney and K.W.Stevens, Rep.Prog.Physics 16 (1953) 108.

8.5 A.J.Shuskass, Phys.Rev. 127 (1962) 2022.

8.6 J.L.Kolopus, L.V.Holroyd and K.E.Mann, Phys. Stat.Sol. 9 (1965) k95.

8.7 A.H. Van-Vleck and W.G.Penney, Phil.Mag. 17 (1934) 961.

8.8 R.D.Shannon and C.T.Prewitt, Acta.Cryst. B25 (1969) 925.

8.9 N.N. Greenwood, "Ionic crystals lattice defects and non-stoichiometry" Butterworths, London (1958) p.144.

8.10 J.S.Thorp, G.Brown, H.P.Buckley, J.Mat.Sci.9 (1974) 1337.

8.11 M.M.Abraham, C.T.Butler and Y.Chen, J.Chem.Phys.55 (1971)3752.

8.12 J.S.Thorp, M.D.Hossain,and L.J.C.Bluck, J.Mat.Sc.14 (1979), 2853.

8.13 W.Low, Annals.N.Y.Acad.Sci.72 (1958) 71.

8.14 J.S.Thorp, M.D.Hossain, L.J.C.Bluck and T.G.Bushell, J.Mat.Sci.15 (1980) 903.

8.15 J.S.Thorp, R.A.Vasquez, C.Adcock and W.Hutton, J.Mat.Sc.11(1976) 89.

8.16 P.Auzins, J.W.Orton and J.E.Wertz, 'Paramagnetic resonance' V-1 Edt.W.Low, N.Y.(1963),p 90.

8.17 Watanabe.Prog.Theoret.Phys.(Kyoto) 18 (1957) 405.

8.18 M.H.L.Pryce, Phys.Rev. 80 (1950) 1107.

8.19 W.Low and U. Rosenberger, Phys.Rev.116 (1959) 621.

8.20 C.P. Poole,"Electron Paramagnetic Resonance", John Wiley & Sons, N.Y. (1967) p 375.

8.21 J.S.Thorp and M.D.Hossain, J.Mat.Sci. 15 (1980) 1866

8.22 G.Brown, C.J.Krikby and J.S.Thorp, J.Mat.Sc.9 (1974) 65.

CHAPTER NINE

STRAIN BROADENING IN Ni^{2+}/MgO

In this chapter electron spin resonance linewidth of Ni^{2+} in single crystal MgO at 9 GHz was examined both experimentally and theoretically for Ni^{2+} concentration of 1400 ppm. The experimental peak-to-peak linewidth for $\Delta M_s = \pm 1$ transition had a value of about 6 mT over the temperature range 180 K to 20 K and found polar angle dependent. The calculated dipolar linewidth exceeded that observed by a factor of about five ; the ratio of moments $M_4^{\frac{1}{4}}/M_2^{\frac{1}{2}}$ derived from experimental data was 1.34 ; the lineshape was Lorentzian and independent of polar angle. The data suggested that Ni^{2+} entered the lattice substitutionally, occupying magnesium sites, that the linewidth for $\Delta M_s = \pm 1$ transition was determined by exchange narrowing together with inhomogeneous broadening due to internal strain. The angular dependence of the linewidth is given by

$$\Delta H_{\frac{1}{2}} = \left[a(1 - 3F) + bF \right]^{\frac{1}{2}} . \qquad (9.1)$$

with $F = (\sin^2 \Theta_H \cos^2 \Theta_H + \sin^2 \phi_H \cos^2 \phi_H \sin^4 \Theta_H)$

where $\Delta H_{\frac{1}{2}}$ is the integrated linewidth at half intensity ; 'a' = 132 mT^2 and 'b' = 124 mT^2.

9.1 INTRODUCTION

The electron spin resonance (E.S.R.) linewidth results of Cr^{3+}, Co^{2+} and Fe^{3+} in magnesium oxide showed exchange interactions have been described in the previous chapters 4, 5 and 6 respectiely. As a part of further studies on different ions of iron group, a similar investigation has been made of the nickel doped magnesia (Ni^{2+}/MgO) in an attempt to provide specimens of known structural characteristics on which electrical conductivity and dielectric loss measurement might subsequently be made. The e.s.r. spectra of Ni^{2+}/MgO was first observed by Low in 1958 (9.1), where the characteristics parameter of the spin-Hamiltonian for the transition $\Delta M_s = \pm 1$, were calculated for cubic crystalline field and the linewidth assumed due to both dipolar and exchange interactions. Orton et al (9.2, 9.3) were first observed the double quantum line $\Delta M_s = \pm 2$, in Ni^{2+}/MgO in the same position of the transition $\Delta M_s = \pm 1$, where the observed single quantum broad line was dependent on crystal orientation and the appearance of the double quantum line was dependent on the microwave incident power on the sample. Later on the e.s.r. linewidth behaviour of Ni^{2+}/MgO were observed by different authors (9.4, 9.5, 9.6) in different e.s.r. experiments , where they also noticed a variation of linewidth behaviour from sample to sample history and the magnitude of the broadened line was varied from about 3 mT to 27 mT. However, there is little detailed information available either on the question of the sites actually occupied by dopant atoms or the nature of interactions between the latter. Information of this nature has been described in the previous chapter 4 by making a comparison between observed e.s.r. linewidths and those predicted from dipolar broadening. Galeeva and Kochelaev (G-K) in 1977 (9.7) have estimated the numerical value of the e.s.r. linewidth of Ni^{2+} ion in MgO by considering the spherical point defects ; the interaction of paramagnetic ion with symmetric point defects and the spin-spin interaction of

paramagnetic ions via the strain field. So it was decided to compare the experimental linewidths for the transition $\Delta M_s = \pm 1$ of Ni^{2+} / MgO with the theories.

The configuration of Ni^{2+} ion is $3d^8$, $^3F_4$ and the ground term in an octahedral field is the orbital singlet $^3A_2$ ($t_{2g}^6 e_g^2$) ; thus a suitable spin-Hamiltonian is $\mathcal{H} = g\beta \bar{H}.\bar{S}$ (9.6), where $S = 1$. The g value for Ni^{2+}/MgO is 2.2145 (9.2), the deviation from g = 2.0023 being due principally to the admixture of the term $^3T_2$ ($t_{2g}^5 e_g^3$) through the spin orbit coupling (9.6). Therefore the expected e.s.r. spectrum of Ni^{2+}/MgO is a single line at a magnetic field $H_o = \frac{h\nu}{g\beta}$, where the transition $M_s = 1 \overrightarrow{\leftarrow} 0$ and $M_s = 0 \overrightarrow{\leftarrow} -1$ are coincident (9.1). This chapter presents the results of the linewidth comparison made for the $|\pm 1> \longleftrightarrow |0>$ transitions of Ni^{2+}/MgO.

9.2 EXPERIMENTAL RESULTS

The nickel concentration in the specimen examined was 1400 ppm. Initial measurements were made at room temperature to establish the form of the spectrum. An example of this is shown in Figure 9.1. This spectrum at $\Theta_H = 0^o$ and $\phi_H = 0^o$ shows a broad resonance line at about g = 2.215, which is the superposition of the transition $|-1> \longleftrightarrow |0>$ and $|+1> \longleftrightarrow |0>$ and a central dip with the same g value due to the transition $|-1> \longleftrightarrow |+1>$ effected by the absorption of two quanta at moderate microwave power. The field value at which the transition occurred were compared with the values expected for Ni^{2+} in an octahedral site. There was close agreement and on this basis and in view of the similarity between Figure 9.1 and the spectrum reported in the literature (9.6 and 9.8), it was felt justifiable to attribute the spectrum to Ni^{2+} in octahedral sites. The peak-to-peak width of the dip at the centre is 1.4 mT at 293 K. A similar width has been reported in (9.6). It has been

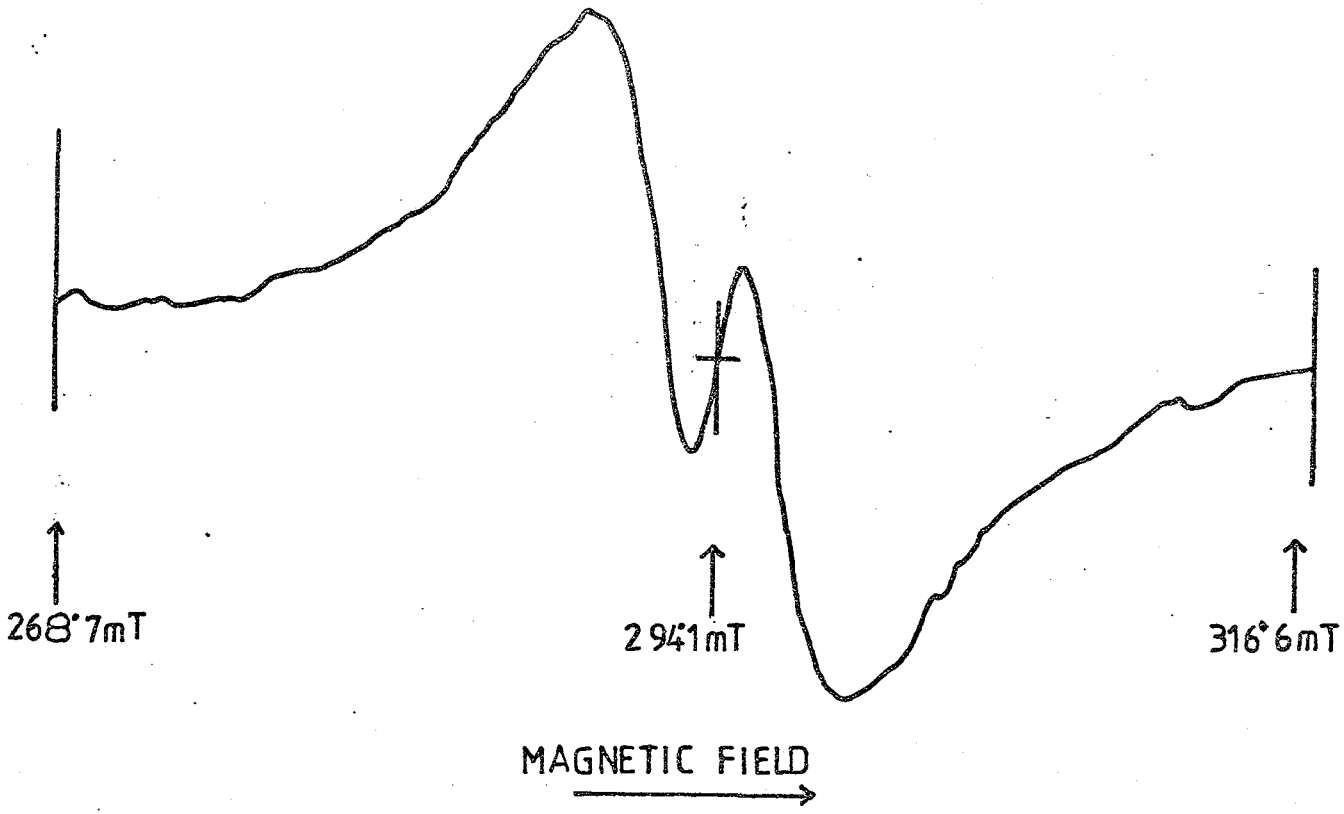

FIG, 9.1 E.S.R spectra of Ni^{2+}/MgO(1400ppm) at 293K, 9·117GHz, $\theta_H = 0°$. The broad line is due to $|\pm 1\rangle \longleftrightarrow |0\rangle$ transition with a dip at the center due to $|-1\rangle \longleftrightarrow |+1\rangle$ transition effected by the absorption of two quanta.

found that the appearance of the dip at the centre depends on the microwave incident power on the sample. The appearance of double quantum line as a function of incident power has been reported in the literature (9.2,9.4 9.6). It was possible to adjust the microwave incident power on the sample to such that the observed transition only for $\Delta M_s = \pm 1$ in the temperature range from 20 K to about 180 K. The appearance of double quantum line in the temperature range from 180 K to 293 K could not be avoided. There was no change in resonance field both with the temperature and the polar angle. The linewidth, defined as the width between points of maximum slopes, ΔH_{ms}, was obtained directly from the derivative plots. The resonance linewidth for $\Delta M_s = \pm 1$ transition was 6.0 mT at $\theta_H = 0^o$ and $\phi_H = 0^o$ in the temperature 20 K to 180 K (a spectrum for $\Delta M_s = \pm 1$ transition at 77 K is shown in Figure 9.2) and above 180 K the linewidth increases (derivative width becomes 10.2 mT at 293 K) with a doublet character as shown in Figure 9.1. The variation of linewidth with temperature at $\theta_H = 0^o$ is shown in Figure 9.3. Walsh (9.4) also observed the temperature independent linewidth in the temperature range 20 K to 77 K for a powdered sample of Ni^{2+}/MgO, having a concentration of about 0.1%. The resonance linewidth ΔH_{ms}, for $\Delta M_s = \pm 1$ transition, was dependent on polar angle, which was the maximum at $\theta_H = 0^o$ and the minimum at about $\theta_H = 45^o$ (when the magnetic field along (100) plane, i.e. $\phi_H = 0^o$) as shown in Figure 9.4 by the dotted line examined at 77 K. Low and Suss (9.9) mentioned that the maximum linewidth at $\theta_H = 0^o$ is a general characteristic of Ni^{2+} ion in the host crystal of alkaline earth oxide.

9.3 THEORETICAL LINEWIDTH

(a) Dipolar Broadening.

It will be assumed in this calculation that the main contribution to homogeneous line broadening is dipole-dipole interaction between Ni^{2+} ions. The second moment $\langle \Delta\omega^2 \rangle$ of the linewidth caused by dipolar inter-

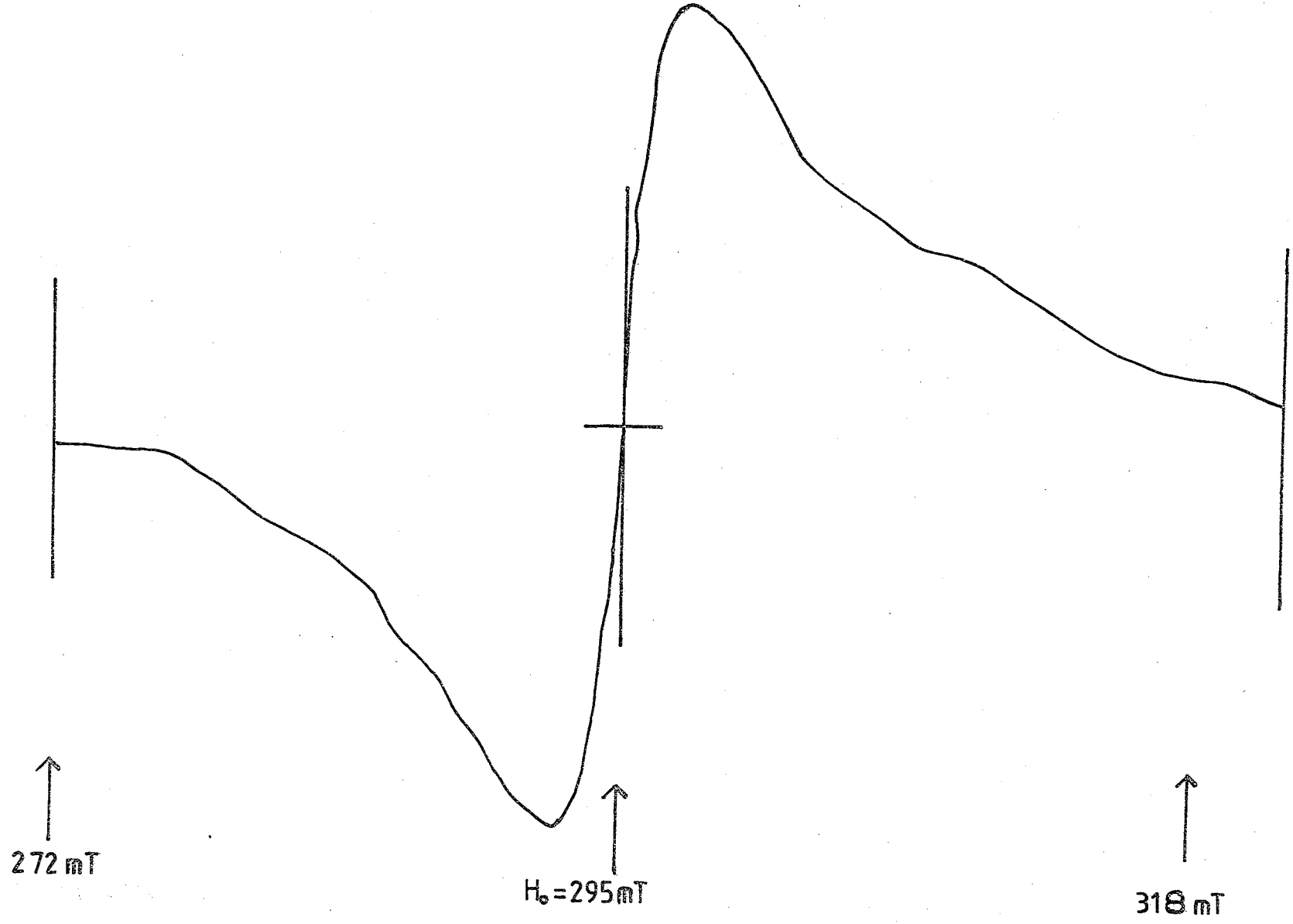

FIG, 9,2 E.S.R. SPECTRA OF Ni^{2+}/MgO(1400ppm), 77K, 9·14GHz, $\Delta Ms = \pm 1$, $\theta_H = 0°$.

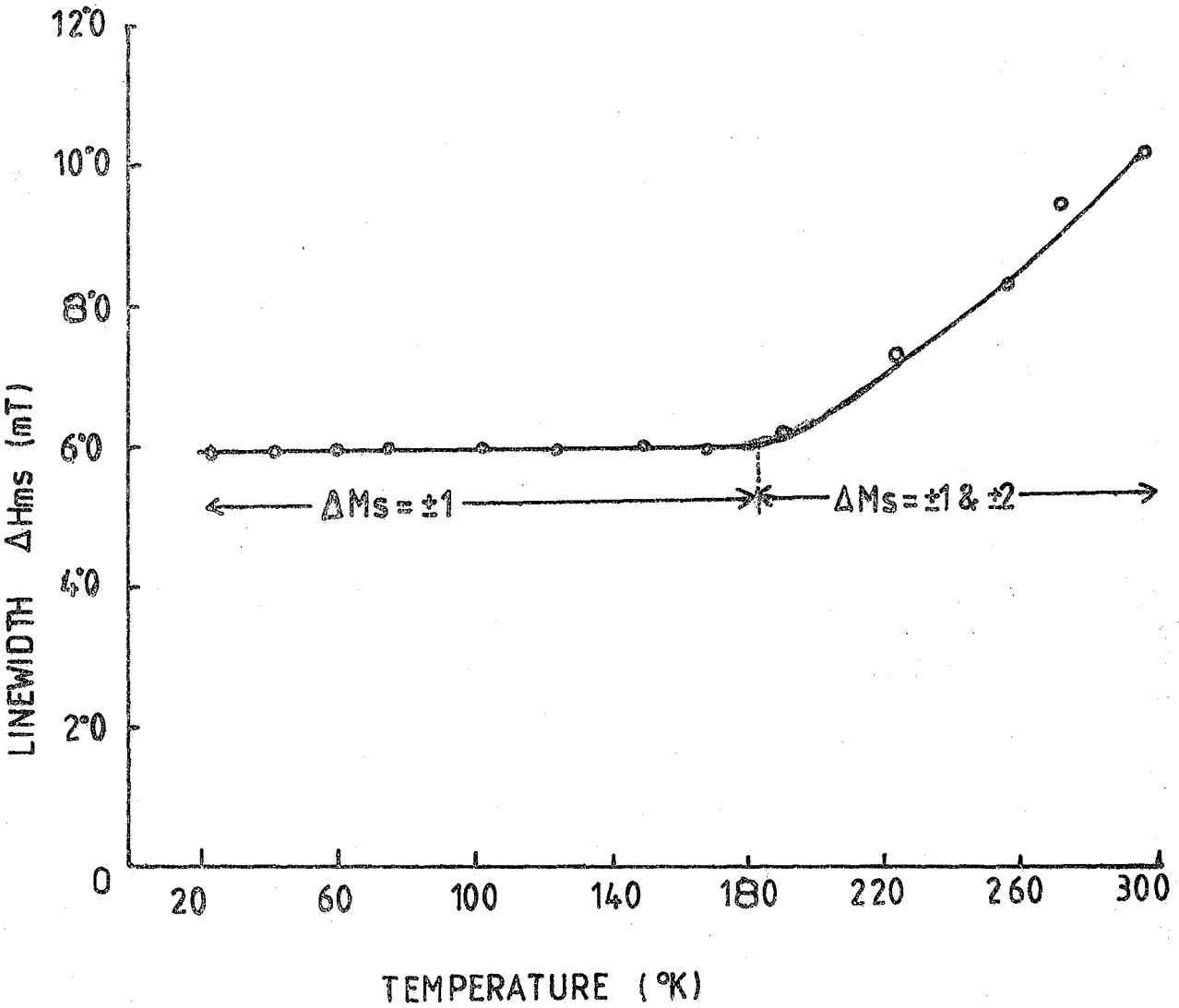

FIG, 9,3 VARIATION OF LINEWIDTH WITH TEMPERATURE; 9·14GHz, $\theta_H = 0°$, Ni^{2+} MgO (1400ppm).

action between identical atoms of Ni^{2+} in MgO has been derived in Section 2.2.1 as

$$\langle\Delta\omega^2\rangle = 2.3989 \times 10^{20}.n.\left[15.9184-5.175\ Y^{*}_{4,0}(\theta_H,\phi_H) - 6.218\ Y^{*}_{4,4}(\theta_H,\phi_H)\right] \qquad (9.2)$$

For $\phi_H = 0^o$, the equation 9.2 becomes totally real ; by substituting the experimental value of n = 0.0014 (i.e. 1400 ppm) and θ_H, the theoretical curve for the variation of dipolar linewidth ΔH_{ms}(dipolar) with polar angle can be obtained and is shown in Figure 9.4 by full line. Since the shape of a dipolar line is Gaussian (9.10) and using the Gaussian lineshape factor for a derivative line (9.11) as

$$G_{Y'(H)} = \left(\frac{H - H_o}{\frac{1}{2}\Delta H_{ms}(\text{dipolar})}\right)\exp\left[-\frac{1}{2}\left\{\left(\frac{H - H_o}{\frac{1}{2}\Delta H_{ms}(\text{dipolar})}\right)^2 - 1\right\}\right] \qquad (9.3)$$

where H_o is the resonance magnetic field, the points for the derivative line ΔH_{ms}(dipolar) at $\theta_H = 0^o$ are calculated and plotted in Figure 9.5(a).

(b) Exchange Narrowing.

It will be assumed in this calculation that the lineshape due to exchange narrowing is Lorentzian and the linewidth independent of doping concentration (Chapters 4 and 5). The predicted half-linewidth Δ (i.e. $\Delta = \frac{2\pi g\beta}{h}.\frac{1}{2}\Delta H_{\frac{1}{2}}$ exch) at half height of the absorption spectrum of Ni^{2+}/MgO due to exchange narrowing can be evaluated by adopting the Anderson-Weiss formula (9.12)

$$\Delta = \frac{\langle\Delta\omega^2\rangle \text{ dipolar}}{J/\hbar} \qquad (9.4)$$

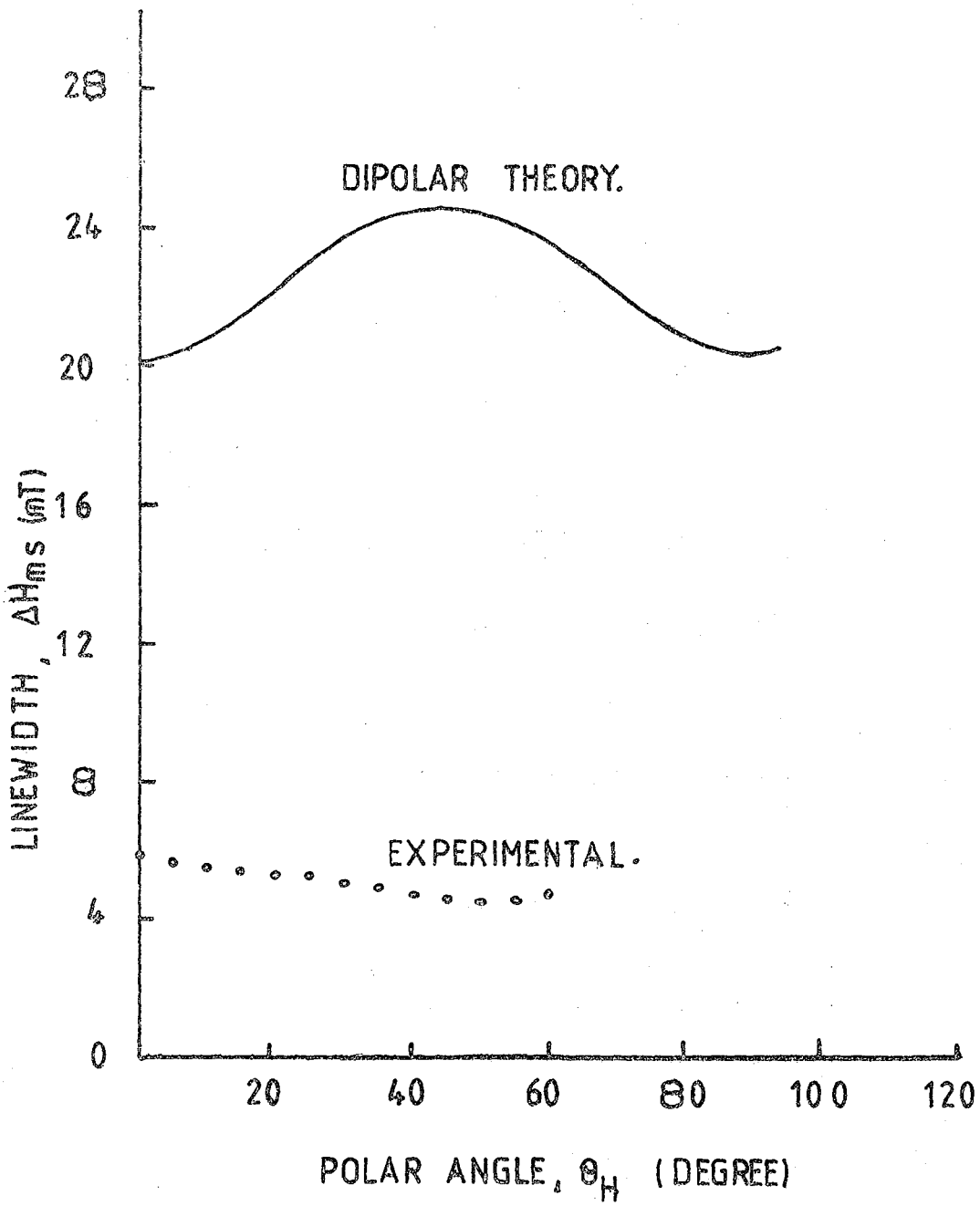

FIG, 9,4 VARIATION OF LINEWIDTH WITH POLAR ANGLE θ_H, 9°14GHz, 77K, $\Delta Ms = \pm 1$, Ni^{2+}/MgO (1400 ppm)

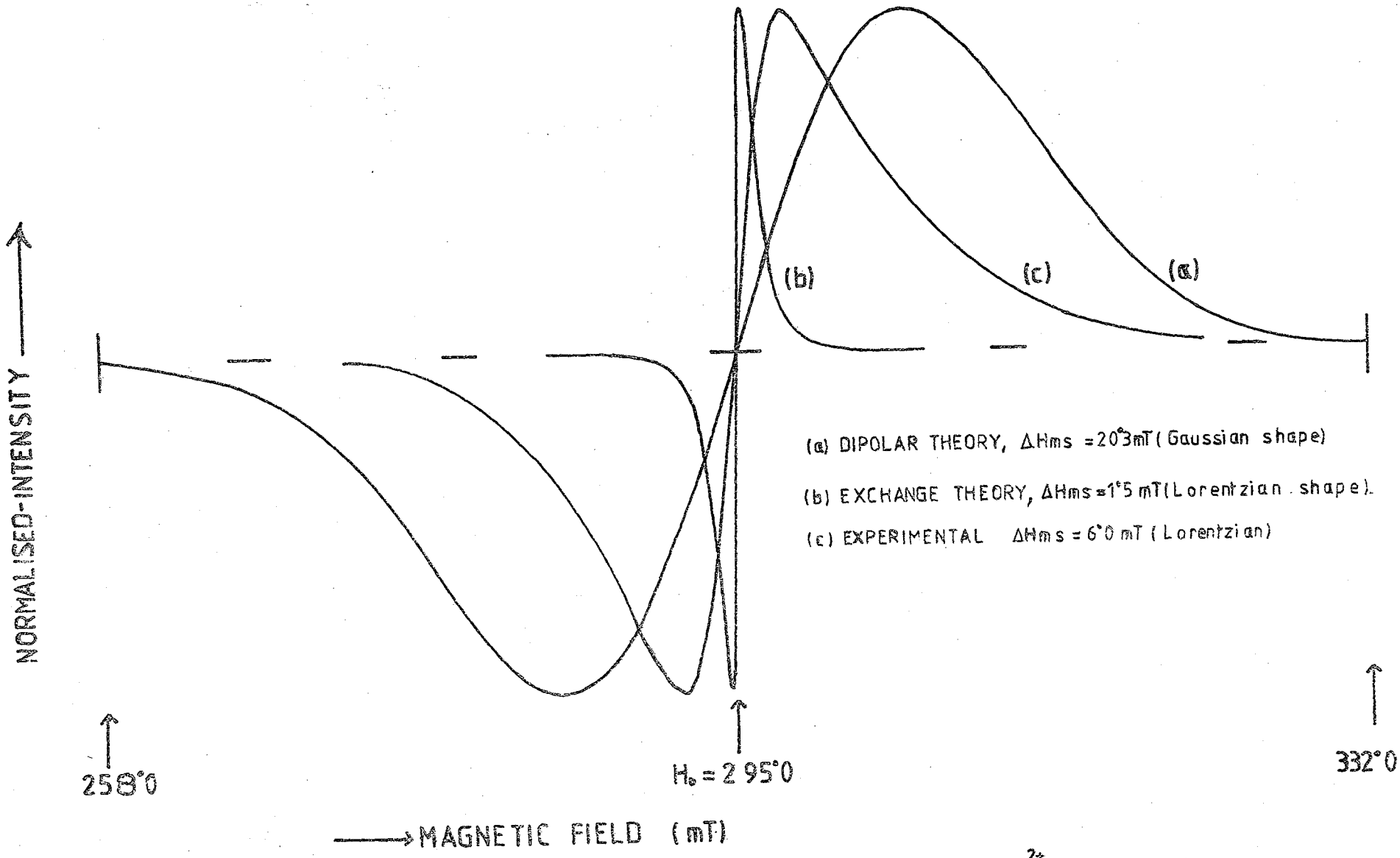

FIG. 9,5 COMPARISON OF DERIVATIVE LINESHAPES OF Ni^{2+}/MgO(1400 ppm), 9·14GHz, $\theta_H = 0$, $\Delta Ms = \pm 1$.

where J is the exchange energy in frequency unit and $\langle \Delta\omega^2 \rangle$ is the second moment caused by dipolar interaction in frequency unit, which can be calculated from equation 9.2.

The MgO crystal and NiO crystal has the same lattice structure and their lattice parameter difference is less than 1% [i.e. for MgO, a_o = 4.212 Å and for NiO, a_o = 4.1686 Å (9.13)] . The exchange energy of NiO is 5.209×10^{12} Hz, which has been calculated from Weiss constant $\theta = 2000^{o}$ k (9.14) by using the relation $J = \frac{3k}{2zS(S+1)}$, where k is Boltzmann constant and for NiO lattice z = 6. One can consider this value of $J = 5.209 \times 10^{12}$ Hz corresponding to 50% of available sites occupied by Ni^{2+} in MgO (i.e. the point corresponding to NiO). Since the exchange energy is linearly proportional to the doping concentration (Chapters 4 and 5), therefore the estimated exchange energy for 1400 ppm of Ni^{2+} ion in MgO is 1.458×10^{10} Hz. Substituting this value of $J = 1.458 \times 10^{10}$ Hz in equation 9.4 and using the Lorentzian shape factor, $\frac{\Delta H_{ms}(\text{exch})}{\Delta H_{\frac{1}{2}}(\text{exch})} = 0.577$ (Chapter 4), the peak-to-peak derivative linewidth can be evaluated as ΔH_{ms} exch = 1.57 mT for Ni^{2+}/MgO (1400 ppm). This value is very close to the exchange narrowing linewidth in the MgO single crystals doped with Cr^{3+}, Co^{2+} and Fe^{3+} (Chapters 4, 5 and 6 respectively). Using the Lorentzian lineshape factor for a derivative line (9.11) as

$$Y'^{L}_{(H)} = \frac{16\left(\frac{H - H_o}{\frac{1}{2}\Delta H_{ms}\ \text{exch}}\right)}{\left[3 + \left(\frac{H - H_o}{\frac{1}{2}\Delta H_{ms}\ \text{exch}}\right)^2\right]^2} \qquad (9.5)$$

and the points for the predicted derivative line ΔH_{ms} (exch) at $\theta_H = 0^{o}$ are calculated and plotted in Figure 9.5(b).

(c) Galeeva and Kochelaev (G-K) Estimation

The e.s.r. linewidths of paramagnetic ions via the strain field on the basis of isotropic elasticity theory have been estimated by Galeeva and Kochelaev (G-K) in 1977 (9.7) and the total linewidth has been given on the assumption of Lorentzian line which is also concentration dependent as

$$\Delta T_{G-K} = \Delta_1 + \Delta_2 + \Delta_3 \qquad (9.6)$$

where

Δ_1 is the linewidth due to interaction of paramagnetic ions with lattice defects.

Δ_2 is the linewidth due to interaction of a paramagnetic impurity.

and Δ_3 is the linewidth due to spin-spin interaction due to strain field.

The expression for Δ_1 has been given as

$$\Delta_1 = \frac{N\, k\, \Omega_o (3 - 2\nu)\, G_{11}}{4\sqrt{3}\, .\, G\, (1-\nu)\, h} \qquad (9.7)$$

where N is the concentration of paramagnetic ion per cm^3 ; $\frac{k}{G} = \frac{2(1+\nu)}{3(1-\nu)}$

where ν is the Poisson ratio ; G_{11} is the spin-phonon coupling constant; Ω_o is a tensor with dimension of volume and has been given by the expression as

$$\Omega_o \simeq \frac{4}{3}\pi \left(R^3_{Ni^{2+}} - R^3_{Mg^{2+}} \right)$$

where $R_{Ni^{2+}}$ and $R_{Mg^{2+}}$ are the radii of the ions Ni^{2+} and Mg^{2+} respectively.

It has been reported by Shannon and Prewitt (9.15) that the effective ionic radius of an ion depends on the coordination of both cation and anion and the electronic spin state. According to them, effective ionic radii based on $R\,(^{vl}O^{2-}) = 1.40$ Å, for $R_{Ni^{2+}}$ is 0.70 Å and for $R_{Mg^{2+}}$ is 0.72 Å. On substituting these values for Ω_o, equation 9.7 becomes negative. Hence the linewidth Δ_1 due to interaction of nickel ions with the lattice defects would be zero. The linewidth Δ_2, due to spin-spin interaction has been given for Ni^{2+}/MgO (9.7) as

$$\Delta_2 = \frac{4\pi^2 N g^2 \beta^2}{9\sqrt{3}\, h} = 1.64\, N \times 10^{-13} \text{ Hz.}$$

The expression for the contribution to the e.s.r. linewidth of the spin-spin interaction due to the strain field is given by G-K (9.7) as

$$\Delta_3 = \frac{\pi N}{30^{5/2} \times 8\, G(1-\nu)h} \Big\{ 3\left[(a+b)^{5/2} - (a-b)^{5/2}\right] - 30(\nu-3)\left[(a+b)^{3/2} - (a-b)^{3/2}\right] + 30^2\,\nu\left[(a+b)^{1/2} - (a-b)^{1/2}\right] \Big\} \frac{G_{44}^2}{6} \tag{9.8}$$

where $a = 9 + 3\nu$, $b = \sqrt{81 + 9\nu^2 - 6\nu}$, $G = \rho v^2$. For Ni^{2+}/MgO, $G_{44} = 36\ cm^{-1} \cong 7.2 \times 10^{-15}$ erg. $\rho = 3.6\ gm/cm^3$ and $v = 6 \times 10^5$ cm/sec. As a result

$$\Delta_3 = 11.34 \times 10^{-16}\, N \text{ Hz} = 0.0113 \times 10^{-13}\, N \text{ Hz.}$$

which shows that Δ_2 is greater than Δ_3.

Therefore the estimated total linewidth of Ni^{2+}/MgO via strain field on the basis of elasticity theory is

$$\Delta T_{G-K} = (1.64 + 0.01134)\ N \times 10^{-13}\ Hz.$$

$$= 1.65134\ N \times 10^{-13}\ Hz. \qquad (9.9)$$

The linewidth estimated in equation 9.9 is an absorption linewidth at half-height, which can be converted to the derivative linewidth ΔH_{ms} (G-K) by using the Lorentzian shape factor as $\frac{\Delta H_{ms}\ (G-K)}{\Delta T_{(G-K)}} = 0.577$.

Therefore the derivative linewidth for a concentration of 1400 ppm Ni^{2+} ions in MgO according to G-K estimation become ΔH_{ms} (G-K) = 0.231 mT, which is less than the values predicted from other theories and also much less than the observed linewidth. The comparison of the predicted linewidths with the experimental linewidth is given in Table 9.1.

Concentration (ppm)	ΔH_{ms} (dipolar) (mT)	ΔH_{ms} (exch) (mT)	ΔH_{ms} (G-K) (mT)	ΔH_{ms} (expt) $\Delta M_s = \pm 1$, 77 K (mT)
1400	20.20	1.57	0.231	6.0

TABLE 9.1 : Comparison between predicted linewidth of Ni^{2+}/MgO on the basis of different theories at $\theta_H = 0^o$ and $\phi_H = 0^o$ together with experimental value.

9.4 DISCUSSION

Two salient features emerge from initial comparison between the experimental result for the as grown crystal and those predicted on the basis of dipolar broadening. In the first place the predicted dipolar linewidth is about 5 times larger than the observed linewidth at $\theta_H = 45^o$; secondly the angular dependence of observed linewidth appears maximum at $\theta_H = 0^o$, where the predicted dipolar linewidth shows maximum at $\theta_H = 45^o$. The discrepancy in the magnitude of the linewidth (observed) is not far greater than those encountered for other ions doped in MgO in which similar comparisons have been made and where the linewidths were determined by exchange narrowing, (Table 9.2).

Doped ions	Predicted linewidth (dipolar)	$M_4^{1/4}/M_2^{1/2}$ greater than	$\frac{\Delta H_{ms}}{\Delta H_{1/2}}$ less than	Lineshape	Refs.
Fe^{3+}	100 times larger than observed	1.42	0.577	Lorentzian	Chapter 6
Cr^{3+}	160 times larger than observed	1.33	0.577	Lorentzian	Chapter 4
Co^{2+}	50 times larger than observed	1.35	0.577	Lorentzian	Chapter 5
Ni^{2+}	5 times larger than observed	1.34	0.577	Lorentzian	Present work

TABLE 9.2 : Comparison of predicted dipolar linewidth with observed linewidth and lineshape of different ions doped in MgO.

To determine the nature of linewidth mechanisms, the observed derivative spectrum was integrated numerically giving the integrated line-

shape as shown in Figure 9.6 and the lineshape factor $\frac{\Delta H_{ms}\ (obs)}{\Delta H_{\frac{1}{2}}\ (obs)}$ was found 0.525. The moment ratio $M_4^{\frac{1}{4}} / M_2^{\frac{1}{2}}$ (M_2 and M_4 are the second and fourth moments respectively) was found 1.34. Both the lineshape factor and moment ratio were found almost independent of polar angle. The value of the lineshape factor and the moment ratio are similar to the figure quoted for Fe^{3+}/MgO, Cr^{3+}/MgO and Co^{2+}/MgO as given in Table 9.2. This suggests that the lineshape is Lorentzian and exchange narrowing is important.

Although the assumed G-K lineshape is the same as the observed Lorentzian lineshape, the magnitude of the strain broadened linewidth, due to point defects considered by G-K, is about 25 times less than the magnitude of the observed broadened line. This proves that the G-K estimation of linewidth, due to point defects, seems to be absent for lower concentration of Ni^{2+} in MgO. On this assumption and comparison with the predicted dipolar linewidth and with derivative (normalized) lineshape (Figure 9.5); since moment ratio greater than 1.33 and lineshape is Lorentzian, it is suggested that the observed line mechanism is due to exchange narrowing. The broadened linewidth (which is about 4 times larger than the estimated linewidth on the basis of exchange mechanism) and the angular dependence of the linewidth, suggests the presence of inhomogeneous strain in the crystal.

To explain the angular dependence of the linewidth, the equation of linewidth due to internal strain (or stress) given by Feher et al (9.16, 9.17) of any transition for any angle (θ,ϕ) of the magnetic field with respect to the cube axes of the crystal can be written as

$$\Delta H_{\frac{1}{2}} = \left[a(1 - 3F) + bF \right]^{\frac{1}{2}} \qquad (9.10)$$

with $F = (\sin^2 \theta_H \cos^2 \theta_H + \sin^2 \phi_H \cos^2 \phi_H \sin^4 \theta_H)$

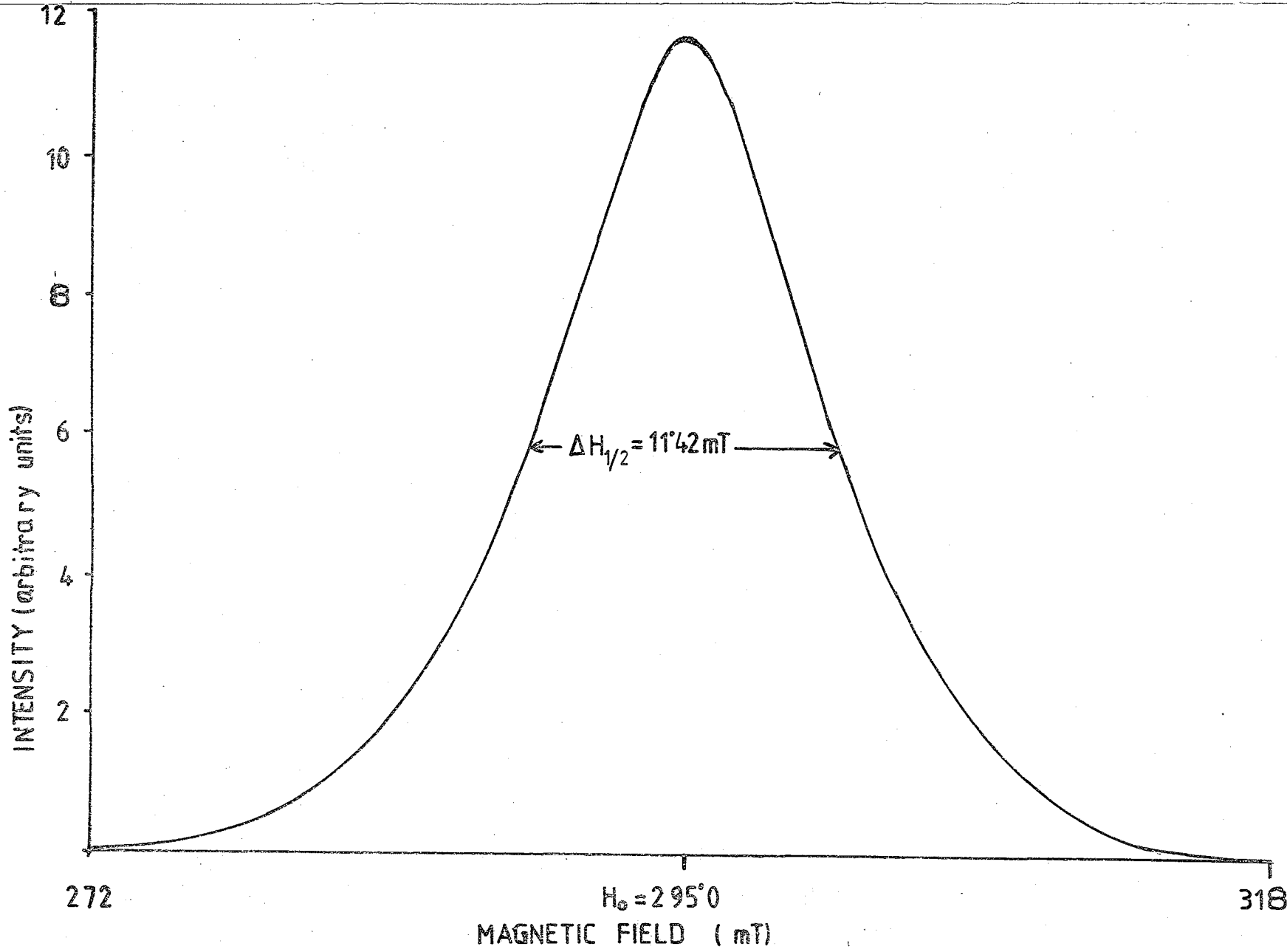

FIG, 9,6 INTEGRATED LINESHAPE FOR Ni^{2+}/MgO(1400ppm), $\theta_H = 0^\circ$, 77K, 9·14GHz, $\Delta Ms = \pm 1$.

where $\Delta H_{\frac{1}{2}}$ is the linewidth at half intensity ; 'a' and 'b' are the constants dependent on the elastic constants and strain (or stress) distribution in the crystal lattice. A good fit of this equation has been found with experimental data as shown in Figure 9.7 by a solid line ; where a = 132 mT^2, b = 124 mT^2 and F = $\sin^2 \theta_H - \sin^4 \theta_H$ (in this experimental situation $\phi_H = 0^\circ$). Therefore the linewidth, when H// [100] (i.e. $\theta_H = 0^\circ$, $\phi_H = 0^\circ$) is

$$\Delta H_{\frac{1}{2}} \left[100\right] = a^{\frac{1}{2}} = 11.5 \quad mT \qquad (9.11a)$$

when H// [111] (i.e. $\theta_H = 54.5^\circ$, $\phi_H = 45^\circ$)

$$\Delta H_{\frac{1}{2}} \left[111\right] = \left(\frac{b}{3}\right)^{\frac{1}{2}} = 6.4 \quad mT \qquad (9.11b)$$

and when H// [110] (i.e. $\theta_H = 45^\circ$, $\phi_H = 0^\circ$)

$$\Delta H_{\frac{1}{2}} \left[110\right] = \left(\frac{a+b}{4}\right)^{\frac{1}{2}} = 8 \quad mT \qquad (9.11c)$$

Therefore $\Delta H_{\frac{1}{2}}$ with H along the directions [111] , [110] and [100] are in the ratios 1:1.25:1.8. These ratios are agreed well with the corresponding ratios 1:1.1:1.5 reported by Orton et al (9.3).

Several mechanisms of inhomogeneous line broadening due to strain have been discussed by Stoneham (9.18), such as (a) strain broadening by point defect arising essentially from a size difference effect and is not likely to make an important contribution here because the ionic radius of the doping ion (Ni^{2+}, 0.70 Å) is less than that of the cation (Mg^{2+}, 0.72 Å) ; (b) strain broadening by line defect (i.e. dislocation) which may be the possible reason here. Lewis et al (9.5) deduce a relation between the width of the spin resonance line and the width of

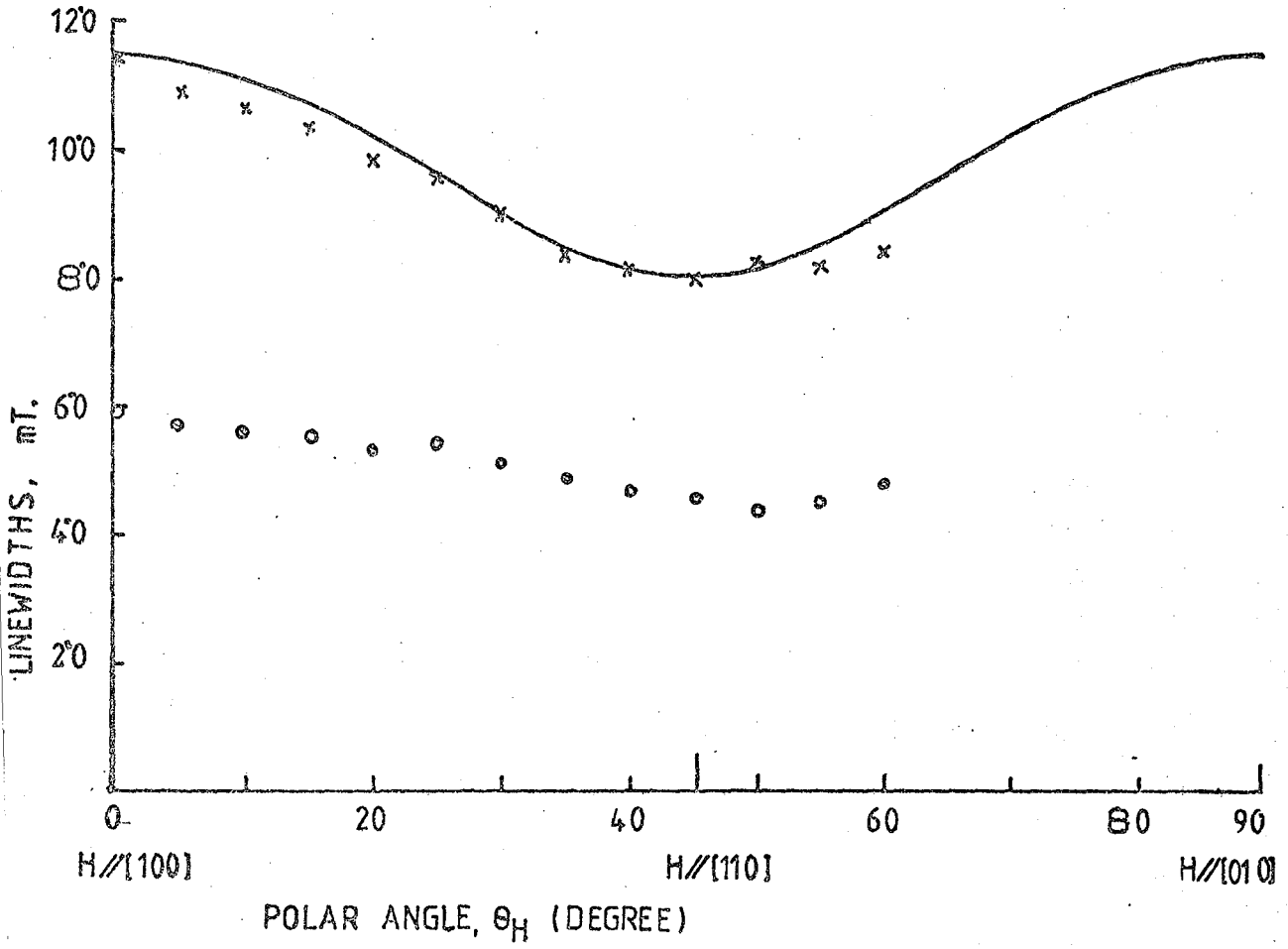

FIG, 9,7 THE ANGULAR DEPENDENCE OF THE LINEWIDTHS FOR Ni^{2+}/MgO (1400 ppm), 9·14GHz, 77K, $\phi_H = 0°$, OPEN CIRCLES, PEAK-TO-PEAK LINEWIDTH, ΔH_{ms}; CROSSES, ABSORPTION-HALF-AMPLITUDE LINEWIDTH, $\Delta H_{1/2}$; AND SOLID LINE IS THE DEPENDENCE PREDICTED BY Eqn. 9,10, FOR $a = 132\,mT^2$ AND $b = 124\,mT^2$.

the strain distribution (irrespective to the shape) as

$$\left.\begin{aligned} \hbar\Delta\omega_{001} &= G_{11}\,\varepsilon_E \\ \hbar\Delta\omega_{111} &= G_{44}\,\varepsilon_T \end{aligned}\right\} \qquad (9.12)$$

where $\Delta\omega$ denotes the full width at half intensity in frequency unit corresponding to the cube axes ; G_{11} and G_{44} are the coupling coefficients [for Ni^{2+}/MgO, $G_{11} = 57\ cm^{-1}$, $G_{44} = 36\ cm^{-1}$ (9.19)] ; ε_E and ε_T are the full width of the strain distribution at half intensity corresponding to H// [100] and H// [111] respectively. According to Stoneham's notation (9.20),

$$\left.\begin{aligned} \varepsilon_E &= \frac{1}{2}\ \varepsilon_{001} \\ \varepsilon_T &= \frac{4}{3}\ \varepsilon_{111} \end{aligned}\right\} \qquad (9.13)$$

Using equations 9.12 and 9.13 together with the experimental values, the ratio of $\frac{\varepsilon_{001}}{\varepsilon_{111}}$ becomes 3.01, which is very close to the theoretical value of 2.3 given by Stoneham (9.20) for strain broadening due to dislocations. The predicted shape of the line (due to strain by dislocation) will be Lorentzian along [100] and become nearly Gaussian along [111] (9.20). In fact, the experimental lineshape for different ions doped in MgO were Lorentzian, which were unlike the predicted shape considered by Stoneham as shown in Table 9.3. The calculated ratio $\frac{\varepsilon_{001}}{\varepsilon_{111}}$ = 3.01 and observed Lorentzian shape suggests that the angular dependence of the broadened line of Ni^{2+}/MgO is due to the presence of strain which arises from inhomogeneous dislocations.

IONS doped in MgO	$\frac{\varepsilon_{001}}{\varepsilon_{111}}$	Refs)	Lineshapes
Mn^{2+}	3.1		
Fe^{3+}	4.0		
Fe^{2+}	3.2 2.5	(9.18)	Experimental lineshapes were Lorentzian
Co^{2+}	1.0		
Ni^{2+}	3.1		
Theory	2.3	(9.20)	Theory predict Lorentzian when H// [100] and nearly Gaussian when H// [111]
Ni^{2+}	3.01	Present work	Lorentzian

TABLE 9.3 : Strain distributed linewidth ratio calculated from e.s.r. data for ions doped in MgO by Stoneham (9.18) together with the calculated value for Ni^{2+}/MgO (1400 ppm).

Finally, it can be calculated from the moment ratio ; $\frac{\varepsilon_{001}}{\varepsilon_{111}}$; Lorentzian lineshape and the magnitude of the linewidth (in comparison with theories) that the observed linewidth in Ni^{2+}/MgO for $\Delta M_s = \pm 1$ is determined by exchange narrowing together with inhomogeneous broadening due to strain.

REFERENCES

CHAPTER NINE

9.1 W. Low, Phys.Rev. 109 (1958) 247.

9.2 J.W. Orton, P. Auzins and J.E. Wertz, Phys.Rev.Letts.41 (1960)128.

9.3 J.W.Orton, P. Auzins, J.H.E.Griffiths and J.E.Wertz, Proc.Phys.Soc. London 78 (1961) 584.

9.4 M.M.Walsh, Phys.Rev. 122 (1961) 762.

9.5 M.F.Lewis, and H.M.Stoneham, Phys.Rev.164 (1967) 271.

9.6 S.R.P.Smith, F.Dravnicks, and J.E.Wertz, Phys.Rev.178 (1969)471.

9.7 N.M.Galeeva; B.I.Kochelaev, Sov.Phys.Solid State 19 (1977)787.

9.8 J.E.Wertz; J.R.Bolton, 'Electron Spin Resonance' p.292 McGraw Hill, N.Y. 1972.

9.9 W.Low; J.T.Suss, Solid State Comn. 2 (1964) 1.

9.10 P.Swarp, Cand.J.Phys. 37 (1959) 848.

9.11 C.P. Poole, 'Electron Spin Resonance' (John Wiley & Sons,N.Y.1967) p.775.

9.12 P.W.Anderson; P.R.Weiss, Rev.Mod. Phys.25 (1953) 269.

9.13 R.W.C. Wyckoff, 'Crystal Structure' V-1. Interscience.N.Y.1965 Chapters V and VI.

9.14 C.R.C.Handbook (for physics and chemistry) 57th Ed. 1977-78 p.E.120.

9.15 R.D.Shannon and C.T.Prewitt, Acta.Cryst.B25 (1969) 925.

9.16 E.Feher and M.Weger, Bull.Am.Phys.Soc 7 (1962) 613.

9.17 E.Feher, Phys.Rev.136A (1964) 145.

9.18 A.M.Stoneham, Rev.Mod.Phys. 41 (1969) 82.

9.19 G.Watkins and E.Feher, Bull.Am.Phys.Soc 7 (1962) 29.

9.20 A.M.Stoneham, Proc.Phys.Soc.London 89 (1966) 909.

CHAPTER TEN

DIELECTRIC PROPERTIES

In this chapter the dielectric properties of pure and doped MgO have been measured at the temperatures between 293 K to 100 K, over the frequency range 500 Hz to 30 kHz. The samples examined were MgO (4N), Co^{2+}/MgO (300 ppm to 9900 ppm Co) and Ni^{2+}/MgO (130 ppm to 1400 ppm). The dielectric constant ε' for doped MgO has been found to be higher than the undoped MgO. The measured dielectric constants ε' of Co^{2+}/MgO were found slightly concentration dependent, which may be matched with the concentration dependence behaviour of exchange energy. Low temperature measurements of ε' indicate that Co^{2+}/MgO has the greater temperature dependence of polarizability than pure MgO and Ni^{2+}/MgO. At room temperature, the variation of the real part of the conductivity with frequency over the measured frequency range followed $Re\sigma(\omega) \alpha \quad \omega^{n}$, with n = 0.86 for Co^{2+}/MgO and n = 0.853 for Ni^{2+}/MgO and undoped MgO. The data fits well with the "universal dielectric law" $\varepsilon'' \quad \alpha \ \omega^{n-1}$ $(n < 1)$.

10.1 INTRODUCTION

An important feature of dielectrics (insulators) is the presence of extrinsic (or low temperature) and intrinsic (or high temperature) conductivity. Extrinsic conductivity is the conductivity when the source of charge carrier is impurity ions or defects resulting from impurities and intrinsic conductivity is the conductivity due to the host crystal ions and the thermally created defects. Conductivity studies in the temperature range above 800^{o} C have been made as follows:- The static intrinsic conductivity of pure MgO and doped MgO (0.01 % Fe) by Mittof in 1959 (10.1) and 1962 (10.2) ; the surface conductivity (static) of single crystal MgO doped with NiO (5%) by Choi et al in 1973 (10.3) ; the a.c. bulk conductivity (frequency below 100 kHz) of pure single crystal by Osburn et al in 1977 (10.4) and of polycrystalline MgO doped with CoO (1.1%) by Devies in 1963 (10.5). It was found that the conductivity of MgO dominated by impurities. Lewis and Wright in 1968 (10.6), first measured the static bulk conductivity of single crystal MgO (the impurity content of about 850 ppm with major impurities of Ca, Fe, Al, Na, Si) in the temperature range 400^{o}C to 750^{o}C, where it was shown that the conductivity mechanism was due to electron hopping between impurity sites in the crystal rather than to oxygen ion transport suggested by Devies in 1963 (10.5). Several theories of hopping conduction (10.7, 10.8), indicate that a frequency dependence of the real part of the conductivity following a $Re\sigma(\omega) \alpha \omega^{n}$ law should be observed with $n < 1$. More recently Jonscher in 1977 (10.9) has suggested that several hopping models may lead to this behaviour and has shown further a wide range of materials which follow the "Universal dielectric law" according to which $\varepsilon''(\omega) \alpha \omega^{n-1}$, where again $n < 1$.

So far no previous measurements of dielectric constant and conductivity on doped MgO single crystal at room temperature have been

published. The aims of this chapter are to measure the dielectric constant and loss for single crystals of undoped MgO(4N), Co^{2+}/MgO and Ni^{2+}/MgO in the frequency range from 0.5 kHz to 30 kHz at room temperature and hence to establish the frequency variation of dielectric constant and loss, which will indicate the conduction mechanism. Although most of the measurements were made at room temperature, for few specimens, the temperature dependence of dielectric constant at the temperature range from 100 K to 293 K were also made to observe the effect of temperature on dielectric constant.

10.2 EXPERIMENTAL

The purity of the undoped MgO sample examined was 4N, i.e. 99.99% purity. The cobalt concentration in the specimens examined range from 310 ppm to 9900 ppm (all these concentrations have been studied for e.s.r. measurements as described in Chapter 5) and the nickel concentration in the specimens examined ranged from 130 ppm to 1400 ppm (where 1400 ppm concentration has been studied for e.s.r. measurements as described in Chapter 9). All the specimens were cut with a diamond wheel cutting machine ; the large area faces of the specimens were polished to a 0.25 micron finish using a precision polishing machine. Specimens dimensions were typically 10 mm x 10 mm x 0.3 mm and circular gold electrodes of 6mm diameter were evaporated on the opposite polished faces to ensure good electrical contact.

10.2.1 Room Temperature Measurements

The dielectric properties of the specimens were measured at room temperature over the frequency range 500 Hz to 30 kHz using a Wayne-Kerr bridge (Type. B224). For room temperature measurement, a dielectric testing jig made with crap brand tufnol insulators of the type described elsewhere (10.10), was used to hold the specimen. In the bridge the

conductance G and capacitance C of the specimens were determined as functions of applied frequency and the data was used to derive the real part of the conductivity Re(σ), the loss tanδ, and the real part of the dielectric constant ε', from the relations

$$Re(\sigma) = \frac{d}{Ag} \; G \; (mho\text{-}m^{-1}) \tag{10.1}$$

$$\tan\delta = \frac{G}{\omega C} = \frac{\varepsilon''}{\varepsilon'} \tag{10.2}$$

and

$$\varepsilon' = \frac{C}{\varepsilon_o} \cdot \frac{d}{Ag} \tag{10.3}$$

where ω is the angular frequency, d the specimen thickness in meter, Ag the area of the gold electrode in meter^2 and ε_o is the permittivity of free space having a value of 8.854 pF m^{-1}. Using the different edge correction formulae described in the literature (10.11), the equation 10.3 was modified to

$$\varepsilon' = \frac{C}{C_{og} + C_{eg}} = \frac{C_S - C_{AIR} + C_{OB} + C_{eB}}{C_{og} + C_{eg}} \tag{10.4}$$

where C_S is the measured capacitance with the specimen mounted in the jig and C_{AIR} is the capacitance at the same jig electrode spacing without specimen and

$$\left.\begin{aligned} C_{og} &= \frac{\varepsilon_o Ag}{d} \\ C_{OB} &= \frac{\varepsilon_o A_B}{d} \\ C_{eg} &= \frac{111.3\ Dg}{8\pi}\left[\ell n\ \frac{8\pi Dg}{d} - 3\right] \\ C_{eB} &= \frac{111.3\ D_B}{8\pi}\left[\ell n\ \frac{8\pi D_B}{d} - 3\right] \end{aligned}\right\} \tag{10.5}$$

where Dg and D_B are the diameters of the gold and brass electrodes respectively in meter and assuming the ratio of the thickness of gold electrodes to the thickness of the sample less than 0.01. The output of the external oscillator applied to the bridge was 2 V r.m.s. The room temperature measurements were made in air.

10.2.2 Low Temperature Measurements

The low temperature measurements were made using a similar type of jig as that used at room temperature, by installing the jig inside a helium cryostat as shown in Figure 10.1. The cryostat itself, being metals provides the shielding to minimize the pick up. The temperature dependent dielectric constant measurements were made by observing the change in capacitance of the sample as its temperature was varied in the range 100 K to 293 K. Temperature measurements were made with a copper-copper-constantan thermocouple, which was mounted on one of the electrodes. The measurements were made in the presence of nitrogen gas at constant pressure. The specimens also get a constant pressure of about 5.5 Newton/cm^2 due to the weight of the upper jig. Since the dielectric constant of the specimen is relatively insensitive to frequency in the low frequency range, the measurements were made at the single frequency 1.592 kHz, which was the internal frequency of the bridge.

In general, isotropic and cubic materials obey the Clausius-Mosotti equation (10.12) as regards the dielectric constant,

$$\frac{\varepsilon'-1}{\varepsilon'+2} = \frac{1}{3}\frac{\alpha_m}{V} \qquad (10.6)$$

where $\left\{\frac{\alpha_m}{V}\right\}$ is the polarizability per unit volume. The temperature dependence of the dielectric constant is only obtained by differentiating

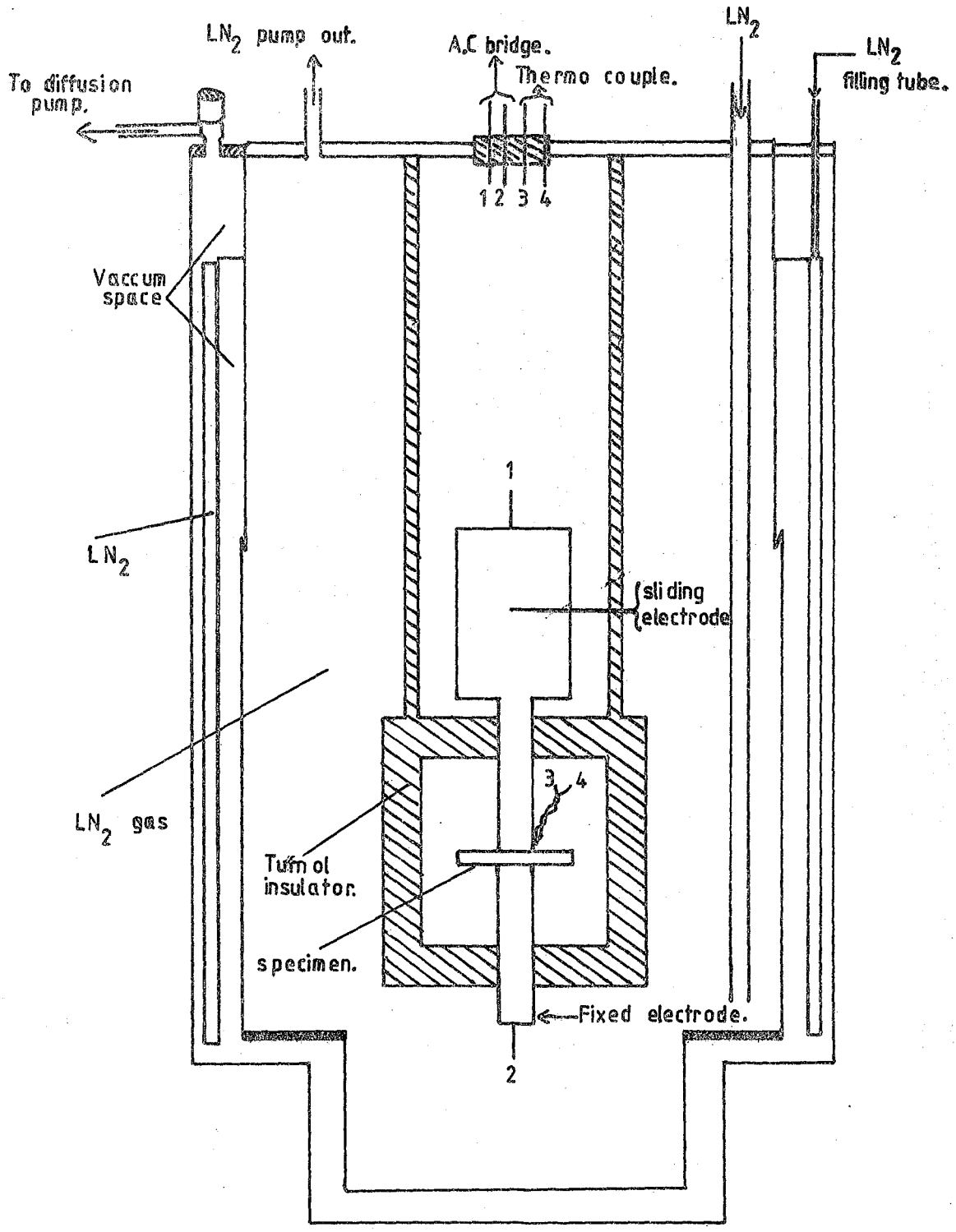

FIG, 10,1 DIELECTRIC TESTING JIG FOR LOW TEMPERATURE.

Equation 10.6, with respect to temperature T at constant pressure P,(10.13)

$$\frac{1}{(\varepsilon'-1)(\varepsilon'+2)}\left(\frac{\partial\varepsilon'}{\partial T}\right)_P = -\frac{1}{3V}\left(\frac{\partial V}{\partial T}\right)_P + \left[\frac{1}{\alpha_m}\left(\frac{\partial\alpha_m}{\partial P}\right)_T \Big/ \frac{1}{V}\left(\frac{\partial V}{\partial P}\right)_T\right] \cdot \frac{1}{3V}\left(\frac{\partial V}{\partial T}\right)_P$$

$$+ \frac{1}{3\alpha_m}\left(\frac{\partial\alpha_m}{\partial T}\right)_V = K + L + M \qquad (10.7)$$

The first item K describes the direct effect of volume expansion, the second term L represents the increase of the polarizability of a given number of particles as a result of the expanding volume, and the third term M indicates the temperature dependence of the polarizability itself (at constant volume).

Bosman and Havinga in 1963 (10.13) have discovered an interesting experimental relationship between the dielectric constant and its temperature dependence which holds for a surprising large and diversified number of materials. It appears that the temperature dependence of a dielectric constant, $K + L + M = \frac{1}{(\varepsilon'-1)(\varepsilon'+2)}\left\{\frac{\partial\varepsilon'}{\partial T}\right\}_P$ is positive for ε' smaller than about 20 and negative for larger values of ε'.

10.3 EXPERIMENTAL RESULTS

10.3.1 At 293 K

The dielectric constant data obtained at 1.592 kHz (the internal frequency of the bridge) are summarized in Table 10.1 in which the values given under 'present work' represent averages of several measurements on each individual specimen with an error of ± 0.08 for ε'. The frequency

References	Samples	Doping Concentration (ppm)	Frequency (kHz)	ε'	tanδ
Present work	Undoped MgO	4N	1.592	9.45	7.6×10^{-3}
	Ni^{2+}/MgO	130	"	9.50	6.5×10^{-3}
		370	"	9.50	6.5×10^{-3}
		1400	"	9.52	6.19×10^{-3}
	Co^{2+}/MgO	310	"	9.59	6.69×10^{-3}
		1250	"	9.60	6.57×10^{-3}
		1900	"	9.58	6.24×10^{-3}
		2500	"	9.63	7.28×10^{-3}
		3300	"	9.70	6.19×10^{-3}
		4800	"	9.72	5.73×10^{-3}
		8200	"	9.74	6.1×10^{-3}
		9900	"	9.35	4.79×10^{-3}
Hippel (10.14)	Pure	-	$0.1-10^5$	9.65	$< 3 \times 10^{-4}$
Yamashita et al (10.15)	"	-	Static	9.80	-
Goyal (10.16)	"	-	Static	9.34	-
Bosman et al (10.13)	"	-	250	9.80	-
Barties et al (10.17)	"	-	1 & 10	9.958	-

TABLE 10.1 : Dielectric data for MgO, Ni^{2+}/MgO, Co^{2+}/MgO at 293 K, 1.592 kHz.

variations of dielectric constant ε' for pure MgO, Ni^{2+}/MgO and Co^{2+}/MgO in the frequency range of 0.5 kHz to 30 kHz are shown in Figure 10.2. It was found that the frequency variations for all the specimens were very similar in form. There was no significanct difference between the behaviour of pure MgO and Ni^{2+}/MgO specimens. A very slight increase in ε' from 9.59 ±0.08 for 310 ppm Co^{2+} to 9.72 ± 0.08 for 8200 ppm Co^{2+} was found. The variation of dielectric constant with doping concentrations of Ni^{2+} and Co^{2+} in MgO are shown in Figure 10.3 at a frequency of 1.592 kHz. The values of dielectric constant for the specimens of Ni^{2+}/MgO are independent of concentration.

The conductivity variation with frequency, derived directly from the experimental data (assuming that the d.c. contribution was negligible) is shown by the continuous line of Figure 10.4(a) for Co^{2+}/MgO and of Figure 10.4(b) for Ni^{2+}/MgO. Over the frequency range 0.5 kHz to 30 kHz, these fit well with the relation

$$Re\sigma(\omega) \propto \omega^{n} \qquad (10.8)$$

where n has the value 0.86 for Co^{2+}/MgO and 0.853 for Ni^{2+}/MgO and undoped MgO at 293 K.

With regard to the dielectric loss, tan δ, there were slow decreases in magnitude as a function of frequency (of similar form for all the specimens) but not in sequence with the doping concentrations of Co^{2+} in MgO as shown in Figure 5(a). It was found that the variation of tanδ with concentrations were less sensitive with frequencies below 10 kHz. The variation of ε'' with frequency for Co^{2+}/MgO was derived from Figure 10.2 and Figure 10.4(a) and is given in Figure 10.5(b). Similar variations of dielectric loss and tan δ with frequency for Ni^{2+}/MgO are shown in

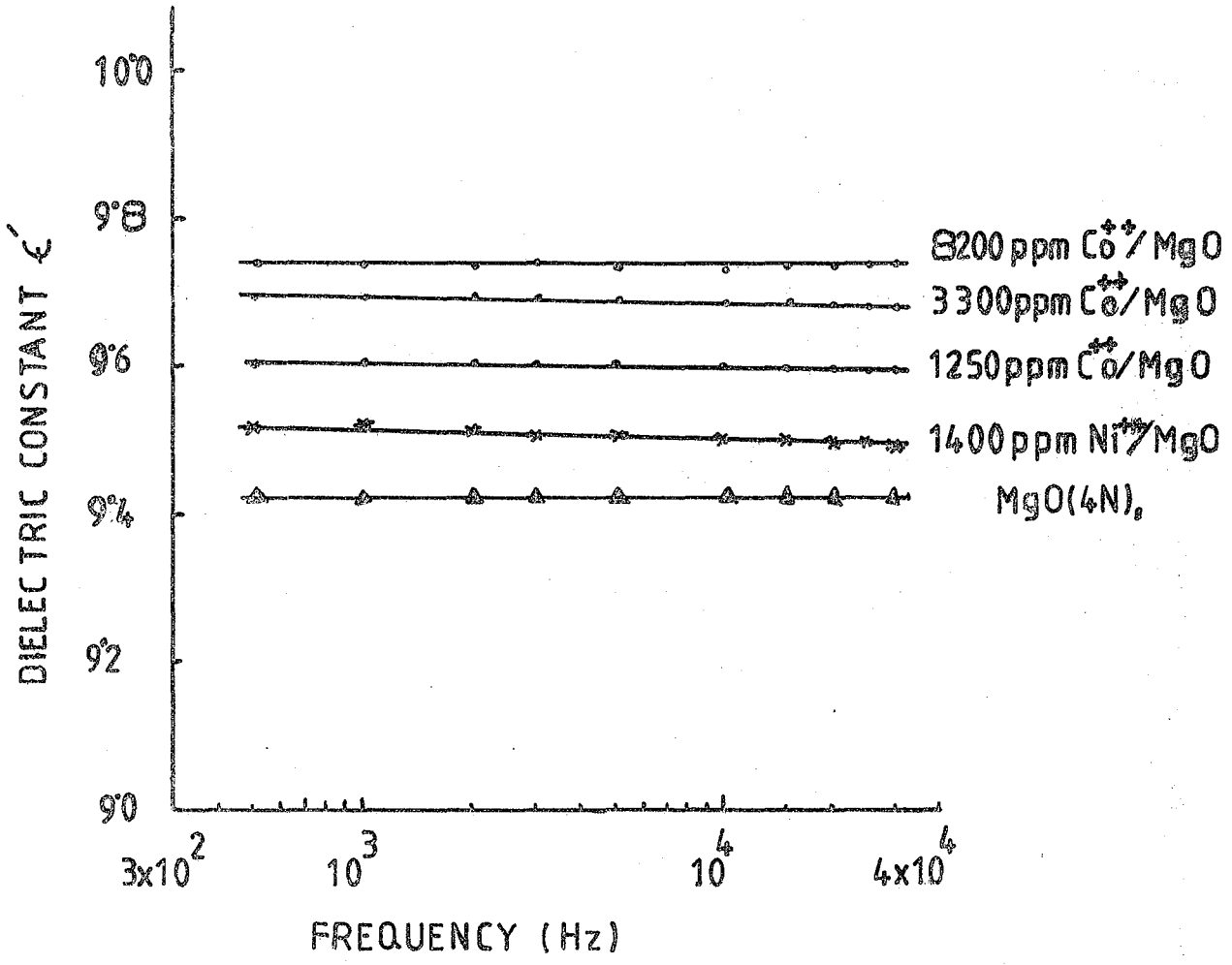

FIG, 10,2 FREQUENCY DEPENDENCE DIELECTRIC CONSTANT ϵ'; DOPED AND UNDOPED MgO , 293K.

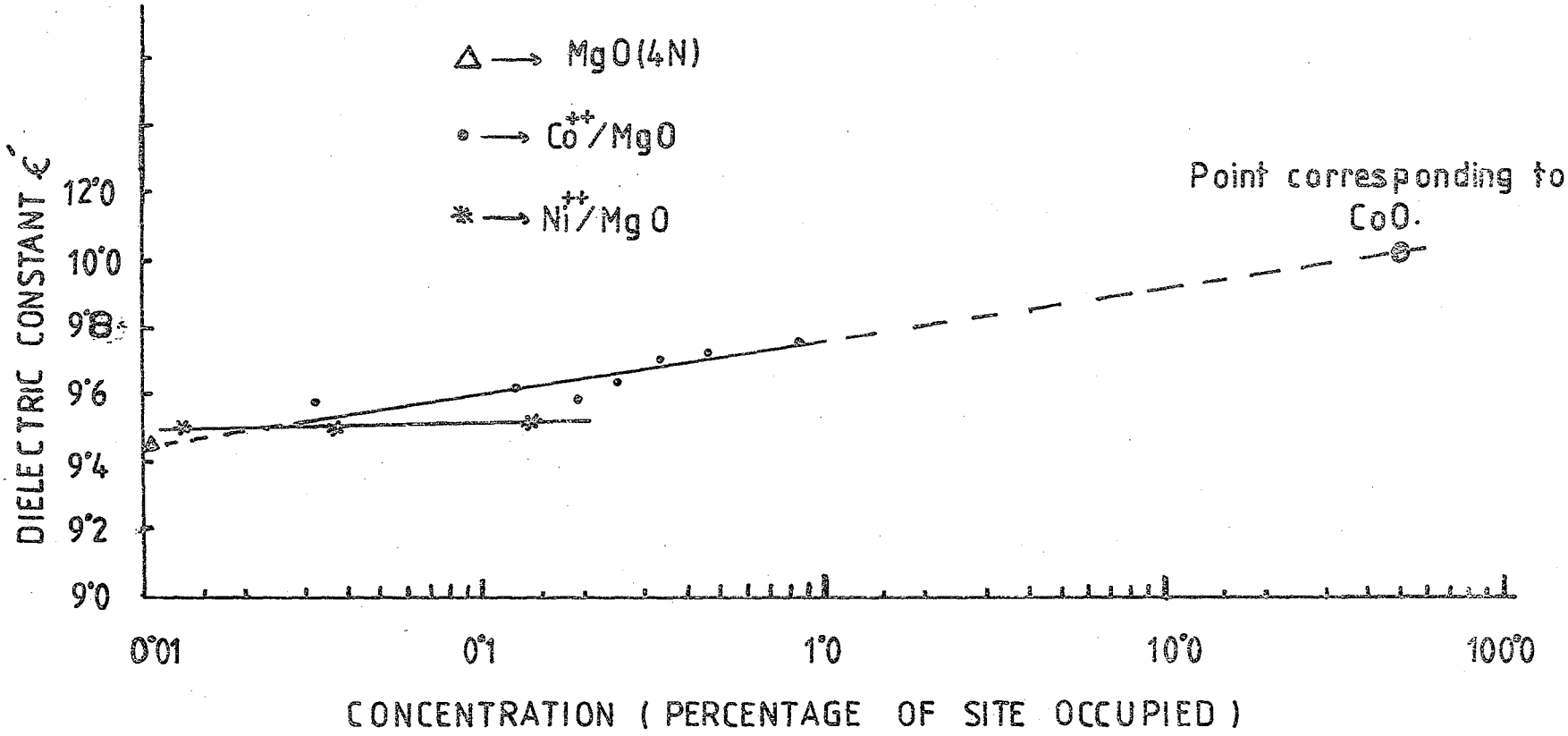

FIG, 10,3 CONCENTRATION VERSUS DIELECTRIC CONSTANT OF Co^{++}/MgO AND Ni^{++}/MgO, 293K, 1·592KHz.

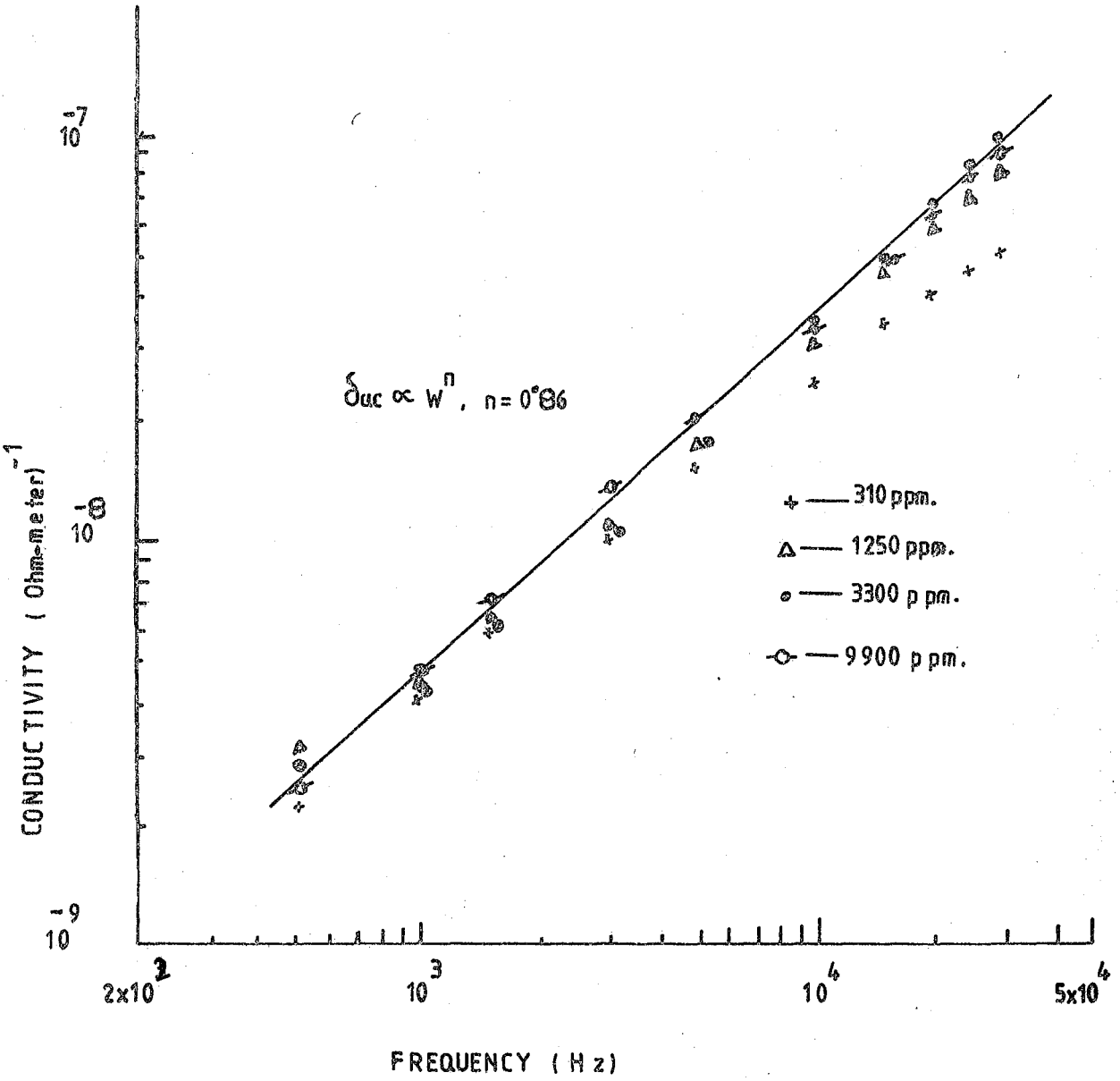

FIG, 10,4(a) THE FREQUENCY DEPENDENCE OF CONDUCTIVITY, Co^{2+}/MgO, 293K.

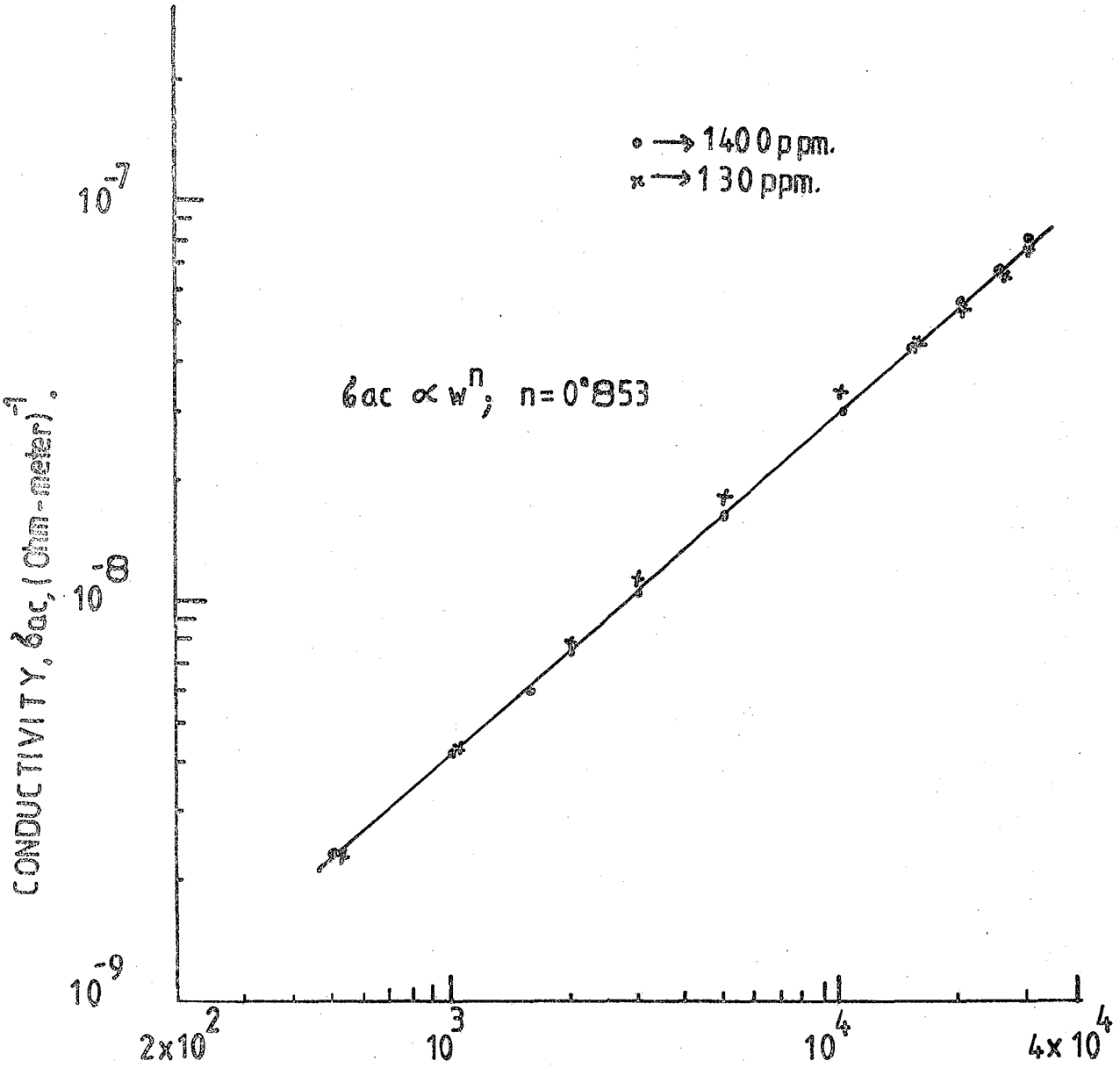

FIG, 10,4 (b). THE FREQUENCY DEPENDENCE OF CONDUCTIVITY FOR Ni^{++}/MgO, 293K.

Figure 10.6. The variation of conductivity with Co concentrations in MgO at different frequencies are shown in Figure 10.7. It was assumed that there was a very little increase in conductivity with concentration, as shown by the continuous lines. The slopes of the conductivity plots were a bit higher above 10 kHz. For Ni^{2+}/MgO, the conductivity is almost the same as for pure MgO (4N) sample and is also independent of the Ni^{2+} concentration.

10.3.2 Below 293 K

The results of the measurements for the temperature dependence of dielectric constant,

$$\left[\frac{1}{(\varepsilon'-1)(\varepsilon'+2)}\right]\left(\frac{\partial\varepsilon'}{\partial T}\right)_P = K + L + M,$$ are given in Table 10.2.

Samples	Concentration (ppm)	Dielectric constant ε' at 293 K	Frequency kHz	Temperature (^{o} K)	$\frac{1}{(\varepsilon'-1)}\frac{1}{(\varepsilon'+2)}\left(\frac{\partial\varepsilon'}{\partial T}\right)_P$ at 293 K, (K^{-1})	Refs
Undoped MgO	4N	9.45	1.592	100-293	$(1.31\pm0.21)\times10^{-5}$	
Ni^{2+}/MgO	1400	9.52	1.592	100-293	$(1.26\pm0.12)\times10^{-5}$	Present
	130	9.50			$(1.16\pm0.12)\times10^{-5}$	
	8200	9.74			$(1.80\pm0.14)\times10^{-5}$	
Co^{2+}/MgO	4800	9.72	1.592	100-293	$(1.69\pm0.39)\times10^{-5}$	
	1900	9.58			$(1.26\pm0.12)\times10^{-5}$	
Pure MgO	-	9.8	Static	Uncertain but >293K	1.19×10^{-5}	(10.19)
Pure MgO	-	9.8	Static	"	1.76×10^{-5}	(10.18)
Pure MgO	-	9.8	250	293-423	1.05×10^{-5}	(10.13)
Pure MgO	-	9.96	1 and 10	50-293	0.998×10^{-5}	(10.17)

TABLE 10.2 : Temperature dependence of dielectric constant, undoped MgO, Ni^{2+}/MgO and Co^{2+}/MgO.

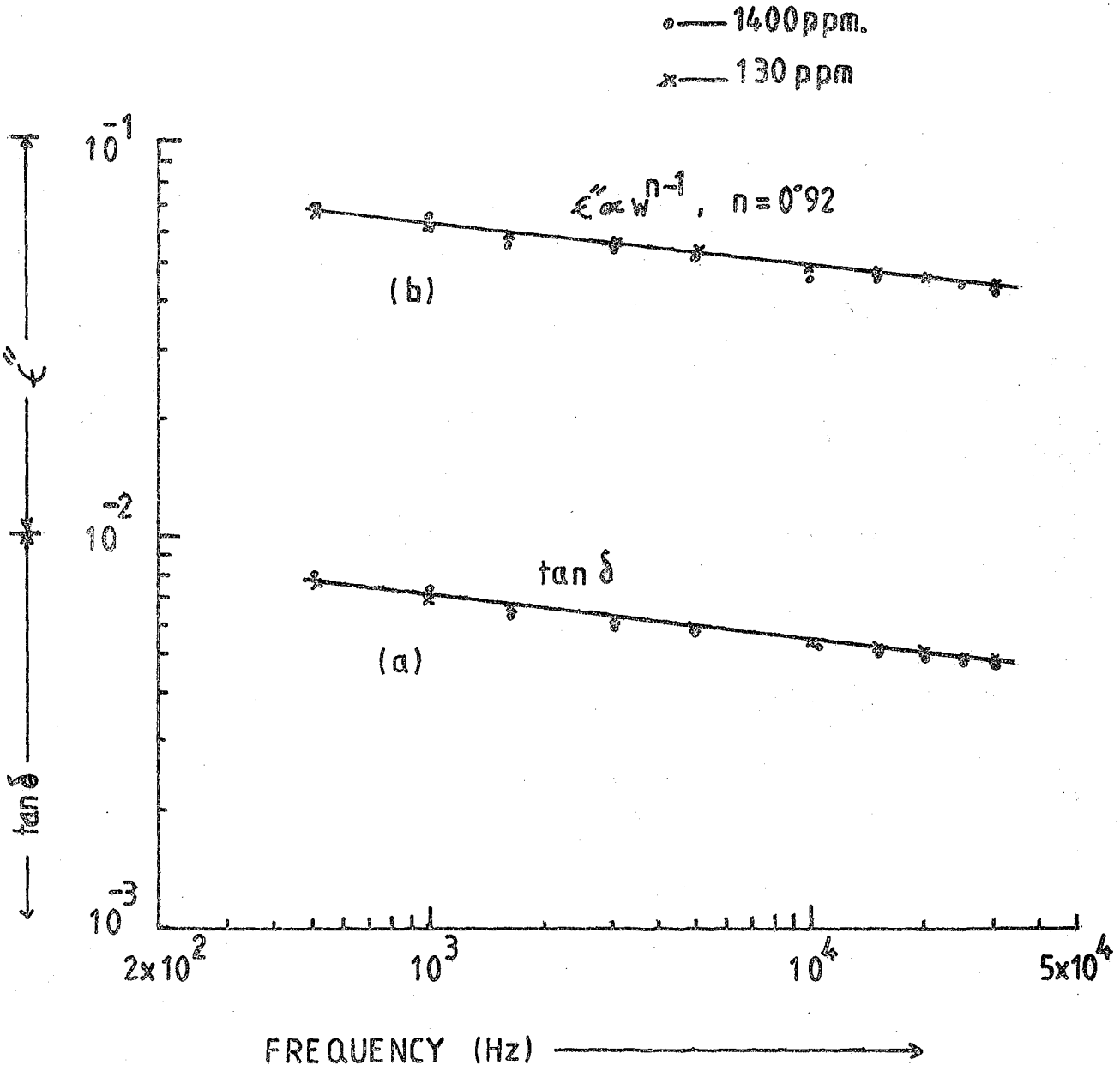

FIG, 10,6 THE FREQUENCY DEPENDENCE OF (a) tan δ & (b) DIELECTRIC LOSS ϵ'' ; FOR Ni^{++}/MgO ; 293K.

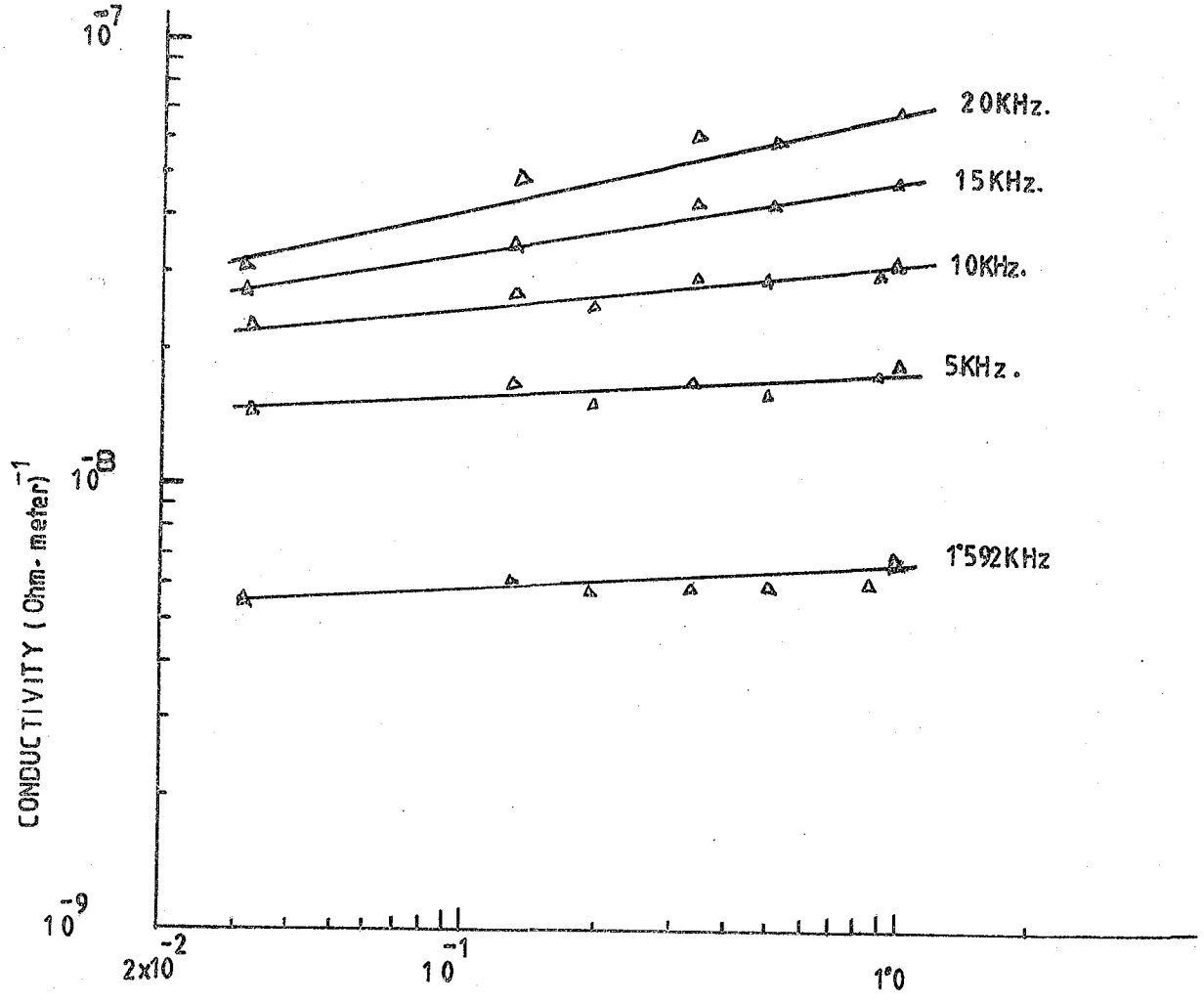

FIG, 10,7 CONCENTRATION VS CONDUCTIVITY OF Co^{2+}/MgO AT LOW FREQUENCY: 293K.

These values and the root mean square errors attached to them are based on the results of several measurements. The typical variation of dielectric constant with temperature is shown in Figure 10.8. The (K + L + M) value for undoped and doped MgO at 293 K are given in Table 10.2 (under present work), is about 30% less than that reported by Krishnan (10.18) and about 30% greater than that by Bosman et al (10.13) and Barties et al (10.17) ; however, the derived value for undoped MgO does agree with the literature value 10.19. For Ni^{2+}/MgO, the (K + L + M) values are independent of doping concentrations and very near to the pure MgO value $(1.31\pm0.21)\times10^{-5}.k^{-1}$. But for the specimens of Co^{2+}/MgO, these values seem to be concentration dependent giving greater values for the higher doping concentrations as shown in Table 10.2.

10.4 DISCUSSION

The measured values of dielectric constant ε' are less than three of the values reported in the literature (10.13, 10.15, 10.17) for pure MgO and greater than one (10.16). Since the e.s.r. data (as shown in Chapter 5) and the lattice parameter data (10.20) did not show any change in lattice structure of MgO with doping concentrations of Co^{2+} (up to 9900 ppm), the slight increase in dielectric constant with doping concentration could be matched with the exchange energy. A comparison of the dielectric constant ε' with exchange energy J for some oxides having similar lattice structures to MgO are given in Table 10.3.

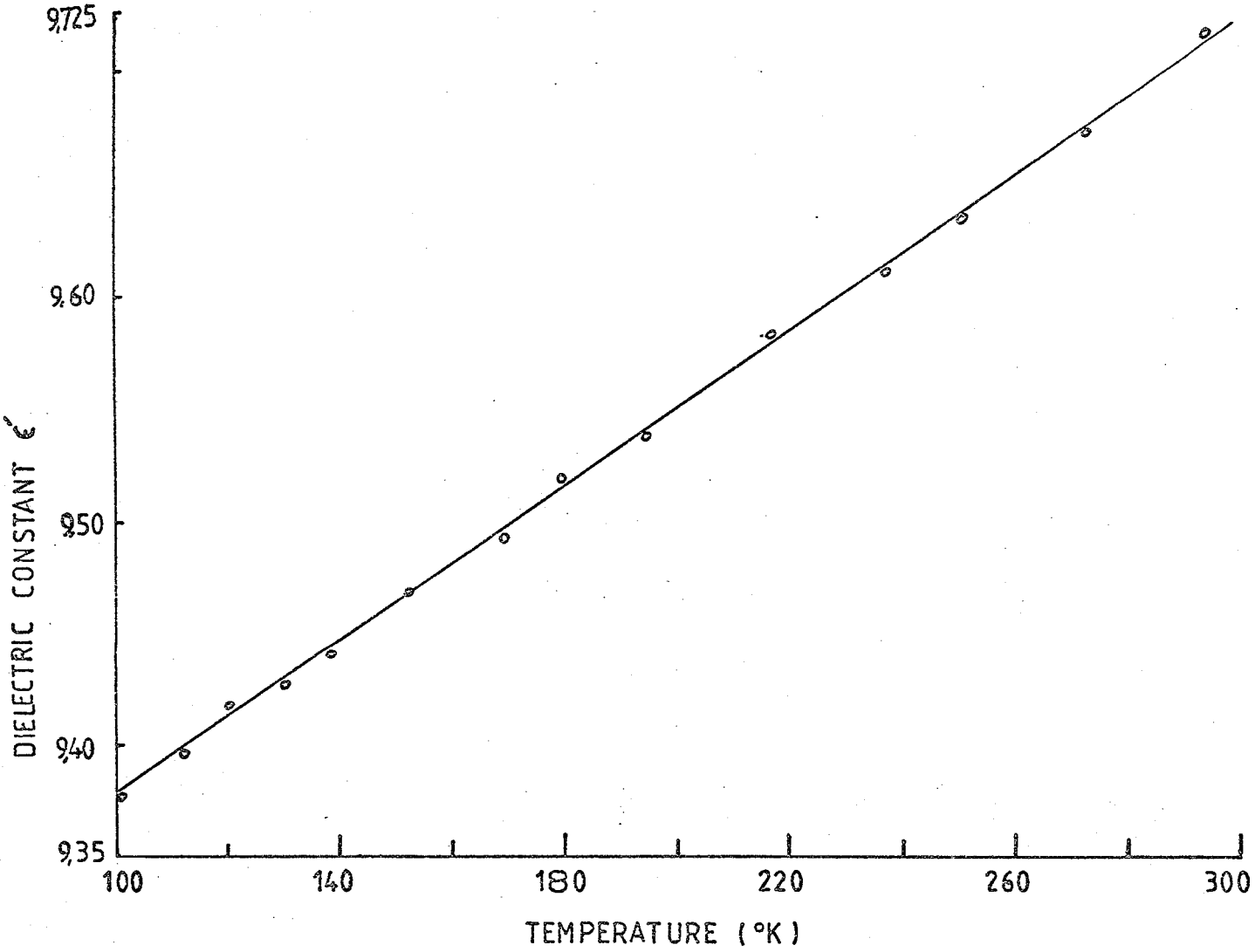

FIG, 10,8 TEMPERATURE DEPENDENCE DIELECTRIC CONSTANT ε'; Co^{2+}/MgO(4800ppm); 1°592 KHz.

F.c.c. single crystal	Lattice space group Ref.(10.21)	Exchange Energy		Dielectric constant ε' at 293 K		
		J (GHz)	Refs.	Frequency (Hz)	ε'	Refs
FeO	O_h^5	162.5	(10.22)	2×10^6	14.2	(10.24)
CoO	O_h^5	143.7	(10.22)	$10^2 - 10^9$	12.9	(10.25)
NiO	O_h^5	114.6	(10.23)	10^5	11.9	(10.25)
Co^{2+}/MgO	O_h^5	6 to 77	Chapt. 5	1.592×10^3	9.5-9.74	Present work

TABLE 10.3 : Comparison of the published data for exchange energy J and dielectric constant ε' of some metal oxides and Co^{2+}/MgO.

From this table, it can be assumed that the real part of the dielectric constant ε' is proportional to the exchange energy for the same type of crystal structure. Since the exchange energy of Co^{2+}/MgO increased linearly with doping concentration (Chapter 5), therefore the slight increase in dielectric constant with concentration can be considered as due to the increase in exchange energy. The e.s.r. linewidth of Ni^{2+}/MgO (Chapter 9) has determined by exchange narrowing together with strain broadening due to dislocations. Possibly, due to the relative absence of exchange mechanism in Ni^{2+}/MgO, the dielectric constant ε' of Ni^{2+}/MgO is very near to the undoped MgO crystal.

It has been shown in Chapter 5 that Co^{2+} entered the MgO lattice substitutionally in Mg^{2+} site. When 50% of the available sites of MgO

are substituted by Co^{2+}, the lattice will correspond to CoO, so dielectric constants of Co^{2+}/MgO for concentrations of 500,000 ppm (i.e. 50% of the sites occupied by cation), can be the value for pure CoO. The measured value of ε' for CoO is 12.9 (10.25) and the measured values of ε' for MgO by different authors at low frequency are less than 12.9 as shown in Table 10.1. If one extrapolated the dielectric constant ε' for 0.01% impurity (which is the point corresponding to 4N pure MgO), the value of ε' becomes 9.42 (as shown in Figure 10.3) which is very close to the experimental value $\varepsilon' = 9.45$ for undoped MgO. So it can be proposed that the dielectric constant ε' for Co^{2+}/MgO is slightly increased with doping concentrations of Co^{2+}. The extrapolation of the law frequency ε' corresponding to the point CoO is 10.4 (as shown in Figure 10.3), which is very much lower than the actual value of $\varepsilon' = 12.9$ (10.25) for CoO. This shows that the exchange energy (which has been interpreted as the hopping frequency (10.26)) has a relatively small contribution to the dielectric constant ε' for Co^{2+}/MgO. Such a small influence of hopping frequency in dielectric constant is one of the criteria for hopping conduction as described in (10.9).

In a wide range of low conductivity materials, for frequency dependence of the conductivity involves two components, such that the measured conductivity $\sigma_m(\omega)$ is related to the true conductivity $\sigma'(\omega)$ by

$$\sigma_m(\omega) = \sigma'(\omega) + \sigma \text{ d.c.} \qquad (10.9)$$

and that the frequency variation $\sigma(\omega)$ follows

$$\sigma'(\omega) \alpha \omega^n \qquad (10.10)$$

where usually $0.7 < n \leq 1$ at low temperatures. There is general agreement

that the a-c conductivity in hopping systems will follow Equation (10.10). With the present materials the experimental evidence indicates that $\sigma_{d.c.}$ is negligible (as shown in Figure 10.4(a) and 10.4(b)) and $\sigma'(\omega)$ is proportional to ω^n with n = 0.86 for Co^{2+}/MgO and n = 0.853 for Ni^{2+}/MgO at room temperature over the frequency range 0.5 kHz to 30 kHz. The very small increase in conductivity of Co^{2+}/MgO with doping concentration (as shown in Figure 10.7) can be matched with the increase in exchange energy with doping concentration of Co^{2+} and the conductivity of Ni^{2+}/MgO similar to pure MgO can be matched with the relative absence of exchange energy in the Ni^{2+}/MgO samples (Chapter 9).

The dielectric loss data fit well with the 'Universal law' suggested by Jonscher (10.9) according to which

$$\varepsilon'' \alpha \omega^{n-1} \quad \text{where} \quad n < 1 \qquad (10.11)$$

for the Co^{2+}/MgO, n = 0.80 and for Ni^{2+}/MgO, n = 0.92 (calculated from the Figure 10.5(b) and 10.6(b) respectively).

The positive value of (K + L + M) for all the samples at room temperature confirms the Bosman and Havinga rule for $\varepsilon' < 20$. The concentration dependence of (K + L + M) for Co^{2+}/MgO may be matched with the increase in exchange energy with doping concentration of Co^{2+} in MgO. The (K + L + M) value for Ni^{2+}/MgO is similar to undoped MgO indicating that by doping Ni^{2+} in MgO, the dielectric behaviour of the samples does not show measurable change. The greater value of (K + L + M) for Co^{2+}/MgO than the undoped MgO and Ni^{2+}/MgO indicates the greater temperature dependence of polarizability in Co^{2+}/MgO.

Since both Co^{2+} and Ni^{2+} are divalent ions substituting them in the MgO lattice, it does not create any extra vacancy (Chapter 5 and Chapter 9) so from the above discussions of the basis of exchange energy

and dielectric behaviour of the samples, it can be concluded that the conductivity mechanisms may be due to hopping from dopant sites.

REFERENCES

CHAPTER TEN

10.1 S.P. Mitoff, J. Chem.Phys. 31 (1959) 1261.

10.2 S.P. Mitoff, J.Chem.Phys. 36 (1962) 1383.

10.3 J.S. Choi, H.Y.Lee, K.H.Kim, J.Phys. Chem. 77 (1973) 2430.

10.4 C.M.Osburn and R.W.Vest, J.Amer.Ceram. Soc. 54 (1971)428.

10.5 M.D.Devies, J. Chem. Phys. 38 (1963) 2047.

10.6 T.J.Lewis and N.J.Wright, Brit.J. App. Physics 1 (1968) 441.

10.7 M. Polack, Phil.Mag. 23 (1971) 519.

10.8 N.F.Mott and E.A.Davis, 'Electronic Process in Non-Crystalline Materials', Oxford Univ.Press, London, 1971.

10.9 A.K.Jonscher, Nature 267 (1977) 673.

10.10 J.S.Thorp and E.A.Ammar, J.Mat.Sc. 10 (1975)918.

10.11 A.H.Scott and H.L. Curtis, J.Res.Nat.Bur.Stand.22 (1939) 741.

10.12 H. Frölich, 'The theory of dielectric' 2nd Edn. Clarendon Press, Oxford, 1958.

10.13 A.J.Bosman and E.E.EHavinga, Phys. Rev. 129 (1963) 1593.

10.14 A.R.V.Hippel, 'Dielectrics materials and applications' John Wiley & Sons, N.Y. 1954.

10.15 J. Yamashita and T.Kurosawa, J.Phys. Soc. Japan 10 (1955) 610.

10.16 S.C.Goyal, J.Appl.Phys. (U.S.A.) 49 (1978) 4503.

10.17 R.A.Barties and P.A.Smith, Phys.Rev.B7 (1973) 3885.

10.18 R.S.Krishnan,'Progress in Crystal Physics', Inter.Sc.Pub.N.Y. 1958, V.1 - p 193.

10.19 Table of dielectric materials, M.I.T. Cambridge, Massachusetts, 1957-V-5.

10.20 L.J.C.Bluck, M.Sc. Thesis, 1979, p 15 ,Durham University, (unpublished).

10.21 J.F.Cornwell, 'Group theory and electronic energy bands in solid', North Holland, 1969.

10.22 P.W.Anderson, Solid State Physics, 14 (1963) 99.

10.23 B.F.Law and D.J.Newman, J.Phys. C 6 (1973) 3245.

10.24 Young and Frederikse, J.Phys.Chem.Ref. Data 2 (1973) 313.

10.25 K.V.Rao and A. Smakula, J.App.Phys. USA 36 (1965) 2031.

10.26 C. Kittel, 'Introduction of Solid State Physics', p 604, 4th Edn. John Wiley & Sons, N.Y. 1971.

CHAPTER ELEVEN

CONCLUSION

In this chapter the linewidths of Cr^{3+}/MgO, Fe^{3+}/MgO, Co^{2+}/MgO, Ni^{2+}/MgO and Gd^{3+}/MgO are compared both in respect of magnitude and mechanisms. It is shown that the exchange energy of S-state ions is greater than F-state ions. The estimation of exchange energies for different oxides have also been shown. Vacancy rule and effective spin value of the dopants have been proposed, and their nuclear spin have also been discussed. It is shown how the magnitude of the dipolar linewidth is related to the lattice parameter and to the dopant electron spin value.

11.1 LINEWIDTH AND MECHANISMS

The e.s.r. results of Cr^{3+}/MgO (Chapter 4), Co^{2+}/MgO (Chapter 5), Fe^{3+}/MgO (Chapter 6), Gd^{3+}/MgO (Chapter 8) and Ni^{2+}/MgO (Chapter 9) confirmed that the observed peak-to-peak linewidths ΔH_{ms} for $\Delta M_s = \pm 1$ transitions were very narrow in comparison to the predicted dipolar broadening theory. The calculated dipolar linewidths exceeded those observed by factors of about 5 to 100 according to the dopant's configuration these factors being higher for trivalent Cr^{3+}, Fe^{3+} and Gd^{3+} than the divalent Co^{2+} and Ni^{2+}. The measured linewidths were independent of concentration over the range examined for Cr^{3+}/MgO (800 ppm-15100 ppm) ; Co^{2+}/MgO (310 ppm to 9900 ppm) and Fe^{3+}/MgO (2300 ppm-4300 ppm) which in contrast to the $(\text{concentration})^{\frac{1}{2}}$ variation expected from dipolar theory. The polar angle independence of the linewidth for Cr^{3+}/MgO (temperature range from 293 K to 15 K) ; Co^{2+}/MgO (temperature range from 65 K to 4.2 K) and Gd^{3+}/MgO was also in contrast to dipolar theory. The polar angle dependences of linewidth for Cr^{3+}/MgO (15 K to 4.2 K) and Ni^{2+}/MgO (180 K to 20 K) confirm the presence of internal strain.

Dopants in MgO	Effective ionic radii-Ref.(11.1)	Concentration (ppm)	Peak-to-peak linewidth (mT)	Exchange Energy J (GHz)	Weiss-Constant θ (K)	10 Dq in MgO	
						Value (cm^{-1})	Refs
Cr^{3+}	0.615 Å	800-15100	0.5	4.39-102.6	3.15-73.7	22700	(11.2)
Fe^{3+}	0.645 Å	2300-4300	0.6	26.05-57.53	43.77-96.65	13800	(11.3)
Co^{2+}	0.735 Å	310-9900	2.0	6-77	0.88-11.12	9600	(11.4)
Ni^{2+}	0.70 Å	1400	6.0	2.912	-	8600	(11.5)
Gd^{3+}	0.938	310	0.3	15	-	-	-

TABLE 11.1 : Summary of the e.s.r. linewidth results of doped MgO.

From Table 11.1, it may be concluded that there was no correlation between the ionic radius of the dopants and the observed linewidths, because of the random magnitude of the linewidths corresponding to the ionic radius. The measured 'g' values and the fitting of the spectra by spin-Hamiltonian of cubic symmetry suggested that all the dopants (Cr^{3+}, Fe^{3+}, Co^{2+}, Ni^{2+} and Gd^{3+}) entered the magnesium sites, though the dopants have different valency and ionic radius than the host cation Mg^{2+}. For all the crystals the ratio of the moments $M_4^{\frac{1}{4}} / M_2^{\frac{1}{2}}$ derived from the experimental data were greater than 1.33 and the lineshapes were Lorentzian. These moment ratios and the lineshape confirmed that the linewidths were determined by exchange narrowing mechanisms. The value of the exchange energies in the crystal are dependent on the dopants configuration (i.e. on the total spin states, which will be discussed in the section 11.3) and proportional to the doping concentration.. A corresponding conclusion is also true for Weiss constant θ . The comparison between the crystal field splitting factor 10 Dq of the dopants in MgO and the measured linewidth indicate a correlation between them, where they have opposite trends.

11.2 CONCENTRATION AND LINESHAPE

It has been calculated by Kittel and Abrahams (11.6) that for the fractional concentration $f > 0.1$ the lineshape is approximately Gaussian with a width proportional to $f^{\frac{1}{2}}$ and for $f < 0.01$ the lineshape is approximately Lorentzian with a width proportional to f. Here, in contrast, the experimental results of doped MgO showed that the linewidths (for the measured concentrations from 0.00031 to 0.0115) were independent of concentration and lineshapes were Lorentzian. The slight increase in linewidth of Co^{2+}/MgO with concentration (Chapter 5) were due to cross-relaxation between Co^{2+} ions (as cross-relaxations proportional to the concentration). The relatively broadened line of Ni^{2+}/MgO than Fe^{3+}/MgO and Cr^{3+}/MgO can be matched with the strain coefficient G_{11} for these ions

in MgO as shown in Table 11.2.

Dopants in MgO	Linewidth ΔH_{ms} (mT)	Measured Strain Coefficient G_{11} in MgO with reference	
		G_{11} (cm^{-1}/unit strain)	Reference
Cr^{3+}	0.5	0.6	E.S.R. Measurements
Fe^{3+}	0.6	5.1	by Zdansky (11.7)
Ni^{2+}	6.0	57	

TABLE 11.2 : Comparison between linewidths and strain coefficient G_{11} in MgO.

The linewidth ratios of Cr^{3+}/MgO : Fe^{3+}/MgO : Ni^{2+}/MgO are 1:1.2:12 which are compared well with the corresponding ratios for strain coefficient G_{11} as 1:8.5: 95.

11.3 COMPARISON OF EXCHANGE ENERGIES

To compare the exchange energies of iron group ions (Cr^{3+}, Fe^{3+}, Co^{2+}) in single crystal MgO, the exchange energy J in Fe^{3+}/MgO have been evaluated from the data previously reported in the literature (11.8) coupled with further measurements of lineshape for single crystal specimens containing 2300 ppm and 4300 ppm of Fe^{3+} respectively.

The lineshapes for the $+\frac{1}{2}$ to $-\frac{1}{2}$ transition in these specimens, derived by integration of derivative plots recorded at 9.1 GHz, are shown in Figure 11.1 which illustrates their Lorentzian shape; the lineshape factors, defined as the ratio of the derivative peak-to-peak linewidth (ΔH_{ms}) to the integrated linewidth at half height ($\Delta H_{1/2}$), were 0.479 and 0.57 respectively. Furthermore, the values of the moment ratio $M_4^{\frac{1}{4}} / M_2^{\frac{1}{2}}$

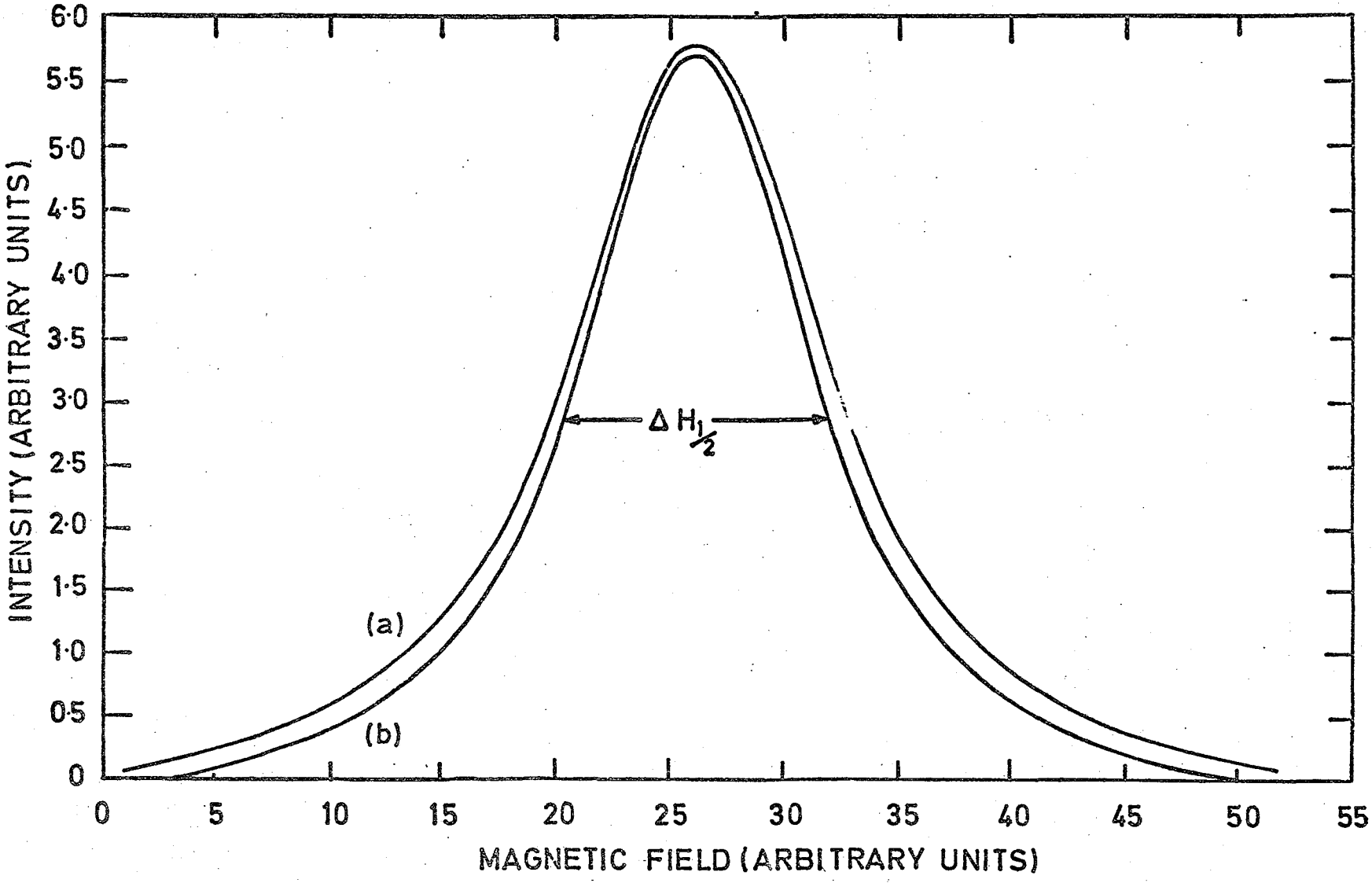

FIG. 11.1 INTEGRATED LINESHAPES FOR (a) 2300ppm Fe, (b) 4300ppm Fe, 77K, 9·165GHz, $\theta_H = 0°$.

(where M_2 and M_4 are the second and fourth moments of the line) were 1.48 and 1.42 respectively. Consequently, having shown that these two line-shapes were Lorentzian, it was considered justifiable to extend this to all the specimens examined in (11.8) using a shape factor of 0.57. On this basis values of exchange energy J have been derived and the variation of J with iron concentration is shown in Table 11.3.

Iron Concentration (ppm)	Exchange Energy, J (GHz)	Weiss-Constant, θ (K)
140	1.80	3.02
310	4.17	7.00
710	9.72	16.33
2,300	26.05	43.77
4,300	57.53	96.65

TABLE 11.3 : Values of exchange energy and Weiss constant for various concentrations of Fe^{3+} in MgO.

A plot of J versus concentration shows a linear dependence up to 4300 ppm Fe^{3+}, (Figure 11.2). If the Fe^{3+} line is extrapolated to a concentration representing 66.6% of available sites occupied by Fe^{3+} (i.e. to the point corresponding to Fe_2O_3), an exchange energy of 8.59×10^{12} Hz is obtained ; this compares well with the value of 10.493×10^{12} Hz for Fe^{3+} in α-Fe_2O_3 obtained from measurements of the intensity of e.s.r. pair spectra (11.9). The values of Weiss constant θ have also been calculated (by the method described in Chapter 4) and these are also tabulated in Table 11.3. The Weiss constant is linearly dependent on the dopant concentration in a manner similar to that described both for Cr^{3+}/MgO (Chapter 4) and also for Co^{2+}/MgO, (Chapter 5).

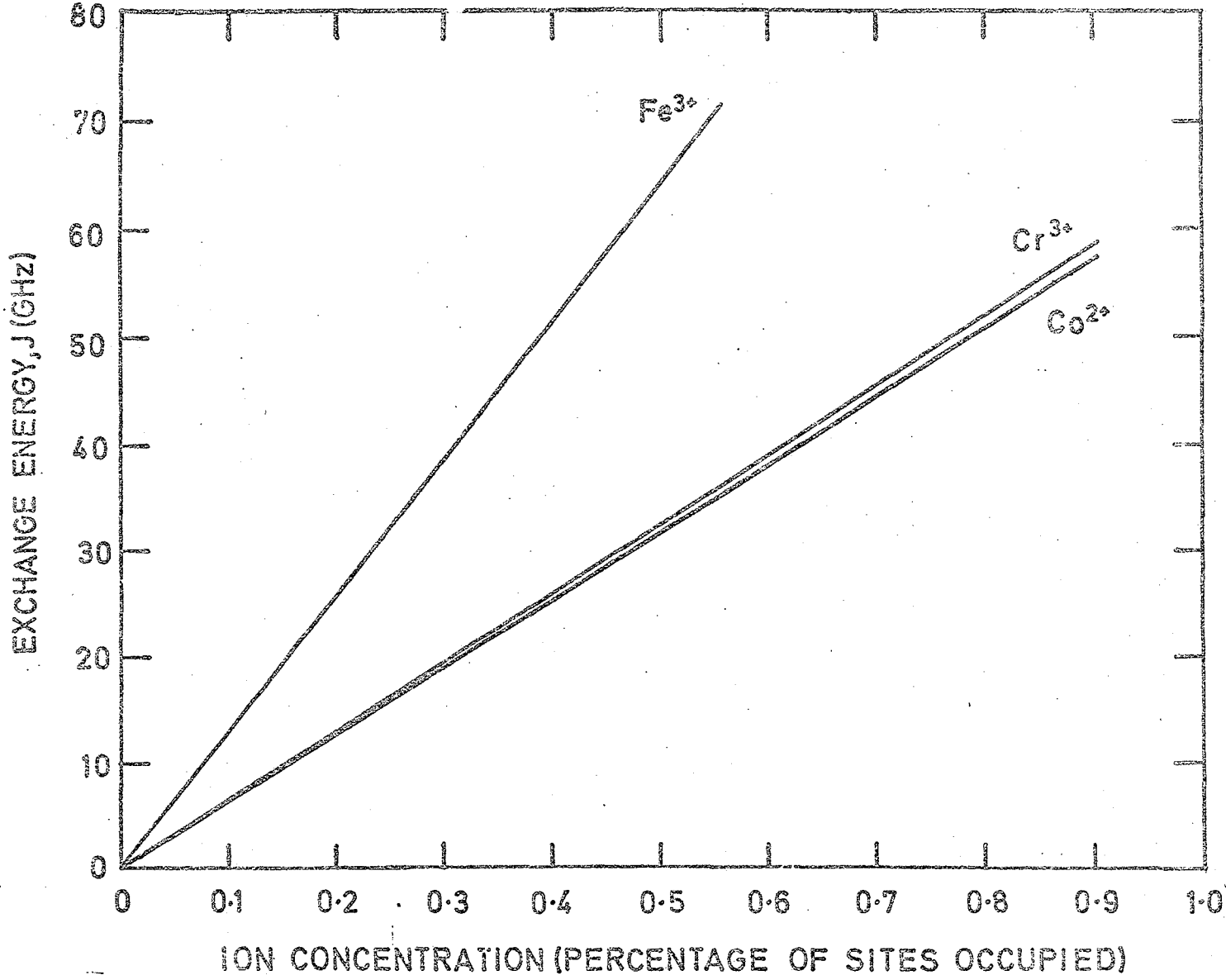

FIG. 11.2 THE VARIATION OF J WITH CONCENTRATION FOR IRON GROUP IONS IN MgO.

The collected data for iron, chromium and cobalt can be compared with the predictions of the general rules for the behaviour of the exchange energy for different ions in the same crystal lattice. According to Anderson, (11.3) these are, firstly that the exchange energy for a trivalent ion will be greater than that for a divalent ion and secondly that an ion with a d^5 configuration will have a greater exchange energy than one having a d^3 configuration. Here the comparison has been made by deriving the slopes of the exchange energy-concentration variations for each ion, shown in Figure 11.2. The numerical data is given in Table 11.4.

Ion and Configuration	Slope Hz.(Conc %)$^{-1}$	References
Fe^{3+}, $3d^5$, $^6S_{5/2}$	12.9 x 10^{10}	This work
Cr^{3+}, $3d^3$, $^4F_{3/2}$	6.57 x 10^{10}	Chapter 4
Co^{2+}, $3d^7$, $^4F_{9/2}$	6.40 x 10^{10}	Chapter 5

TABLE 11.4 : Comparison of data for three iron group ions in MgO.

It can be seen that, for any given concentration,

$$J(Fe^{3+}) > J(Cr^{3+}) > J(Co^{2+})$$

and also that the exchange energy for the S-state ion is greater than for

the F-state ions.

For the given doping concentration of 310 ppm, a comparison of exchange energies for the ions Gd^{3+}, Fe^{3+}, Cr^{3+} and Co^{2+} in MgO with the electron spin value is shown in Table 11.5.

IONS	Ground State	Electron Spin Value	Concentration (ppm)	Exchange energy J(GHz)	References
Gd^{3+}	$^8S_{7/2}$	$\frac{7}{2}$	310	15	Chapter 8
Fe^{3+}	$^6S_{5/2}$	$\frac{5}{2}$	310	4.17	Table 11.3
Cr^{3+}	$^4F_{3/2}$	$\frac{3}{2}$	310	2.03	All these values have been calculated from the slope for J (Table 11.4)
Co^{2+}	$^4F_{9/2}$	$\frac{3}{2}$	310	1.98	

TABLE 11.5 : Comparison of exchange energy for different ions with their electron spin value.

This table shows that exchange energy is higher for higher electron spin value and also substantiates that S-state ions have greater exchange energy than F-state ions in the same host lattice MgO, irrespective of their periodic group.

11.4 ESTIMATION OF EXCHANGE ENERGIES FOR DIFFERENT OXIDES

The lattices of Fe_2O_3 (or Cr_2O_3) can be regarded as a point, corresponding to the situation when 66.6% of the available sites of MgO occupied by Fe^{3+} (or Cr^{3+}) and 50% of the available sites by Co^{2+} will correspond to CoO. From the slopes of the exchange energy concentrations variation of Fe^{3+}, Cr^{3+} and Co^{2+} ions in MgO (as shown in Figure 11.2 and Table 11.4), the exchange energies of Fe_2O_3, Cr_2O_3 and CoO have been estimated and compared with the reported exchange energies of these oxides (as shown in Table 11.6).

Oxides	Estimated from the slopes in Fig 11.2 J(Hz)	Literature value with reference	
		J (Hz)	References
Fe_2O_3	8.59×10^{12}	10.493×10^{12}	(11.9)
Cr_2O_3	4.38×10^{12}	3.75×10^{12}	(11.3)
CoO	3.2×10^{12}	6.29×10^{11}	(11.10)

TABLE 11.6 : Estimation of exchange energies

This comparison agreed well with the literature values and thus supports the validity of estimation of exchange energies.

11.5 VACANCY RULE

The observed narrow linewidths (less than about 0.6 mT) of the trivalent dopants Fe^{3+}, Cr^{3+} and Gd^{3+} in the single crystal MgO were less than the predicted dipolar linewidths (more than about 10 mT) and the general behaviour of the spectra of these ions confirmed that the cubic

symmetry was preserved to a high order, despite the fact that the dopants have greater valency than the host cation Mg^{2+}. As the dopants go substitutionally, to maintain the neutrality of the crystals, either there have been some positive ion vacancies or negative ion interstitials. Since the spectra fitted with cubic spin-Hamiltonians, since the linewidths are very narrow, and since these dopants have large exchange energies, this evidence seems to suggest that there are no interstitial ions in the neighbourhood of the crystals Fe^{3+}/MgO, Cr^{3+}/MgO and Gd^{3+}/MgO. So vacancies may be one Mg^{2+} ion for every two trivalent ions in the magnesium sites and the distribution of vacancies should be uniform throughout the crystals to preserve the cubic symmetry. This uniform distribution of vacancies holds for Fe^{3+} and Gd^{3+} in the temperature range from 293 K to 4.2 K and for Cr^{3+} in the temperature range from 293 K to about 15 K.

11.6 EFFECTIVE SPIN

The observation of a single fine structure line for each of Cr^{3+}, Co^{2+}, Ni^{2+} and Gd^{3+} in MgO single crystals indicates that the effective spin value for the above ions is $S' = \frac{1}{2}$, though their actual spins are $S \geq 1$ and the allowed transition of $\Delta M_s = \pm 1$ can be given by the simple spin-Hamiltonian $h\nu = g\beta H$. For this effective spin $S' = \frac{1}{2}$, the empirical energy levels for these ions in the host lattice MgO can be proposed as shown in Figure 11.3, where two levels, diverging linearly with H, with slopes $\pm \frac{1}{2}\ g\ \beta H$.

11.7 NUCLEAR SPIN

Hyperfine structures were found in Cr^{3+}/MgO (Chapter 4) and Co^{2+}/MgO (Chapter 5). The observation of four hyperfine lines

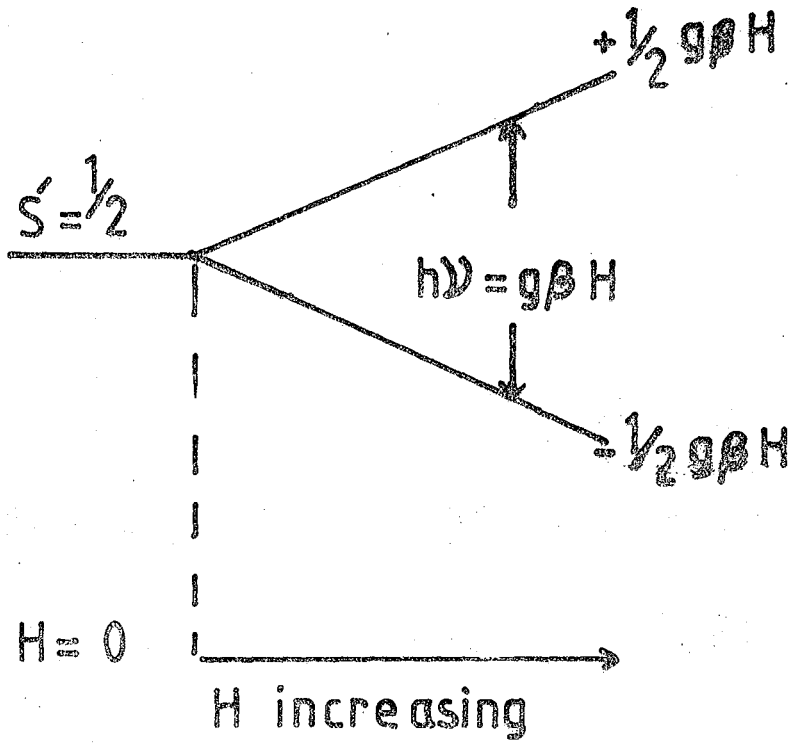

FIG, 11,3 Energy levels for $s'=\frac{1}{2}$; Zeeman effect in an applied field H, with allowed transition at $h\nu = g\beta H$.

for Cr^{3+} and eight hyperfine lines for Co^{2+} in MgO permitted the confirmation of the nuclear spin I of Cr^{53}, $I = \frac{3}{2}$ and Co^{59}, $I = \frac{7}{2}$.

11.8 DIPOLAR LINEWIDTHS OF TRIVALENT IONS DOPED IN ALKALINE EARTH OXIDES

The prediction of dipolar linewidths (e.s.r.) in the MgO lattice for transition ions Fe^{3+} (11.8), Cr^{3+} (Chapter 4) and Gd^{3+} (Chapter 8) have been shown, where the calculated linewidths are found much larger than the experimental linewidths and the linewidth mechanisms are exchange narrowing instead of dipolar broadening. Dipolar linewidth for Cr^{3+} in Al_2O_3 (11.11) and Gd^{3+} in $CaWO_4$ (11.12) have been calculated by Thorp et al and the calculated linewidths are well agreed with the experimental dipolar linewidths. This proves that the linewidth mechanisms of the same ion in the different lattices are different. E.S.R. spectra for Fe^{3+} in CaO (11.13) and SrO (11.14) ; for Cr^{3+} in CaO (11.15) and SrO (11.16) ; for Gd^{3+} in CaO (11.17) and SrO (11.18) have been reported. These reported spectra showed cubic symmetry in the CaO lattice with the indication that trivalent impurities replace Ca^{2+} ions without disturbing the local symmetry, while in the SrO lattice the symmetry are low. These reported lines were not compared with the dipolar broadening theory. Here the prediction of dipolar linewidths for Fe^{3+}, Cr^{3+}, and Gd^{3+} in the host lattices of CaO and SrO ; and a comparison between dipolar linewidths to the reported linewidths for these ions (Fe^{3+}, Cr^{3+}, Gd^{3+}) in the host lattices MgO, CaO, Al_2O_3 and $CaWO_4$, are given.

Magnesium oxide (MgO), Calcium oxide (CaO) and Strontium oxide (SrO) are the alkaline earth oxides, having the same crystal structure type of Nacl (11.19) in which the divalent cation lies at the centre of an octahedran of six O^{2-} ion. Wyckoff (11.19) gave the lattice parameter of MgO at 21° C as $a_o = 4.2112$ Å , of CaO as $a_o = 4.8105$ Å and for SrO at

25^{o} C as a_o = 5.1602 Å. It will be assumed in the calculation that the main contribution to homogeneous line broadening is dipole-dipole interactions between like ions. The unit cells of alkaline earth oxides (MgO, CaO, SrO) are face centred cubic of space group O_h^5 as indicated by Cornwell (11.20). It has been reported that Fe^{3+}, Cr^{3+} and Gd^{3+} can be substituted in the CaO lattice (11.13, 11.15, 11.17) and in the SrO lattice (11.14, 11.16, 11.18) for the cation sites. In order to calculate the dipolar linewidth, a complete tabulation of these sites is needed. It is found sufficient to consider eight unit cells with the dopant ion as common corner because the contribution from remote cells is negligible. The r,θ,ϕ values of all the calcium sites in CaO lattice and of all the strontium sites in SrO have been given in Appendix I, Table A1 and Table B1 respectively. The second moment of the linewidth caused by dipolar interactions between identical atoms in cubic oxide lattice has been shown by Thorp et al (11.8) to be

$$\langle\Delta\omega^2\rangle = \frac{3}{4} S(S+1)\left(\frac{g^2\beta^2}{\hbar}\right)^2 .n.\left[\frac{4}{5}\sum r_{jk}^{-6} + \frac{32\pi}{35} Y^{*}_{4,0}(\theta_H,\phi_H) \sum_k r_{jk}^{-6} Y_{4,0}(\theta_K,\phi_K) + \frac{64\pi}{35} Y^{*}_{4,4}(\theta_H,\phi_H) \sum_k r_{jk}^{-6} Y_{4,4}(\theta_K,\phi_K)\right] \quad (11.1)$$

where $\langle\Delta\omega^2\rangle$ is the second moment and the symbols have their usual meaning as described in Chapter 2. Equation 11.1 has two parts, the first relating only to the atomic parameters, the second describing the particular crystal

system, which is known as geometrical part. The atomic part

$\left\{ \frac{3}{4} S(S+1) \left(\frac{g^2 \beta^2}{\hbar} \right)^2 .n \right\}$ for different ions in the same host

lattice has the different values, while the geometrical part has the same value. Using Appendix 1, Table A.11 for CaO and Table B11 for SrO, the geometrical part of Equation 11.1 can be evaluated respectively as

$$\left[\quad\right]_{CaO} = \left\{ 7.15864 - 2.3271\ Y^{*}_{4,0}(\theta_H,\phi_H) - 2.7561\ Y^{*}_{4,4}(\theta_H,\phi_H) \right\} \times 10^{45}\ .\ cm^{-6} \quad (11.2)$$

and

$$\left[\quad\right]_{SrO} = \left\{ 4.69943 - 1.4986\ Y^{*}_{4,0}(\theta_H,\phi_H) - 1.8244\ Y^{*}_{4,4}(\theta_H,\phi_H) \right\} \times 10^{45}\ .\ cm^{-6} \quad (11.3)$$

when $\theta_H = 0^\circ$, and $\phi_H = 0^\circ$ (which corresponds to H// [100] plane), the above equations reduces to

$$\left[\quad\right]_{CaO} = 5.18936 \times 10^{45}\ cm^{-6} \quad (11.4)$$

$\theta_H = 0^\circ$

$\phi_H = 0^\circ$

and

$$\left[\quad\right]_{SrO} = 3.43119 \times 10^{45}\ cm^{-6} \quad (11.5)$$

$\theta_H = 0^\circ$

$\phi_H = 0^\circ$

The total dipolar broadening is given by the square root of the sum of second moments of the individual dipolar interactions. This must be converted into the peak-to-peak derivative linewidth ΔH_{ms}, for comparison with the experimental results. This is done by using the equation

$$\Delta H_{ms} = \frac{\sqrt{<\Delta\omega^2>}}{\pi} \cdot \frac{\partial H}{\partial \nu} \quad \text{Tesla} \qquad (11.6)$$

where the parameter $\frac{\partial H}{\partial \nu}$ obtained from the relation $\frac{\partial H}{\partial \nu} = \frac{h}{g\beta}$.

By evaluating the atomic part and geometrical part for different ions (Cr^{3+}, Fe^{3+} and Gd^{3+}) doped in CaO and SrO ; and using the transformation equation 11.6, ΔH_{ms} can be calculated.

Crystal	Ions and Configuration ⟶	$Cr^{3+}, 3d^3, {}^4F_{3/2}$, $S = \frac{3}{2}$	$Fe^{3+}, 3d^5, {}^6S_{5/2}$, $S = \frac{5}{2}$	$Gd^{3+}, 4f^7, {}^8S_{7/2}$, $S = \frac{7}{2}$
MgO	g-value ⟶	1.98 Ref(11.2)	2.0037 Ref(11.21)	1.992 Ref(11.22)
	ΔH_{ms} (dipolar) (mT) ⟶	661.6. $\sqrt{n}$	1024.6. $\sqrt{n}$	1364.2. $\sqrt{n}$
CaO	g-value ⟶	1.9732 Ref (11.15)	2.0052 Ref(11.13)	1.9913 Ref(11.17)
	ΔH_{ms} (dipolar) (mT) ⟶	442.096. $\sqrt{n}$	686.68. $\sqrt{n}$	914.52. $\sqrt{n}$
SrO	g-value ⟶	1.9638 Ref (11.16)	2.004 Ref(11.14)	1.9918 Ref(11.18)
	ΔH_{ms} (dipolar) (mT) ⟶	358.59. $\sqrt{n}$	557.7. $\sqrt{n}$	744.01 $\sqrt{n}$

TABLE 11.7 : Predicted dipolar linewidth for an unknown concentration n, when H// $[\bar{1}00]$ plane and $\theta_H = 0^o$.

A comparison of the calculated dipolar linewidths of the dopants (Cr^{3+}, Fe^{3+} and Gd^{3+}) in the lattices MgO (a_o = 4.2112 Å), CaO (a_o = 4.8105 Å) and SrO (a_o = 5.1602 Å) for the same concentration n is given in Table 11.7 and the calculated values are plotted for n = 100 ppm as a function of lattice parameters as shown in Figure 11.4. From the Table 11.7 and Figure 11.4 it is concluded that :-

(a) The dipolar linewidth of a given ion decreases linearly with the increases of the host lattice parameter and smaller lattice parameter causes greater magnitude of the dipolar linewidth.

(b) In a given host lattice, the dipolar linewidth of the dopants are proportional to the spin value of the ions and the greater linewidth corresponds to the higher spin.

A comparison of the predicted dipolar linewidths for Fe^{3+}, Cr^{3+} and Gd^{3+} with the reported experimental linewidths in different lattices are given in Table 11.8. All the data considered here were taken at 77 K (because at this temperature the relaxation effect to linewidth were negligible), H// [100] plane at $\theta_H = 0^o$ and in X-band spectrometers except for $Gd^{3+}/CaWO_4$ and Cr^{3+}/Al_2O_3 in Q band spectrometers. From Table 11.8 it can be concluded that the ratio of the dipolar linewidth to the reported linewidth is higher for the lower radius of sphere (which contains 64 sites corresponding to 8 unit cells). These ratios of linewidths for the CaO lattice lie in between the ratios for the exchange narrowing and dipolar mechanisms. So it would be interesting for future work to test which one of these linewidth mechanisms holds true for doped CaO.

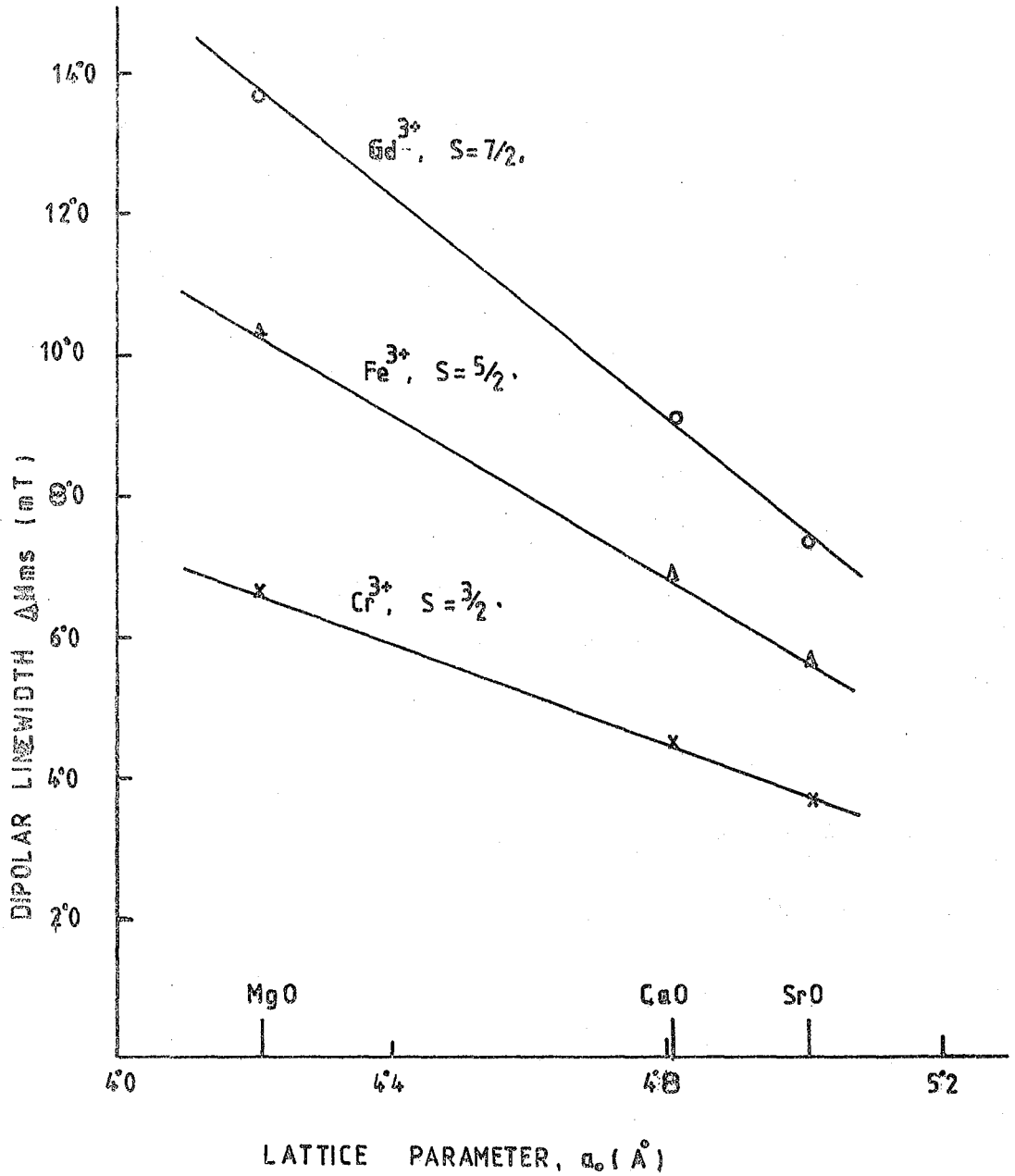

FIG.11.4 LATTICE PARAMETER VERSUS DIPOLAR LINEWIDTH. (x —— Chromium, Δ —— Iron and o —— Gadolinium), n =100ppm.

Host Crystals	Radius of sphere which contains 64 sites corresponds to 8 unit cells	Dopants	Concentration (refer to % of cation site)	Reported linewidth ΔH_{ms} (mT)	Reported linewidth Refs	Dipolar linewidth ΔH_{ms} (mT)	Ratio = $\frac{\Delta H_{ms}(\text{dipolar})}{\Delta H_{ms}(\text{reported})}$	Reported
MgO	7.294 Å	Cr^{3+}	0.08%	0.47	Chapter 4	18.7	40	Exchange-
		Fe^{3+}	0.071%	0.62	(11.8)	23.67	38	narrowing
		Gd^{3+}	0.031%	0.30	Chapter 8	23.3	77	
CaO	8.332 Å	Cr^{3+}	0.001%	0.087	(11.15)	1.398	16	Not mentioned
		Fe^{3+}	0.107%	0.70	(11.13)	22.5	32	
		Gd^{3+}	0.043%	1.2	(11.17)	19.13	16	
Al_2O_3	13.015 Å	Cr^{3+}	0.02%	1.2	(11.11)	6.0	5	Dipolar
$CaWO_4$	13.5794 Å	Gd^{3+}	0.001%	0.3	(11.12)	2.1	7	Dipolar

TABLE 11.3 : Comparison between the dipolar linewidths and the reported experimental linewidths.

REFERENCES

CHAPTER ELEVEN

11.1 R.D.Shannon and C.T. Prewitt, Acta.Cryst.B25 (1969) 925.

11.2 W.Low, Phys. Rev. 105 (1957) 801.

11.3 P.W.Anderson, Solid State Physics 14 (1963) 99.

11.4 W.Low, Phys. Rev. 109 (1958) 256.

11.5 W. Low, Phys. Rev. 109 (1958) 247.

11.6 C. Kittel and E.Abrahams, Phys.Rev.90 (1953) 238.

11.7 K. Zdansky, Colleque Ampere, XIV,North Holland, (1967), p.295.

11.8 J.S.Thorp, R.A.Vasquez, C.Adcock, W. Hutton, J.Mat.Sci.11 (1976)89.

11.9 R.L.Garifullina, M.M.Zaripov & V.G.Stephonov, Sov.Phys.Solid State 12 (1970), 43.

11.10 S.Geschwind, "Electron Paramagnetic Resonance", Plenum Press, N.Y.1972.

11.11 J.S. Thorp, H.P.Buckley, J.Mat.Sci.9 (1974) 1499.

11.12 J.S.Thorp, G.Brown and H.P.Buckley, J.Mat.Sci.9 (1974) 1499.

11.13 A.J.Shuskus, Phys. Rev.127 (1962) 1529.

11.14 P. Auzins, J.W.Orton and J.Wertz, "Paramagnetic resonance", V.1 Page 90, Edt. W.Low, Acad.Press, N.Y.1963.

11.15 W.Low, R.S.Robinson, Phys.Lett 1 (1962) 316.

11.16 W.Low, J.T.Suss. Phys.Lett.11 (1964) 115.

11.17 A.J.Shuskus, Phys.Rev.127 (1962) 2022.

11.18 A.J.Shuskus, J.Chem.Phys.41 (1964) 1885.

11.19 R.W.Wyckoff, "Crystal Structure"V-1,Inter.Sci.N.Y.1965.

11.20 J.F.Cornwell, "Group theory of electronic energy bands in solids", North Holland, 1969

11.21 W.Low, Ann.N.Y.Acad.Sci.72 (1958) 69.

11.22 M.M.Abraham, L.A.Boatner, Y.Chen and J.L.Kolpus, Phys.Rev.B4 (1971) 2853.

APPENDIX I

TABLE A1 : Values of r, θ , and φ for calcium sites in eight unit cells of CaO, taking the common corner as the origin of the polar co-ordinates.

a	b	c	r (Å)	θ°	φ°
½	½	0	3.4015	90	45
-½	½	0	3.4015	90	135
-½	-½	0	3.4015	90	225
½	-½	0	3.4015	90	315
0	½	½	3.4015	45	90
0	-½	½	3.4015	45	270
0	-½	-½	3.4015	135	270
0	½	-½	3.4015	135	90
½	0	½	3.4015	45	130
-½	0	½	3.4015	45	180
½	0	-½	3.4015	135	0
-½	0	-½	3.4015	135	180
0	0	1	4.8105	0	-
0	0	-1	4.8105	180	-
1	0	0	4.8105	90	0
0	1	0	4.8105	90	90
-1	0	0	4.8105	90	180
0	-1	0	4.8105	90	270
½	½	1	5.8916	35.26	45
-½	½	1	5.8916	35.26	135
-½	-½	1	5.8916	35.26	225
½	-½	1	5.8916	35.26	315
½	½	-1	5.8916	144.74	45
-½	½	-1	5.8916	144.74	135
-½	-½	-1	5.8916	144.74	225
½	-½	-1	5.8916	144.74	315
½	1	½	5.8916	65.91	63.44
-½	1	½	5.8916	65.91	116.56
½	1	-½	5.8916	114.09	63.44
-½	1	-½	5.8916	114.09	116.56
-½	-1	½	5.8916	65.91	243.44
½	-1	½	5.8916	65.91	296.56
-½	-1	-½	5.8916	114.09	243.44
½	-1	-½	5.8916	114.09	296.56
1	½	½	5.8916	65.91	26.57
1	-½	½	5.8916	65.91	233.43
1	½	-½	5.8916	114.09	26.57
1	-½	-½	5.8916	114.09	333.43
-1	½	½	5.8916	65.91	153.43
-1	-½	½	5.8916	65.91	206.56
-1	½	-½	5.8916	114.09	153.43
-1	-½	-½	5.8916	114.09	206.56
1	0	1	6.8030	45	0
-1	0	1	6.8030	45	180
1	0	-1	6.8030	135	0
-1	0	-1	6.8030	135	180
0	1	1	6.8030	45	90
0	-1	1	6.8030	45	270
0	1	-1	6.8030	135	90
0	-1	-1	6.8030	135	270
1	1	0	6.8030	90	45
-1	1	0	6.8030	90	135
-1	-1	0	6.8030	90	225
1	-1	0	6.8030	90	315
1	1	1	8.3320	54.74	45
-1	1	1	8.3320	54.74	135
-1	-1	1	8.3320	54.74	225
1	-1	1	8.3320	57.74	315
1	1	-1	8.3320	125.26	45
-1	1	-1	8.3320	125.26	135
-1	-1	-1	8.3320	125.26	225
1	-1	-1	8.3320	125.26	315

r(Å)	θ^{o} k	ϕ^{o} k	N(No. of sites)	$Y_{4,0}(\theta_k,\phi_k)$	$Y_{4,4}(\theta_k,\phi_k)$	$Nr^{-6} \times 10^{45} cm^{-6}$	$Nr^{-6}Y_{4,0}(\theta_k,\phi_k) \times 10^{45} cm^{-6}$	$Nr^{-6}Y_{4,4}(\theta_k,\phi_k) \times 10^{45} cm^{-6}$
3.4015	90	45	4	0.3174	-0.4425	2.5825	0.8197	-1.1427
3.4015	45	0	8	-0.3438	0.1106	5.1649	-1.7757	0.5712
4.8105	0	-	2	0.8463	0.000	0.1614	0.1366	0.000
4.8105	90	0	4	0.3174	0.4425	0.3228	0.1025	0.1428
5.8916	35.26	45	8	-0.1528	-0.04917	0.1913	-0.0292	-0.00094
5.8916	65.91	26.57	16	-0.1087	-0.0861	0.3826	-0.0416	-0.03294
6.8030	45	0	8	-0.3438	0.1106	0.0793	-0.0273	0.00088
6.8030	90	45	4	0.3174	-0.4425	0.0396	0.0126	-0.01752
8.3320	54.74	45	8	-0.3291	-0.1967	0.0239	-0.0078	-0.00047
					SUM	8.9483	-0.8102	-0.4799

TABLE AII : Trigonometrical parameters for the calcium sites in 8 unit cells of CaO.

TABLE B1 : Values of r, Θ and φ for strontium sites in eight unit cells of SrO, taking the common corner as the origin of the polar co-ordinates.

a	b	c	r (Å)	Θ	φ
½	½	0	3.6488	90	45
-½	½	0	3.6488	90	135
-½	-½	0	3.6488	90	225
½	-½	0	3.6488	90	315
0	½	½	3.6488	45	90
0	-½	½	3.6488	45	270
0	½	-½	3.6488	135	90
0	-½	-½	3.6488	135	270
½	0	½	3.6488	45	0
-½	0	½	3.6488	45	180
½	0	-½	3.6488	135	0
-½	0	-½	3.6488	135	180
0	0	1	5.1602	0	-
0	0	-1	5.1602	180	-
1	0	0	5.1602	90	0
0	1	0	5.1602	90	90
-1	0	0	5.1602	90	180
0	-1	0	5.1602	90	270
½	½	1	6.3199	35.26	45
-½	½	1	"	35.26	135
-½	-½	1	"	35.26	225
½	-½	1	"	35.26	315
½	½	-1	"	144.74	45
-½	½	-1	"	144.74	135
-½	-½	-1	"	144.74	225
½	-½	-1	"	144.74	315
½	1	½	"	65.91	63.44
-½	1	½	"	65.91	116.56
½	1	-½	"	114.09	63.44
-½	1	-½	"	114.09	116.56
-½	-1	½	"	65.91	243.44
½	-1	½	"	65.91	296.56
-½	-1	-½	"	114.09	243.44
½	-1	-½	"	114.09	296.56
1	½	½	6.3199	65.91	26.57
1	-½	½	6.3199	65.91	333.43
1	½	-½	6.3199	114.09	26.57
1	-½	-½	6.3199	114.09	333.43
-1	½	½	6.3199	65.91	153.43
-1	-½	½	6.3199	65.91	206.56
-1	½	-½	6.3199	114.09	153.43
-1	-½	-½	6.3199	114.09	206.56
1	0	1	7.2976	45	0
-1	0	1	7.2976	45	180
-1	0	-1	7.2976	135	0
-1	0	-1	7.2976	135	180
1	1	0	7.2976	90	45
-1	1	0	7.2976	90	135
-1	-1	0	7.2976	90	225
1	-1	0	7.2976	90	315
0	1	1	7.2976	45	90
0	-1	1	7.2976	45	270
0	1	-1	7.2976	135	90
0	-1	-1	7.2976	135	270
1	1	1	8.9377	57.74	45
-1	1	1	8.9377	54.74	135
-1	-1	1	8.9377	54.74	225
1	-1	1	8.9377	54.74	315

$r(\mathring{A})$	θ^{o} K	ϕ^{o} K	N(No.of sites)	$Y_{4,o}(\theta_k,\phi_k)$	$Y_{4,4}(\theta_k,\phi_k)$	$Nr^{-6} \times 10^{45} cm^{-6}$	$Nr^{-6}Y_{4,o}(\theta_k,\phi_k) \times 10^{45} cm^{-6}$	$Nr^{-6}Y_{4,4}(\theta_k,\phi_k) \times 10^{45} cm^{-6}$
3.6488	90	45	4	0.3174	-0.4425	1.6949	0.5379	-0.7499
3.6488	45	0	8	-0.3438	0.1106	3.3899	-1.1654	0.3749
5.1608	0	-	2	0.8463	0.0000	0.10593	0.0896	0.0000
5.1608	90	0	4	0.3174	0.4425	0.21186	0.0672	0.09374
6.3199	35.26	45	8	-0.1528	-0.04917	0.1255	-0.01917	-0.00617
6.3199	65.91	26.57	16	-0.1087	-0.0861	0.2511	-0.02729	-0.02160
7.2976	45	0	8	-0.3438	0.1106	0.0529	-0.01818	0.00580
7.2976	90	45	4	0.3174	-0.4425	0.0265	0.00841	-0.0113
8.9377	54.74	45	8	-0.3291	-0.1967	0.0157	0.00516	-0.0030
					SUM	5.87429	-0.52177	-0.31759

TABLE BII : Trigonometrical parameters for the strontium sites in 8 unit cells of SrO.

PUBLICATIONS

1. 'Electron Spin Resonance Linewidths of Cr^{3+} in Magnesium Oxide"

   J.S.Thorp, M.D.Hossain, L.J.C.Bluck, J.Mat.Sci.14 (1979) 2853.

2. "Electron Spin Resonance Linewidths of Co^{2+} in Magnesium Oxide"

   J.S.Thorp, M.D.Hossain, L.J.C.Bluck, T.G.Bushell, J.Mat.Sci.15 (1980) 903.

3. "Exchange Energies of Iron Group Ions in Single Crystal MgO"

   J.S.Thorp, M.D.Hossain, J.Mat.Sci 15 (1980) 1866.

4. "E.S.R.Line Broadening of Fe^{3+} in Fe/MgO at Low Temperatures"

   J.S.Thorp, M.D. Hossain, J.Mat.Sci.15 (1980) (to be published).

5. "E.S.R. Line Broadening in Cr^{3+}/MgO at Liquid Helium Temperatures"

   J.S.Thorp, M.D.Hossain, J.Mat.Sci. (to be published)